Durham E-Theses

Three dimensional unsteady flow for an oscillating turbine blade

Bell, David Lloyd

How to cite:

Bell, David Lloyd (1999) *Three dimensional unsteady flow for an oscillating turbine blade*, Durham theses, Durham University. Available at Durham E-Theses Online: http://etheses.dur.ac.uk/4794/

THREE DIMENSIONAL UNSTEADY FLOW FOR AN OSCILLATING TURBINE BLADE

David Lloyd Bell

School of Engineering, University of Durham

A dissertation submitted to the University of Durham
for the degree of Doctor of Philosophy

March 1999

Declaration

I declare that no material presented within this dissertation has submitted towards a degree at this or any other university
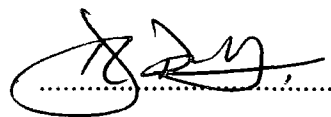
David Lloyd Bell

In memory of Mick Page

Acknowledgements

There are so many people to thank, and I am sure I will omit a few. I would therefore like to begin by thanking all those who have contributed towards this work and assisted me during what has been, for the most part, an enjoyable time in my life.

I must first thank Dr. Li He for whom I have the greatest respect as a mentor, colleague and friend. His continual support and guidance has been excellent.

The technicians of the electrical, electronic and mechanical workshops also require praise, most especially Mr. Brian Blackburn, Mr Ian Garret, Mr. Ray Mand, Mr. Allan. Swan and of course Mr. Ian Glassford, for his constructive and direct input during the design and construction of the experimental test facility. I would also like to mention some of my colleagues and friends: Dr. J. Ismael, Dr. Wei Ning, Kenji Sato and all the boys of the legendary E.P. Pannini.

Most of all I would like to thank my parents, Mari and Thomas for all their love, support and encouragement.

Abstract

An experimental and computational study, motivated by the need to improve current understanding of blade flutter in turbomachinery and provide 3D test data for the validation of advanced computational methods for the prediction of this aeroelastic phenomenon, is presented.

A new, low speed flutter test facility has been developed to facilitate a detailed investigation into the unsteady aerodynamic response of a turbine blade oscillating in a three dimensional bending mode. The facility employs an unusual configuration in which a single turbine blade is mounted in a profiled duct and harmonically driven. At some cost in terms of modelling a realistic turbomachinery configuration, this offers an important benefit of clearly defined boundary conditions, which has proved troublesome in previous work performed in oscillating cascade experiments. Detailed measurement of the unsteady blade surface pressure response is enabled through the use of externally mounted pressure transducers, and an examination of the techniques adopted and experimental error indicate a good level of accuracy and repeatability to be attained in the measurement of unsteady pressure.

A detailed set of steady flow and unsteady pressure measurements, obtained from five spanwise sections of tappings between 10% and 90% span, are presented for a range of reduced frequency. The steady flow measurements demonstrate a predominant two dimensional steady flow, whilst the blade surface unsteady pressure measurements reveal a consistent three dimensional behaviour of the unsteady aerodynamics. This is most especially evident in the measured amplitude of blade surface unsteady pressure which is largely insensitive to the local bending amplitude. An experimental assessment of linearity also indicates a linear behaviour of the unsteady aerodynamic response of the oscillating turbine blade.

These measurements provide the first three dimensional test data of their kind, which may be exploited towards the validation of advanced flutter prediction methods.

A three dimensional time-marching Euler method for the prediction of unsteady flows around oscillating turbomachinery blades is described along with the modifications required for simulation of the experimental test configuration. Computational solutions obtained from this method, which are the first to be supported by 3D test data, are observed to exhibit a consistently high level of agreement with the experimental test data. This clearly demonstrates the ability of the computational method to predict the relevant unsteady aerodynamic phenomenon and indicates the unsteady aerodynamic response to be largely governed by inviscid flow mechanisms. Additional solutions, obtained from a quasi-3D version of the computational method, highlight the strong three dimensional behaviour of the unsteady aerodynamics and demonstrate the apparent inadequacies of the conventional quasi-3D strip methodology.

A further experimental investigation was performed in order to make a preliminary assessment of the previously unknown influence of tip leakage flow on the unsteady aerodynamic response of oscillating turbomachinery blades. This was achieved through the acquisition of a comprehensive set of steady flow and unsteady pressure measurements at three different settings of tip clearance. The steady flow measurements indicate a characteristic behaviour of the tip leakage flow throughout the range of tip clearance examined, thereby demonstrating that despite the unusual configuration, the test facility provides a suitable vehicle for the investigation undertaken. The unsteady pressure data show the blade surface unsteady pressure response between 10% and 90% span to be largely unaffected by the variation in tip clearance. Although close examination of the unsteady pressure measurements reveal subtle trends in the first harmonic pressure response at 90% span, which are observed to coincide with localised regions where the tip leakage flow has a discernible impact on the steady flow blade loading characteristic.

Finally, some recommendations for further work are proposed

Table of Contents

3. The Low Speed Flutter Test Facility

4. Data Acquisition and Reduction

5. The Experimental Results and Discussion

6. The Computational Method, Results and Discussion

7. The Influence of Tip Leakage on the Oscillating Blade Flow

8. Concluding Remarks

Nomenclature

a Undisturbed speed of sound, m/s

Ap_n Amplitude of the nth harmonic pressure response, Pa

B_C Bending amplitude at tip non-dimensionalised with chord

B_L Local bending amplitude, non-dimensionalised with chord

C Blade chord, m

Cp Blade surface pressure coefficient, $\quad Cp = \dfrac{P - P_2}{(\overline{P_{01}} - \overline{P_2})}$

$|Cp_n|$ Amplitude of the nth harmonic pressure coefficient, $\quad |Cp_n| = \dfrac{Ap_n}{(\overline{P_{01}} - \overline{P_2})B_C}$

dA   Projected blade surface area per unit span normal to the direction of bending

e Internal energy, J/kg

EO Engine order

f Frequency, Hz

h   Blade span, m

k Reduced frequency, $\quad k = \dfrac{\omega C}{V_{ref}}$

k_t Reduced frequency (pressure waves in cylindrical pipes), $\quad k_t = \dfrac{\omega R}{a}$

M Mach number

P Pressure, Pa

$P.S.$ Pressure surface

R Tube radius, m

Re Reynolds number, based on chord and reference velocity

s Displacement of the blade surface (defined in figure 3.2), m; pitch length, m

S Shear wave number, $\quad S = R\sqrt{\rho\omega/\mu}$

$S.S.$ Suction surface

t Time, s

T Time period, s

u	Axial velocity, m/s
v	Tangential velocity, m/s
V_{ref}	Reference (isentropic exit) velocity, m/s, $\quad V_{ref} = \sqrt{\dfrac{2(\overline{P_{01}} - \overline{P_2})}{\rho}}$
w	Radial velocity
W	Work, J
x	Chordwise location when presented in non-dimensional form (x/C); otherwise axial co-ordinate, m
y	Tangential co-ordinate, m
Y	Coefficient of total pressure loss, $\quad Y = \dfrac{\overline{P_{01}} - P_0}{(\overline{P_{01}} - \overline{P_2})}$
$\overline{Y}$	Pitch averaged total pressure loss coefficient, $\quad \overline{Y} = \dfrac{\int_s Yu\,dy}{\int_s u\,dy}$
z	Radial or spanwise co-ordinate, m
α	Inlet flow angle relative to axial direction, defined in figure 3.2, degrees
α'	Blade inlet angle relative to axial direction, defined in figure 3.2, degrees
$\overline{\alpha}$	Pitch-averaged exit flow angle, $\quad \overline{\alpha} = Tan^{-1}\left[\dfrac{s\int_s vu\,dy}{(\int_s u\,dy)^2}\right]$
β	Exit flow angle relative to axial direction, defined in figure 3.2, degrees
β'	Blade exit angle relative to axial direction, defined in figure 3.2, degrees
ϕ_n	Phase angle of the nth harmonic pressure response, degrees
μ	Dynamic viscosity, Pas
ρ	Density, kg/m^3
τ	Tip clearance or gap, m
ω	Angular velocity, rad/s
ξ_C	Local aerodynamic damping coefficient, $\quad \xi_C = \int_C \dfrac{-\pi B_L|Cp_1|Sin\phi_1}{CB_C}\,dA$
ξ	Coefficient of aerodynamic damping, $\quad \xi = \dfrac{1}{h}\int_h \xi_C\,dz$

Subscripts

0	Stagnation or total parameter
1	Inlet parameter; 1st harmonic
2	Outlet parameter; 2nd harmonic

Chapter One

Introduction

1.1 General Background

The study of aeroelasticity, as described by Collar (1947), is concerned with the interaction between aerodynamic, inertial and elastic forces, and the influence of these forces upon the behaviour of structures. Since aeroelastic events are generally undesirable, the emphasis of related work is often upon the development of understanding and accurate prediction tools in order to prevent instabilities from arising. Such work spans many engineering disciplines. Mechanical structures may suffer excitation from wind on land and waves at sea, and in aeronautics the problem is well documented for lifting and control surfaces. Here, however, we are concerned with problems encountered through the unsteady aerodynamic and aeroelastic behaviour of axial-flow turbomachines.

The growth of interest in unsteady aerodynamic and aeroelastic instabilities in turbomachines has been motivated by the fact that they have become limiting factors both in terms of performance and engine life-cycle. This situation has arisen through the drive to increase performance and reduce machine weight, especially for aeronautic applications where engine size and weight is of paramount importance. Current trends in design, towards higher aspect ratios and lighter blades accompanied by increases in aerodynamic loading, provide conditions which are conducive to aeroelastic instabilities. And the ensuing incidents of blade failure, high-cycle fatigue and conservative operational margins still represent significant problems for the turbomachine industry. Although the majority of problems have been confined to compressor stages in aircraft engines, the design of turbomachines utilised for power generation has developed to provide challenges in this field. The final stages of low pressure steam turbines, also typified by high aspect ratios and high aerodynamic loading, being particularly susceptible.

There are two basic types of aeroelastic instability in turbomachines: those of a self-excited nature, and those which are forced by unsteady aerodynamic flow phenomenon. In the former case, unsteady aerodynamic forces are induced by low amplitude vibration of blades at or near their natural modes, the original vibration arising through either aerodynamic or mechanical disturbances. When the unsteady aerodynamic forces couple with the blade vibration with a phase relation that leads the blade motion, work is done to the blading and an instability, termed *blade flutter*, occurs. Conversely, in the later case blade vibration is excited by independent unsteady aerodynamic forces. These unsteady aerodynamic forces are usually inherent features of normal machine operation and consequently this type of instability, named *forced response*, characteristically occurs at machine engine orders.
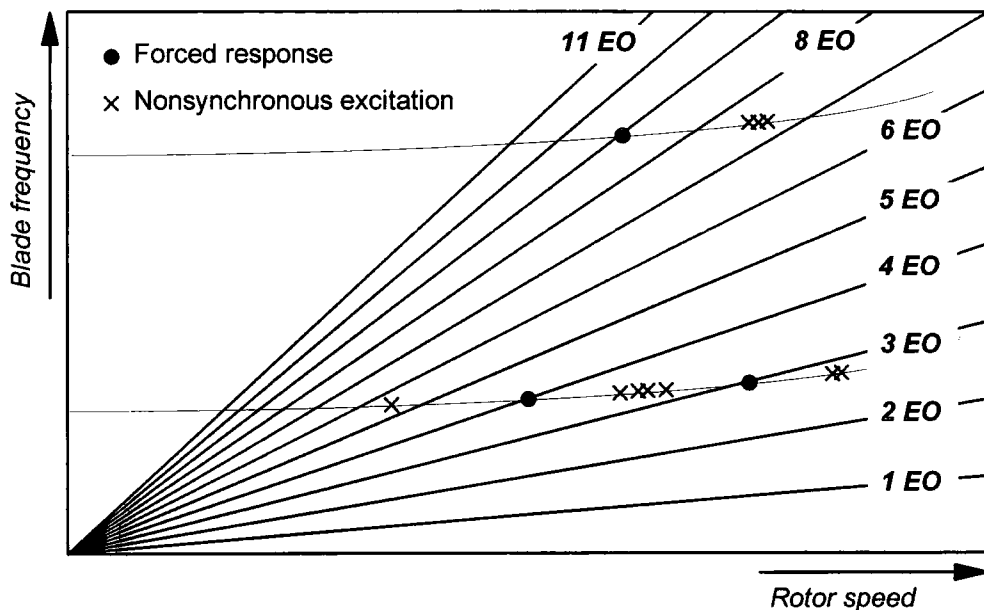
Figure 1.1: Diagnosis of aeroelastic instability with a Campbell diagram

A Campbell diagram, an example of which is shown in figure 1.1, is a useful tool for the diagnosis, and in cases the prevention, of aeroelastic instabilities. In this diagram, natural blade-disc mode frequencies and engine order (EO) lines are plotted against rotor speed. At rotor speeds where blade natural frequencies and machine engine orders coincide, the potential for forced response exists. Therefore blade vibration problems which occur at these synchronous speeds are usually diagnosed as forced response, whilst instabilities which occur at non-synchronous speeds are deemed to be self-excited. In design procedures, a Campbell diagram can be utilised to reduce the risk of forced response

instabilities. When the potential for instability is identified, measures can be taken to avoid exciting aerodynamic frequencies or shift the natural frequency of blade vibration to prevent synchronous speeds being encountered during normal operation. In cases where this is not possible, mechanical damping may be increased or operational procedures established in order to avoid or quickly pass through resonant engine speeds identified in a Campbell diagram.

Given the information available from a Campbell diagram and the measures described, it would appear that the prevention of forced response is a simple process. Unfortunately, the practical situation is far more complex. Modern turbomachines are plagued by a variety of natural blade-disc frequencies and numerous unsteady exciting aerodynamic frequencies, as observed by Srinivassen (1996). In addition, aircraft engines must be able to perform over a range of speeds, and transient procedures such as start up and shut down mean that resonant speeds cannot always be avoided. In the case of self-excited instability the situation is, if anything, worse. The nature of blade flutter is such that it may occur at any engine speed and at a variety of aerodynamic duties, as will be discussed later. Current design procedures provide little information regarding the likelihood of this instability and preventative measures still tend to be of a passive nature, normally at the expense of aerodynamic performance. Consequently, the issues of forced response and blade flutter remain a focus of current research and will become more pressing in the future as performance margins are consistently pushed.

1.1.1 Forced Response

Research directed at forced response in turbomachinery has largely concentrated upon the quantification of unsteady blade loading generated by the independent unsteady aerodynamic flow phenomena which are responsible for this instability.

Rotor-stator interaction has attracted significant attention as a common cause of this instability, for example Fleeter *et al* (1978) and Manwaring & Wisler (1993). Here, the unsteady aerodynamic disturbance arises due to the fact that adjacent blade rows in a turbomachine move relative to one another. The wakes shed by one blade row are experienced as a periodic disturbance by the downstream relative moving blades. Similarly, the potential flow fields and shock structures locked to the leading and trailing edge regions manifest as periodic unsteadiness, although in this case there maybe significant influence on the upstream relative moving blades as well as the downstream.

3

Circumferential non-uniformities in flow properties, generated by structural features of the inlet geometry or combustion nacelles, may also motivate forced response instability. In the case of combustion nacelles, appreciable distortions in temperature are involved and the unsteady thermodynamic as well as aerodynamic loading of rotor blades requires attention. The unsteady loading induced by this type of unsteady disturbance is particularly difficult to both predict and investigate, because susceptible blading may be located several stages downstream of the source of unsteadiness. In many cases, the most suitable vehicle for experimental investigations and the evaluation of prediction methods is an instrumented machine, e.g. Manwaring *et al* (1997) and Manwaring & Kirkeng (1997).

1.1.2 Self-Excited Instability (blade flutter)

This work is specifically concerned with the self-excited instability of blade flutter. Research into this aeroelastic phenomenon has developed in its own right to form a distinct field of study, quite separate from its counterpart in aeronautical engineering (wing flutter). This is because of the unique aerodynamic and mechanical environment offered by axial-flow turbomachines. There are several important features here. The first, and probably most important distinguishing feature is the aerodynamic and mechanical multiplicity of axial-flow turbomachines. Adjacent blades in turbomachines are strongly coupled aerodynamically and for the most part, mechanically too. The mechanical coupling being provided by contacting surfaces at tip shrouds, part span ties or snubbers, and of course blade supports at the root/hub. The consequence of both these types of coupling is that the natural modes of blade vibration are dependant upon the structural behaviour of the whole bladed-disc assembly, which is subject to a circumferential periodic boundary condition. These conditions usually manifest in a characteristic behaviour whereby adjacent blades in cascade vibrate at a constant relative phase angle during flutter. This interblade phase angle (σ), is an important defining parameter for blade flutter and has possible values, Lane (1956):

$$\sigma = \frac{2\pi n}{N_b} \qquad \textit{where } n = 1,2,3,....,N_b \text{ and } N_b \text{ is the number of blades} \qquad (1.1)$$

The relative stiffness of turbomachinery blades, in comparison to the inertia of the working fluid, also differentiates the problem encountered in turbomachines from its aeronautical equivalent. Blades are relatively stiff compared to aircraft wings and the

influence of the unsteady aerodynamics upon the mode of blade vibration is much less severe. Indeed, the influence of the unsteady aerodynamics upon the mode of blade vibration is most often reasonably assumed to be negligible during blade flutter. This assumption gives rise to a powerful approximate approach to the prediction of blade flutter known as the Energy method, described by Mikolajczak *et al* (1975). In this method, the aeroelastic stability of blades oscillating in a prescribed mode of vibration is determined solely by the aerodynamic work input. If the work done to the blading by the induced unsteady aerodynamics exceeds the mechanical damping of the system then the instability, blade flutter, will occur. Application of the Energy method thus breaks the problem of flutter prediction into two separate constituents: the prescription of natural modes of bladed-disc vibration, and the prediction of unsteady aerodynamic forces induced by blade vibration. It must, however, be acknowledged that the premise of this elementary approach does not universally hold and serious effort has also been directed at developing coupled structural and aerodynamic methods for blade flutter prediction, see for example Marshall (1996).
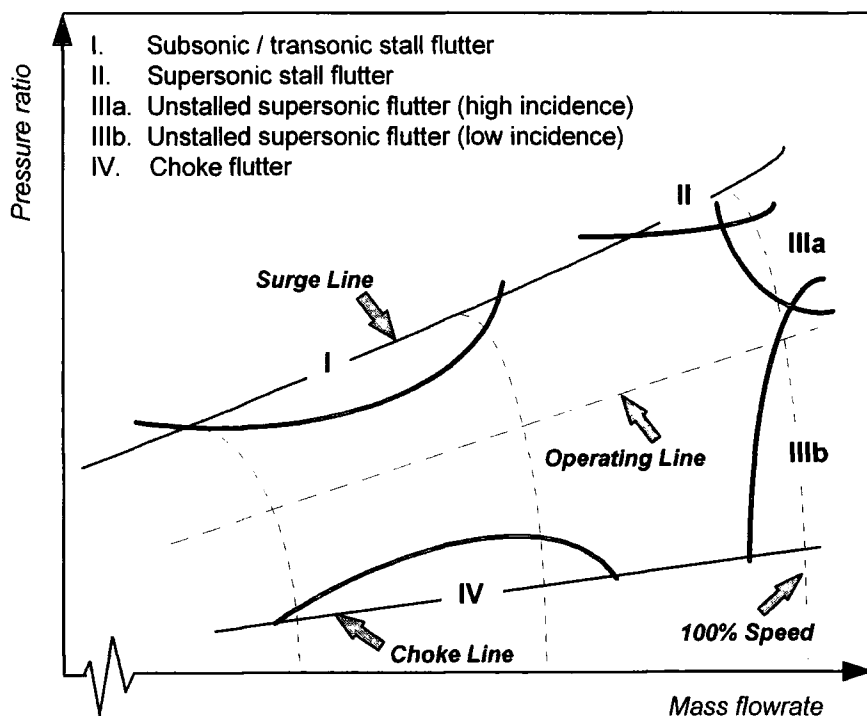
Figure 1.2: Blade flutter boundaries on a compressor characteristic

The numerous incidents of blade flutter in axial-flow compressors has led to the formulation of generic stability margins, shown in figure 1.2 (taken from Sisto 1987a),

and sub-classification of this instability. The classification has been made according to the aerodynamic mode of operation associated with each type of flutter. Under high pressure ratios, where blading is subject to high incidence, there is a risk of the so-called subsonic or transonic stall flutter (region I) at low and intermediate rotor speeds, and supersonic stall flutter (region II) at high speeds. In these types of flutter, the occurrence of massive separation over the suction surface is thought likely to be a strong destabilising aerodynamic influence, as indicated by their names. During high speed operation, compressors may also experience supersonic unstalled flutter at high incidence (intermediate pressure ratios) and low incidence (low pressure ratios), as represented by region III on the compressor map. For this type of flutter, as well as the supersonic and transonic cases of stall flutter, the unsteady behaviour of shockwaves is believed to be an important feature. This is because of the large unsteady aerodynamic forces generated by shockwave motion and unsteady shock-boundary layer interaction, which in some cases may precipitate separation. It is notable that the unstalled supersonic flutter at low incidence cuts the operating line at high speeds and incidents of this instability may influence operation at or near the design point. The final type of flutter to be dealt with here is choke flutter, this occurs near the choke line and consequently receives relatively little attention. In this type of flutter the unsteady shock behaviour is again expected to be important, although for incidents where choke flutter occurs at low incidence the potential for separation on the pressure surface is also believed to be influential in the onset of instability.

Although incidents of blade flutter are less common in axial-flow turbines, the last stage moving blades of these machines have also been identified to be susceptible, e.g. Scalzo (1986). The evolution of these blades - typified by increased loading, higher aspect ratios (and tip speeds) and reduced weight - is the cause of increasing concern and the prevalence of this type of instability is set to rise if increasing performance demands are to be satisfied. This situation has been reflected by a recent growth of interest in flutter research and development within the turbine community. Generic flutter boundaries have not yet, however, been empirically or otherwise established for axial-flow turbines.

The identification of relevant aerodynamic conditions, provided by the classification of flutter in axial-flow compressors and observations in turbines, has been important in directing efforts in this field of research. There is still, however, much to be learnt about the underlying physical mechanisms involved and the accurate prediction of stability margins still alludes state-of-the-art computational methods. Subsequently, there remains a strong dependence on passive techniques to prevent the instability. Tip shrouds and part-

span snubbers, which were preceded by part-span ties, are the most common measures taken. These act at a structural level to increase mechanical damping, stiffen blades and alter natural modes of vibration. Although often effective, these measures are not without their drawbacks. Contacting surfaces on which these methods rely are subject to degradation through rubbing, and the additional mass provided by these features significantly increases the centrifugal force experienced. Furthermore, the intrusive nature of part-span structures inherently impedes aerodynamic performance.

1.2   Unsteady Flow around Oscillating Turbomachinery Blades

Application of the energy method for the prediction of blade flutter has motivated considerable interest in the behaviour of flow around oscillating turbomachinery blades. The general purpose of related work being to enhance current understanding of these unsteady flows and develop accurate and efficient computational methods for their prediction. To clarify the crucial importance of understanding the physical mechanisms responsible for blade flutter, one must realise that this is not simply a matter of academic interest. Moreover, through highlighting the relevant issues, accumulated understanding can suitably direct the development of effective active/passive control techniques as well as the prediction tools which are so actively pursued.

In this section, some of the contemporary issues which occupy experimental and computational efforts in this particular field of research will be discussed, against the background of state-of-the-art techniques and recent advances.

1.2.1   Experimental Work

Experimental investigations into the unsteady flow around oscillating turbomachinery blades have been motivated by the need to improve understanding and provide test cases for the validation of computational prediction methods. In recent years, many of the relevant aerodynamic conditions and parameters have been addressed by some noteworthy experimental studies. The behaviour of flow around various compressor and turbine cascades, oscillating in plunging (2D bending) and torsional modes, has been examined at subsonic, transonic and supersonic speeds, see for example the standard configurations compiled by Bölcs & Fransson (1986). The influence of separation on the aeroelastic stability of oscillating blades has also been addressed under various conditions, for example Buffum *et al* (1998) and He (1998), and parametric studies have examined the

role of reduced frequency[†], incidence and inter-blade phase angle, e.g. Carta & St. Hilaire (1978 & 1980). Now whilst these contributions provide a quite thorough database, all published test cases in open literature remain strictly two dimensional, either through the nature of the experiment or the data collated. The flow within axial-flow turbomachines is however, inherently three dimensional as are the modes of blade vibration. It is therefore apparent, that a comprehensive appreciation of the three dimensional nature of blade flutter is essential for understanding and prediction at practical working conditions. Unfortunately, this is somewhat prohibited by the absence of detailed three dimensional experiments.

Although some measurements have been obtained from instrumented turbomachines, e.g. Barton & Halliwell (1987), the unsteady aerodynamic response of real turbomachinery blades oscillating in three dimensional modes has yet to be determined with sufficient resolution to provide coherent three dimensional test data. And the validity the quasi-3D assumption adopted by some prediction methods largely remains an unknown quantity. In reference to the three dimensional nature of blade flutter, there are two pressing issues which are addressed in the present work. The first pertains to the potential for three dimensional unsteady flow, even though the steady flow field may exhibit two dimensional or more realistically quasi-3D behaviour, due to the three dimensional mode of blade vibration. And the second concerns the behaviour of inherent three dimensional steady flow structures during blade vibration, since these will undoubtedly contrive to generate an unsteady flow that is anything but two dimensional or quasi-3D.

When considering the characteristics of blade types most susceptible to flutter, i.e. high aspect ratios, unshrouded tip sections and significant tip clearances, it becomes clear that the three dimensional flow in the tip endwall region could be influential in terms of the unsteady aerodynamic response to blade vibration. This is because the amplitude of vibration is greatest at the tip section of these blades, and the large unsteady aerodynamic forces induced in this region are likely to make a significant contribution to the overall aerodynamic damping, as demonstrated by Barton & Halliwell (1987). It remains unclear, however, how the dominant three dimensional flow structure in the tip endwall region, associated with the tip leakage vortex and passage secondary flow (shown in figure 1.3.), will influence the unsteady aerodynamic response and therefore the onset of instability.

[†] Reduced frequency, k, is one of the most important governing and descriptive parameters for unsteady aerodynamic phenomenon such as blade flutter. It describes the relative time-scales of convection and unsteady disturbance and is defined, $k = \omega C / V_{ref}$

Outer Casing

Secondary flow
passage vortex

Tip leakage
vortex

Pressure Surface

Suction Surface

Rotation
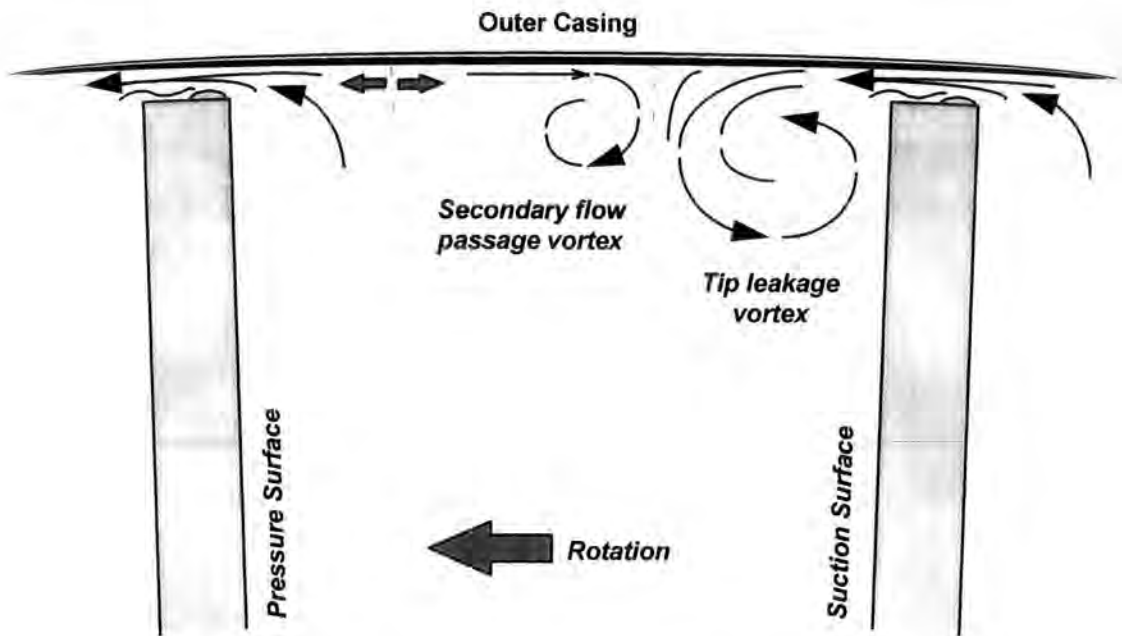
**Figure 1.3: Simplistic impression of secondary flow structures
towards the outer casing of an unshrouded turbine rotor**

There are two basic approaches adopted by experimental investigations. In so called 'free-flutter' experiments, which include those performed on real machines, blades are elastically mounted in order to asses their aeroelastic stability. In these experiments the emphasis is usually upon the identification of flutter stability margins and susceptible aerodynamic conditions, rather than detailed assessment of the unsteady flow. When applied to a linear cascade this method of approach does, however, experience some difficulty in obtaining a tuned aeroelastic system which exhibits the periodicity characteristic of flutter under practical circumstances. To some extent, this difficulty can be overcome by adopting the alternative approach with 'driven blades'. In experiments of this kind, blades in cascade are driven in a prescribed mode of vibration and the resulting unsteady flow investigated. Whilst this approach should provide a well defined phase-shifted periodic blade vibration, there remains some difficulty in maintaining a gapwise periodic unsteady flow in linear cascades, as demonstrated Buffum & Fleeter (1993).

The measurement of unsteady flow phenomena in experiments performed with driven blades presents further challenges. High temporal and spatial resolution of unsteady blade surface pressure distribution is both difficult and expensive to achieve in moderate to high

Mach number experiments, largely because of the high frequency of blade vibration required to match realistic reduced frequencies. In such experiments, expensive, high frequency response surface mounted pressure transducers have to be employed, the number of which is usually restricted for reasons of practicality and cost. At low speeds the situation is, however, somewhat relaxed by the lower blade frequencies involved, see for example Carta & St. Hilaire (1978). And for very low speed applications, He & Denton (1991) demonstrated that outboard pressure transducers can be utilised without appreciable loss in temporal accuracy of unsteady pressure measurement. This approach significantly reduces the expense incurred and allows detailed measurement of blade surface unsteady pressure response with a limited number of transducers

1.2.2 Computational Methods

At present there are two widely accepted approaches to the computational prediction of unsteady flows around oscillating turbomachinery blades. These being time-linearised methods, e.g. Verdon & Casper (1982), Hall *et al* (1994) and Marshall & Giles (1997), and nonlinear time-marching methods, e.g. Gerolymos (1993) and He & Denton (1994).

Time-linearised methods, which will be discussed in more detail in chapter 2, are based upon the assumption that the unsteady flow is composed of a small harmonic perturbation to the steady flow state. This allows the governing equations to be linearised and the unsteady flow to be calculated in the frequency domain. Whilst being computationally efficient, these methods are limited by the linear assumption and in cases where strong non-linear effects exist the validity of these methods breaks down. In reference to this, areas of particular concern are the unsteady behaviour of transonic flows, where shock wave motion and shock boundary layer interaction are important, and unsteady viscous flows, where the response of separated regions maybe influential, viz. stall flutter.

Non-linear effects can be included by adopting an unsteady time-marching method. In this approach, the unsteady non-linear governing equations are formulated and discretised in time-accurate form, and solved by marching the equations in time from an initial value condition to a converged periodic state. Despite efforts to enhance the computational efficiency of these methods, for example the two-grid temporal acceleration proposed by He (1993), they remain extremely computationally expensive compared to their time-linearised counterpart. Furthermore, for blade flutter prediction there is an added

complexity of applying the periodic boundary condition associated with blade vibration at non zero values of interblade phase angle. For solution in a single-blade-passage domain this involves the implementation of a sophisticated phase shifted periodic boundary condition, which will be discussed in Chapter 2.

Although, both of the approaches described have been developed into fully three dimensional inviscid and viscous methods for the prediction of unsteady flow around oscillating blades, the absence of challenging 3D test cases prevents any realistic validation. Not only does this affect the confidence with which these methods can be applied, but moreover it restricts their development, because areas of deficiency cannot be readily identified.

1.3 Overview of Present Work

The present work is motivated by the urgent need for detailed assessment of the three dimensional nature of unsteady flows around oscillating turbomachinery blades. In this experimental and computational study, the unsteady flow around a turbine blade oscillating in a three dimensional bending mode is investigated at depth. The primary objectives being to improve current understanding, provide three dimensional test cases for the validation of computational prediction methods and examine the ability of a 3D time-marching Euler method to capture the relevant unsteady aerodynamics. The research project, documented herein, is broken into four parts.

A low speed experimental test facility has been commissioned specifically for the purposes of this investigation. At the working section of the test facility a single prismatic turbine blade is mounted in a profiled duct and driven at a harmonic rate in a three dimensional bending mode. The unique configuration offered by this facility allows the three dimensional unsteady flow around the blade to be investigated in a clearly defined aerodynamic environment. And the use of outboard mounted pressure transducers, which is permitted by the low speed and scale of the facility, enables detailed measurement of the unsteady blade surface pressure response without prohibitive cost.

In the first part of the work, Chapters 3 and 4, the test facility is described and discussed in detail with special emphasis placed upon the philosophy behind the design. The experimental procedure is also specified and the validity of the technique adopted for unsteady pressure measurement is examined. An evaluation of experimental error and

repeatability, which concludes this section, provides some further justification of the approach adopted.

In Chapter 5, a complete set of steady flow and unsteady pressure measurements generated by the test facility are presented and discussed. In this part of the investigation, the unsteady pressure response of the whole blade surface, to vibration in a three dimensional mode, is examined over a range of reduced frequency and the three dimensional nature of the unsteady aerodynamics assessed. The steady flow blade surface pressure distribution and the results of five-hole probe traverses at inlet and exit provide the aerodynamic background for the unsteady experiments and demonstrate a predominant two dimensional steady flow within the working section. Whilst the unsteady blade surface pressure measurements, which are provided for five spanwise sections between 10% and 90% span, clearly show a three dimensional behaviour of the unsteady aerodynamics. An assessment of linearity, which is also included, demonstrates a linear aerodynamic response to the blade vibration. The present results provide detailed three dimensional test cases with clearly defined boundary conditions, which maybe utilised towards the validation of advanced computational methods and represent the first of their kind.

The third part of this work, presented in chapter 6, deals with the computational phase of the investigation. The principal objective here is to evaluate the ability of an extended three dimensional time-marching Euler method to capture the relevant unsteady aerodynamics exhibited by the experimental test data. The computational results and accompanying discussion are also intended, however, to provided further insight into the behaviour of the unsteady flow. The first part of chapter 6 describes the basic computational method and the special modifications required for simulation of the experimental test configuration. Following this, a series of steady and unsteady flow solutions are presented and discussed. Throughout the range of reduced frequency, very good agreement is demonstrated between the computational solutions and the experimental test data, although some discrepancies are observed in regions where the viscous behaviour of the unsteady aerodynamics is believed to be influential. Additional solutions, obtained from a quasi-3D version of the computation method, are also included. These highlight the three dimensional nature of the measured unsteady pressure response and demonstrate the limitations of the quasi-3D approach.

The fourth part of this study (Chapter 7) is concerned with the influence of tip leakage upon the unsteady aerodynamic response of oscillating turbomachinery blades. This has

practical implications for the aeroelastic stability of high aspect ratio blades with unshrouded tip sections, due to the large clearances that exist and because the contribution towards aerodynamic damping is likely to be significant from the tip region. In order to make a preliminary assessment of the importance and extent of the potential influence, a series of steady flow and unsteady blade surface pressure measurements are compared for the oscillating turbine blade over a range of tip clearance. The steady flow measurements, which again provide the aerodynamic background for the unsteady tests, show characteristic behaviour of the tip leakage flow with increases in clearance and demonstrate that, despite the unusual configuration, the test facility provides a suitable vehicle for the type of investigation undertaken. The detailed unsteady pressure measurements - obtained from pressure tappings located between 10% and 90% span - show the unsteady aerodynamic response of the oscillating turbine blade to be largely unaffected by the change in tip clearance, although subtle, but consistent, trends are evident in the unsteady pressure response recorded at the 90% span location. To the authors knowledge, this is the first work to address the influence of three dimensional endwall flow structures upon the local unsteady aerodynamic response of oscillating turbomachinery blades.

The investigation is brought to conclusion in chapter 8, where some recommendations for future work are also proposed.

Chapter Two

Review of Previous Work

A detailed historical perspective of developments in the understanding and prediction of blade flutter is beyond the scope of the present work. To this end, the reader is directed to the excellent reviews made by Fleeter & Jay (1987), Sisto (1987), Srinivassen (1997) and Verdon (1993). Rather, the objective of this chapter is to discuss advances particularly relevant to this work, in order to further emphasise the present motivation.

2.1 Background

Almost throughout the entire development of axial-flow compressors blade flutter has been a recognised cause of concern, with the first incident being reported by Shannon as far back as 1945, see Shannon (1945). Early attempts to predict and suppress this instability, that followed this pioneering work, relied upon empirical design correlations which had their genesis in the previous experience of wing flutter. These correlations were based upon the data generated by experimental performance testing at that time and related critical values of reduced frequency to certain operational conditions, typically incidence angle and relative Mach number (Mikolajczak, 1976). During the intervening years an extensive test data base has been accrued by turbomachine manufacturers, and this empirical approach to the prediction of flutter has subsequently developed in sophistication. Modern correlations incorporate an increasing number of aerodynamic and structural parameters that define the critical conditions for the onset of instability. Although these correlations may often prove successful, because of the strong historical influence upon the evolution of blading within the turbomachine industry, they are strictly limited to the envelope of empiricism and cannot be confidently applied to original or new designs that transcend previous experience. Motivated by this fundamental limitation

and made feasible by the rapid development of computational technology, an alternative approach to the prediction of blade flutter has been sought with increasing vigour during the past three decades. Here, we refer to the development of computational fluid dynamic (CFD) methods for the prediction of flow around oscillating turbomachinery blades. This theoretical approach does not suffer the inflexibility of the empirical correlations and can equally be applied to the problems more recently encountered in axial-flow turbines, for which relatively limited data is available.

It must be acknowledged, however, that the successful exploitation of both the empirical and CFD approach to the prediction of blade flutter has been, and will continue, to be dependant upon the quality of experimental data. Whilst this is obvious for the empirical approach, to illustrate this point for CFD one must realise that it is not an exact science. At present, all computational fluid dynamic methods incorporate some level of approximation or an assumption regarding the behaviour of flow. A rigorous validation procedure, involving comparison with experimental test data, is therefore required to determine the accuracy, limitations and robustness of these methods.

2.2 Experimental Research

Whilst all experimental work directed at blade flutter shares a common objective to enhance understanding of the basic physical mechanisms, the specific role of experimental research has changed somewhat with the shift in focus from empirical correlations to computational fluid dynamic methods for prediction purposes. Experimental work conducted during the late 1940's and throughout the 1950's, much of which was confined to industry, concentrated upon the identification of flutter stability margins and the acquisition of data which was specifically required in order to formulate the early correlations. More recently, however, the emphasis of experimental work has gradually moved towards the provision of validation test data for computational fluid dynamic methods, although it should be recognised that parametric studies remain both a useful and integral part of experimental research. Despite this change in motivation and objectives, the fundamental challenge for experimental work has remained the same: that of the acquisition of useful and accurate data.

Three basic types of experimental facility have been employed to investigate unsteady flow around oscillating turbomachinery blades, and this forms the basis of the following discussion of previous work. The objective being to highlight the worth, relative merits

and problems associated with each type of facility as well as illustrate the contributions made by various authors.

2.2.1 High Speed Rotating Facilities

Full-scale turbomachines and rotating test facilities, instrumented for experimental measurements, provide the most realistic vehicle for the investigation of blade flutter, because they allow all relevant aerodynamic and mechanical conditions to be reproduced. At present, they are also the only device through which flutter stability margins can be determined with any level of confidence and therefore contribute some of the most meaningful data for empirical correlations. Furthermore, the test configurations provided by this type of experimental work represent the ultimate benchmark for the examination and validation of computational prediction methods.

Unfortunately, high speed rotating facilities are extremely expensive and the acquisition of detailed and accurate data represents a significant challenge. All data obtained from these facilities must be transferred from a rotating to a fixed frame of reference and unsteady flow measurements must be referenced to the vibratory motion of the blading for meaningful analysis. The extreme environment offered by these facilities also places high demands upon the miniature, high frequency response instrumentation required for this type of work. Considerable effort is required to both minimise and compensate for the sensitivity of these instruments to variations in temperature, and effects introduced by installation and acceleration[†], e.g. Manwaring & Wisler (1993) and Manwaring *et al* (1997). The durability of blade surface mounted instruments presents additional problems, as demonstrated by Manwaring *et al* (1997) whom experienced transducer signal failure during testing of a low-aspect ratio transonic fan, most probably due to severe centrifugal forces. Despite these difficulties, however, some useful data and important findings have resulted from this type of experimental work.

In order to determine the onset of instability, facilitate the analysis of unsteady flow measurements and enhance basic understanding, various efforts have been directed at the

---

[†] The acceleration associated with the rotation and vibration of blading can lead to false measurements from surface mounted pressure transducers. In a similar manner, the transmission of blade strain to these sensitive instruments, which can arise through inappropriate installation, may also result in erroneous measurements.

measurement of blade stress levels and mode shapes during blade flutter. Stargadter (1977) obtained some optical measurements of fan blade deflections during stall flutter, using a laser light source and small mirrors located at various radial heights on several blade surfaces. The results enabled the magnitude of blade vibration both in bending and torsion to be determined and qualitatively demonstrated the entrainment of frequencies, although neither an interblade phase angle or nodal diameter pattern was resolved by the measurements. Qualitative evidence for resonant vibration at constant interblade phase angle was, however, provided by the nodal diameter patterns recorded in holographic images presented by Mikolajczak *et al* (1975) for a stationary rotor and by Barton & Halliwell (1987) for a scale model rotor. In the former work (Mikolajczak *et al*, 1975), it was also reported that time-averaged flow measurements from a fan experiencing stall flutter had revealed that aerodynamic losses did not appreciably increase when the instability was encountered. This, combined with reported incidents near peak compressor efficiency, suggested that separation may not actually be a prerequisite of so called stall flutter, as originally presumed.

High speed rotating facilities have also been utilised for the measurement of unsteady flow around fluttering turbomachinery blades. Barton & Halliwell (1987) presented unsteady blade surface pressure measurements for a transonic fan during unstalled supersonic flutter. In this work, a slip ring was employed to transfer data from the rotating frame, and referencing to the blade vibration was made via measurements from surface mounted strain gauges and a further device which monitored the motion of the tip section by means of an electromagnetic arrangement. The unique contribution of this work was the clear resolution of unsteady blade surface pressure associated with an oscillating passage shockwave, captured by purpose built, strip pressure transducers. This contrasts the relatively poor spatial resolution typically provided by similar work, which results from the geometric and economic constraints upon instrumentation imposed by this type of test facility. The high unsteady pressure and abrupt phase change recorded by the strip transducers clearly demonstrated the influence of the unsteady shockwave upon the stability of the fan, and comparison of measurements from several blades confirmed blade vibration at a constant interblade phase angle. Unfortunately, the measurements were restricted to two spanwise sections at 71% and 93% of blade height. Consequently, the full three dimensional extent of the unsteady aerodynamic response to the blade vibration could not be directly established, although the fair agreement with FINSUP (2D potential flow solver developed by Whitehead, 1982), did suggest a predominantly two dimensional behaviour of the supersonic unsteady flow in the outer span region.

17

Scale model rotors can be utilised to relieve the most prohibitive aspect of this type of work, namely the expense incurred. These facilities, as previously described, have been successfully exploited to investigate the dynamics of blade-disk assemblies, e.g. Barton & Halliwell (1987), and have also demonstrated some ability in the provision of useful flutter boundary data for full size machines, on a qualitative level at least (Fleeter & Jay, 1987). They also serve an important function as a preparatory test device, although the restrictions upon instrumentation, imposed by the reduced scale, make them an unsuitable candidate for detailed investigation of unsteady flow behaviour.

In the closure of this section, a final point of caution must be raised regarding experimental work performed in high speed rotating facilities: Due to its commercially sensitive nature, the number of publications and technology reported is unlikely to be a true reflection of past or present investment, or state-of-the-art.

2.2.2 Annular Cascades

For aeroelastic applications, stationary annular cascades are typically employed to model the behaviour of an existing blade row at a specific radial height. Therefore, despite the inherent three dimensional nature of these facilities, they are usually intended to provide a two dimensional aerodynamic and mechanical environment and normally utilise prismatic turbomachinery blades, see for example the fourth standard configuration (Bölcs & Fransson, 1986).

These facilities share many of the qualities exhibited by high speed rotating facilities, the most important of which is the infinite multiplicity, but offer some additional benefits too. The reduced investment required both in time and money makes them an attractive alternative to rotating facilities and a viable option for experimental research within academia, where relatively modest funds are available. The absence of centrifugal forces also reduces the demands upon instrumentation and the stationary frame of reference eases the process of data acquisition. There are, however, some disadvantages associated with this type of experimental facility, some of which will become more apparent in following discussion of linear cascades. The reduced scale frequently adopted in the design of these facilities makes it difficult to simultaneously match all relevant parameters for complete physical similarity, restricts accessibility and prevents detailed instrumentation. Uniform inlet flow conditions are also difficult to realise in annular cascades and reasonably complex inlet geometries are required, for example Körbächer &

Bölcs (1994). Moreover, when conducting 'two dimensional' experiments in annular cascades it is important to be aware of the three dimensional flow effects associated with a significant change in radius and those generated by the flow in the endwall regions.

The flexibility of annular cascades lends itself to both free flutter testing and experiments performed with driven blades, see for example Jutras *et al* (1980) and Kobayashi *et al* (1995) respectively. Jutras *et al* (1980) conducted a parametric free flutter test program to investigate flutter in mid-stage compressor designs, using a tuned, 'two dimensional' annular cascade which simulated conditions at 87.5% span in an existing compressor rotor. Considerable effort was taken in this work to maintain two dimensionality in terms of key aerodynamic properties over the outer half span of the cascade, whilst the inner half span was manipulated to tune the blading without serious prejudice to the cascade aerodynamics. The annular cascade successfully reproduced the aeroelastic behaviour of the rotor, suffering both negative incidence choke flutter and positive incidence stall flutter, and the flutter boundaries, parametrically defined by relative Mach number and incidence angle, recorded in the annular cascade were in good agreement with measurements from the rotor. Kobayashi *et al* (1995) investigated shock wave behaviour in an annular cascade of 16 compressor blades, mechanically driven in a torsional mode of vibration at an interblade phase angle of -67.5°. The unsteady behaviour of the shock wave was examined through images provided by a complex CCD-Schlieren imaging system and unsteady pressure measurements from an embedded pressure transducer located at the steady flow shock position on the suction surface. The blade motion, monitored by an eddy-current-type displacement sensor, provided a reference for these measurements. The results showed the unsteady force associated with the shock wave, relative to the blade motion, to shift from an unstable phase lead to a stable phase lag condition as the reduced frequency increased. Spectral analysis of the shock wave movement and unsteady pressure measurements revealed significant 2nd and 3rd order harmonic components which are indicative of nonlinear behaviour.

Körbächer & Bölcs also performed a series of experimental tests in an annular cascade with driven blades. The test cascade utilised in this case consisted of 20 elastically mounted NACA-3506 blades, each fitted with a high speed electromagnetic exciter to control the frequency, amplitude and interblade phase angle of vibration. The results featured steady flow and unsteady pressure measurements, obtained from several blades instrumented with surface mounted pressure transducers, at off design conditions (positive incidence and high Mach number). In the first part of their work (Körbächer & Bölcs, 1994), the repeatability and circumferential periodicity of measurements was scrutinised

and the validity of the linear superposition principle examined. The steady and unsteady pressure measurements demonstrated excellent repeatability (within 95% confidence intervals), but relatively poor circumferential periodicity, which was attributed to the location of probe holders upstream of the blade row. The linear superposition principle was also demonstrated to be inappropriate for the high incidence and high Mach number conditions tested, i.e. the unsteady pressure measurements exhibited nonlinear behaviour. In their subsequent work (Körbächer & Bölcs, 1996), steady and unsteady pressure distributions were analysed over a range of positive incidence angles. The steady flow measurements and flow visualisation revealed an undesirable three dimensional corner stall at the hub endwall, which was observed to grow as the incidence increased. It was also noted that the high amplitude unsteady pressure measurements corresponded with a short supersonic zone near the leading edge, which featured high steady flow pressure gradients. Somewhat surprisingly, however, and in contrast to their previous work, the influence coefficient technique, which is based upon the principle of linear superposition, was established to be valid for all of the cases investigated. This method was subsequently used to determine the influence of neighbouring blades upon the aeroelastic stability of an arbitrary blade. In this annular cascade it was found that the behaviour of a blade itself and its direct neighbours were responsible for the generation of unsteady pressure.

2.2.3 Linear Cascades

The linear cascade is the most cost effective and common type of test facility encountered in experimental research into the behaviour of flow around oscillating turbomachinery blades. Apart from the financial benefits, the relative simplicity offered by these facilities makes them a highly attractive alternative to the high speed rotating facilities and annular cascades previously described. The large scale typically employed in linear cascade experiments, combined with their two dimensional geometry, enables straightforward implementation of detailed instrumentation and provides favourable conditions for flow visualisation. This type of test facility therefore provides an excellent platform for obtaining high resolution measurements of steady and unsteady flow phenomenon and related work has contributed some of the most thorough test data required to enhance understanding and facilitate the validation of computational methods. The additional flexibility provided by linear cascades, in terms of the control over a wide range of aerodynamic parameters, also enables parametric studies to be conducted and voluminous data to be generated with comparative ease.

The application of linear cascade experiments to model the fundamental behaviour of turbomachinery flows during blade flutter is, however, inhibited by their finite nature. In free flutter experiments serious problems are encountered in recreating a tuned aeroelastic system which characterises the phenomenon of blade flutter, as demonstrated by Snyder & Commerford (1974). In their work, a linear cascade of five elastically mounted compressor blades was utilised to parametrically investigate the inception of unstalled supersonic flutter. The results of strain gauge measurements revealed that the individual blades in this cascade vibrated at different amplitudes and at different values of interblade phase angle, although a constant frequency was enforced by tuning the blades' natural frequency. This poor periodicity was, quite correctly, attributed to the fact that the blades in a linear cascade are not aerodynamically coupled in the same manner as those in an infinite cascade. During blade vibration, the end blades in a linear cascade experience a localised and markedly different aerodynamic environment to blades mounted in an infinite cascade, and indeed to those more centrally located in the linear cascade, due to the proximity of the windtunnel sidewalls. A localised unsteady pressure field is therefore established around the end blades, which subsequently exerts an undesirable, although diminished, influence upon the adjacent blades in cascade and so on. In free flutter experiments this situation is further exacerbated. The end blades will inevitably vibrate at a different amplitude and most probably phase to the central blades, thereby exaggerating the localised unsteady flow field generated at the extremities of the cascade. In a discussion of this problem Snyder & Commerford proposed that ".... the *effective finiteness* of the cascade could be greatly reduced if the cascade blades were forced to vibrate at the same (but adjustable) frequency, amplitude and interblade phase angle." Although this measure relieves the problem, some of the following citations demonstrate that difficulties persist in obtaining a phase shifted periodic unsteady flow in linear cascade experiments performed with driven blades, due to the presence of windtunnel sidewalls.

Following the contribution of Snyder & Commerford (1974), linear cascades have most frequently been utilised in experiments performed with driven blades, for example Buffum & Fleeter (1993), Buffum *et al* (1998), Carta & St. Hilaire (1978, 1980), Carta (1983), Hanamura *et al* (1980), Hanamura & Yamaguchi (1995), He (1998a), Fleeter *et al* (1977), Rothrock *et al* (1982) and Shibata & Kaji (1995). Carta & St. Hilaire performed a series of parametric experiments to investigate the unsteady aerodynamics of an oscillating loaded cascade of eleven NACA-65 compressor blades at subsonic conditions near stall. The cascade was placed in the exhaust of a low speed wind tunnel and during

testing all eleven blades were mechanically driven in pitching mode at a prescribed frequency, amplitude and interblade phase angle. The central blade was instrumented for unsteady pressure measurements which were integrated over the blade surface in reference to the blade motion to yield the work done and thereby establish the aeroelastic stability of the cascade. In the first series of tests (Carta & St. Hilaire, 1978) the influence of reduced frequency, interblade phase angle and incidence angle upon pitching stability was examined. For all cases investigated it was observed that the unsteady pressure activity was largely confined to the leading edge region where the highest gradients in the steady state pressure distribution were found. Within the range of parameters tested, the results also demonstrated the interblade phase angle to have the greatest influence upon the stability of the cascade. Indeed, for all tests performed at an interblade phase angle of 0° the cascade was stable, whilst at 45° the cascade was unstable. A secondary finding of this work revealed instances of contrasting behaviour between the aerodynamics of oscillating aerofoils in cascade and in isolation. For the highly loaded aerofoil in cascade, the pressure wave propagated from the trailing edge upstream, whilst for a similarly loaded aerofoil in isolation the unsteady pressure response at the trailing edge lagged that further upstream, most probably due to the occurrence of dynamic stall. At high loading conditions it was also observed that the unsteady pressure response of the cascaded blades included a strong second harmonic component. The second series of tests (Carta & St. Hilaire, 1980) was largely a continuation of the first, extending the range of parameters tested, and the findings were consistent with the previous work. It was, however, additionally observed that unstable conditions were experienced without any evidence to support the existence of stall. This supported the previous reports made by Mikolajczak *et al* (1975) and led to the conclusion that separation is not a prerequisite of so called stall flutter which, incidentally, further illustrates the disparate fundamental behaviour of oscillating cascaded and isolated aerofoils.

Carta (1983) performed some complimentary tests to examine the gapwise periodicity of the unsteady flow in the oscillating linear cascade previously described. In addition to the fully instrumented central blade, for the purposes of this work five other blades were partially instrumented with surface mounted pressure transducers in order to evaluate the blade to blade periodicity of the unsteady flow. The steady and unsteady flow measurements generally demonstrated the cascade to satisfy the periodic condition, although at a high incidence condition some local discrepancies were observed in the amplitude of unsteady pressure response towards the leading edge which, it must be

added, coincided with the region of highest unsteady pressure activity. Buffum & Fleeter (1993) also examined the unsteady periodicity of flow around oscillating aerofoils, this time in a linear cascade of four biconvex aerofoils which were harmonically driven in a torsional mode of vibration. In their work, the periodic condition of flow was determined at various values of interblade phase angle and reduced frequency, through a comparison of steady and unsteady pressure measurements from the two central blades in cascade. It was observed that at certain values of interblade phase angle the cascade exhibited good periodicity whilst at other values the periodicity broke down. A linearised flat plate analysis was utilised to gain insight into the reasons for this behaviour. The calculations indicated that in the cases of poor periodicity, pressure waves generated by the oscillating aerofoils were reflected off the wind tunnel sidewalls back into the cascade, thereby influencing the unsteady aerodynamics. In subsequent experiments performed in this test facility (Buffum *et al*, 1998), a section of the wind tunnel sidewall and the tailboard were replaced with perforated plates (backed with kevlar fibre) in order to minimise acoustic reflections.

The problems experienced by Buffum & Fleeter, and to a lesser extent by Carta, in obtaining periodic unsteady flow have obvious implications for the reliability of their respective test facilities, but moreover, they clearly demonstrate the necessity for this type of work during the commission of oscillating linear cascade experiments.

The difficulty involved in generating a phase shifted periodic unsteady flow in oscillating linear cascades can be avoided by applying the linear influence coefficient technique, proposed by Hanamura *et al* (1980). In this approach a single reference blade in cascade is vibrated and the induced unsteady pressure response measured for all blades. The unsteady aerodynamic behaviour of a tuned cascade of blades, vibrating at an interblade phase angle, is then subsequently determined through the linear superposition of the unsteady pressure response recorded for each blade. Although this approach offers obvious benefits in terms of the required complexity of test facility and experimental procedure, it is strictly limited by the validity of the linear assumption and care must be taken to ensure that the unsteady phenomenon under scrutiny does not exhibit nonlinear behaviour. This technique has, however, been demonstrated to be adequately valid in an experiment performed with an oscillating turbine cascade, which exhibited a short bubble type separation on the suction surface and a large separation on the pressure surface, He (1998b). And the linear influence coefficient technique has also been applied at transonic flow conditions, Hanamura & Yamaguchi (1995).

The recent contributions of He (1998b) and Hanamura & Yamaguchi (1995) are the first references made in the present text to work directed at flutter problems encountered in axial flow turbines, and this illustrates the growing concern expressed by their manufacturers. Previously, the behaviour of flow around oscillating turbine blades was addressed by Rothrock *et al* (1982) in a transonic linear cascade of five blades, which were coherently driven in a torsional mode of vibration at six different values of interblade phase angle and four expansion ratios. Excellent qualitative agreement was observed between the measured unsteady and quasi-steady blade surface pressure distributions and the results indicated a strong coupling between the steady flow field and unsteady aerodynamics of this highly turned cascade. The detailed unsteady pressure measurements presented by He (1998a) demonstrated the influence of bubble type separation upon the unsteady aerodynamics of a turbine cascade oscillating in a torsional mode of vibration. In this work, a short suction surface bubble separation appeared to behave in a quasi-steady manner and have marked effects upon the local unsteady pressure response. An abrupt change in phase was recorded around the point of reattachment which, at the conditions investigated, exerted a stabilising influence. A larger leading edge separation bubble on the pressure surface did not, however, appear to behave in a quasi-steady manner. In the separated region the unsteady pressure contributed towards negative aerodynamic damping, which was largely balanced by the unsteady pressure downstream of the point of reattachment, due to a rapid increase in phase. This work also demonstrated the feasibility of using externally mounted pressure transducers in low speed oscillating cascade experiments. A recent contribution from Norryd & Bölcs (1997) investigated the influence of tip clearance on the unsteady aerodynamic loading at mid-span of an oscillating linear turbine cascade. Their results showed a significant variation in the amplitude of unsteady pressure for different settings of tip gap, although the aerodynamic damping was observed to be largely unaffected.

Whilst it is clear that progress has been made and a serious effort expended in the investigation of blade flutter under a variety of aerodynamic conditions, it is also apparent that the experimental test data in open literature remains strictly two dimensional. Both the linear and annular cascade experiments previously discussed were purposefully intended to generate a two dimensional unsteady flow, primarily in the interests of simplicity. And although three dimensional effects are inherently introduced in the experiments performed with high speed rotating test facilities, the resolution of measurements provided by these facilities is usually limited for reasons of practicality and

little indication is provided of the three dimensional nature of the unsteady flow. Detailed and reliable three dimensional test data is, however, required to enhance understanding of blade flutter under practical working conditions and essential to facilitate both the validation and future development of computational prediction methods.

2.3 Computational Methods

Two approaches have been actively pursued for the computational prediction of unsteady flow around oscillating turbomachinery blades. The first group of methods to be developed, and those most commonly encountered, are based upon the time-linearised assumption and operate in the frequency domain. More recently, the development of these methods has been accompanied by nonlinear time-marching solution procedures, which operate in the time domain and are by comparison expensive in terms of run-time.

2.3.1 Frequency Domain Solution Methods

Time-linearised methods are based upon the premise that the unsteady flow is composed of a small harmonic perturbation to the steady flow state. This assumption allows the time dependant variation of a primitive flow variable to be expressed,

$$\phi(x,t) = \phi_0(x) + \tilde{\phi}(x,t) \quad = \phi_0(x) + \phi_1(x)e^{i\omega t} \tag{2.1}$$

Application of this approach reveals that once the steady flow solution (ϕ_0) is obtained, then the linear equation for the unsteady terms (ϕ_1) can be solved, i.e. the unsteady perturbation is solved separately, although based upon the steady flow solution.

The early time-linearised methods assumed a uniform steady flow, which allowed the equation for the unsteady terms to be globally linearised. Whilst it should be recognised that the simplicity of these numerical models largely reflected the computational capabilities of their time, it must also be noted that they were seriously deficient due to an inability to deal with important effects introduced by blade geometry and flow turning. Local linearised methods were subsequently developed to address this problem. In these methods, a nonlinear solution is obtained for the steady flow, from which spatially varied coefficients are established for the unsteady perturbation equations. This technique therefore enables the effect of steady flow blade loading upon the unsteady flow to be included. Early examples of this method of approach were based upon linearised potential flow equations, e.g. LINFLO (Verdon & Casper, 1982) and FINSUP (Whitehead, 1982).

Later, Hall & Crawley (1989) applied the time-linearisation technique to the unsteady Euler equations. Shock fitting was applied in their method, through linearising the Rankine-Hugonoit relation, to determine both the steady and unsteady behaviour of shock waves. This gave better treatment of transonic flow than the previous linearised potential flow methods, through modelling the generation of vorticity and entropy. Although this method provided good resolution of shock waves, the technique of shock fitting is rather cumbersome especially when applied to unsteady flows. Subsequently, Lindquist and Giles (1994) examined the validity of linearised unsteady Euler equations with shock capturing, which represents a more flexible and efficient approach to the solution of transonic flows. Their work indicated that the artificial viscosity introduced by this technique, which smears the shock, captured shock waves which were consistent with linearised viscous solutions.

The most recent advances in this field of research has been the development and application of three dimensional linearised Euler methods, for example Hall & Lorence (1993) and Hall *et al* (1994), and the linearisation of the 3D Navier-Stokes equations, Holmes *et al* (1997).

Hall & Lorence (1993) presented a 3D linearised Euler method for the calculation of unsteady turbomachinery flows and provided some example solutions, one of which was the fourth standard configuration: A high speed turbine cascade oscillating in a two dimensional plunging mode (Bölcs & Fransson, 1986). Whilst good agreement was demonstrated with the experimental test data obtained at midspan, their 3D solution also indicated significant three dimensional behaviour of the steady and unsteady aerodynamics of this test configuration. Marked variations were observed between the predicted steady flow blade surface pressure distributions at the hub, midspan and tip section, and variations were also evident in the amplitude of unsteady pressure between the hub and tip of the suction surface. Additional comparisons were also made in their work with quasi-3D predictions from LINSUB for hypothetical subsonic helical fan blades vibrating in pitching mode with a linear variation in bending amplitude from hub to tip. The agreement between the 3D and quasi-3D solution was generally poor, with the quasi-3D method predicting a much higher amplitude of unsteady pressure at the tip and a lower amplitude at the hub. Unfortunately, the 3D solutions presented could not be fully corroborated due to the absence of three dimensional test data and their method could not be rigorously validated.

Holmes *et al* (1997) presented the first 3D linearised Navier-Stokes method for the analysis of turbomachinery flutter problems where viscous effects are influential. To

26

model the effects of turbulence in their method, the two equation k-ω turbulence model was linearised with wall functions adopted to avoid the necessity for very fine meshing in the near wall region.

The local time-linearised methods previously described offer three distinct advantages over their nonlinear time-marching counterparts:

- Superior computational efficiency
- Simple and efficient treatment of multiple disturbances through superposition.
- Simple application of phase shifted boundary conditions for single passage solutions of unsteady flow with blades vibrating at a non-zero value of interblade phase angle.

These three features combine to provide efficient 3D design tools which represent a highly attractive and financially viable option for the turbomachine industry. Under certain circumstances there is, however, some concern over the appropriateness of the time-linear assumption for the prediction and analysis of flutter problems. At most flutter conditions the unsteady flow field is dominated by viscous effects and/or the behaviour shockwaves, both of which maybe characterised by nonlinearity even for relatively small amplitudes of blade vibration.

To address the inability of time-linearised methods to deal with nonlinear behaviour, whilst trying to maintain the benefit of good computational efficiency from solution in the frequency domain, Ning & He (1997) proposed a novel computational model: A nonlinear harmonic Euler method for the solution of unsteady flows around oscillating blades. The basis and unique feature of this approach was the assumption that the unsteady flow field is composed of a time-averaged flow plus a small harmonic perturbation. Application of their methodology to the quasi-3D unsteady Euler equations yielded coupled equations for the time-averaged flow and the first order perturbation. The unsteady equations contributed so called "unsteady stress" terms to the time-averaged equations to give some account of nonlinearity, and spatially varied coefficients were obtained from the time-averaged flow field for the unsteady perturbation equations. Unlike the conventional time-linearised approach, where the unsteady perturbation is solved separately, in their method the two sets of equations were solved simultaneously using a strongly coupled Runge-Kutta time-marching scheme. Their method was subsequently developed for the solution of viscous flows (He & Ning, 1997), which showed improvements over the time-linearised approach for cases where the nonlinear behaviour was strong. Some

discrepancies were, however, observed with solutions provided by a nonlinear time-marching method, most probably due to the influence of higher order harmonic components.

2.3.2 Nonlinear Time-Marching Methods

In nonlinear time-marching methods, the governing equations are formulated and discretised in time-accurate form. The equations are then solved in the time domain through marching or stepping the equations in time from an initial condition to a converged state, which is periodic for unsteady turbomachinery flows. The development of these methods for the prediction of unsteady turbomachinery flows has largely been motivated by the need to address rotor-stator interactions as well as oscillating blade flows. The original methods intended for these applications were developed from a platform of established steady flow Euler time-marching methods, for example Jameson *et al* (1981) and Denton (1983). Over the past two decades this method of approach has evolved rapidly from the early developments made by Fransson & Pandolfi (1986) and Huff (1987) amongst others, and sophisticated 3D methods for the prediction of inviscid and viscous unsteady turbomachinery flows are now reasonably common place, for example He & Denton (1993, 1994), and Gerolymos (1993).

The basic advantage of adopting the nonlinear time-marching methodology over the time-linearised is the inclusion of nonlinear effects, which as previously described may be important to viscous and transonic unsteady flows. Unfortunately this benefit comes at great computational expense, both in the terms of CPU time and memory requirements, which seriously detracts from their practical worth. Subsequently, this group of methods is usually the less preferred option of the turbomachinery industry for the calculation of unsteady flows for design purposes.

Two issues contrive to result in the relatively poor computational efficiency of these methods. The first is an inevitable result of performing the calculation in the time domain and the second is associated with the CFL restriction on time step, which is required to ensure the numerical stability of the explicit solution procedures typically employed. For these particular methods the maximum possible time step is defined by the minimum mesh spacing. Although this time step restriction can be effectively relaxed for steady flow calculations through local time-stepping, to guarantee the time accuracy required for unsteady solutions the whole computational domain must be uniformly stepped in time.

For unsteady time-marching calculations, the time step is therefore usually limited beyond that required to obtain acceptable temporal resolution, especially for viscous solutions where the mesh must be refined to resolve boundary layers and wakes. The restriction on time step can be overcome by adopting an implicit numerical scheme, see for example the method validated by Ayer & Verdon (1998). Implicit schemes do, however, involve large matrix inversions at every time step and the gain in computational efficiency obtained through the use of larger time steps may not be as significant as expected.

To include viscous effects in unsteady time-marching solutions, whilst trying to maintain a reasonable level of computational efficiency, He & Denton (1993) developed an inviscid-viscous coupled method. In this method the unsteady Euler and integral boundary layer equations were simultaneously marched in time using an explicit Runge-Kutta scheme, with a transpiration model included to account for boundary layer displacement thickness in the Euler calculations. This approach enabled viscous solutions to be effectively obtained for coarse meshes, thereby relaxing the time step restriction and providing a relatively efficient method. Quasi-steady correlations were, however, required for closure of the integral boundary layer equations. Later, He (1993) proposed a time-consistent two-grid acceleration technique, to enhance the computational efficiency of Navier-Stokes, explicit time-marching calculations. In this method the time step restriction was relaxed though performing calculations at alternate time steps on a fine and coarse mesh, to obtain a solution for the fine. Although this approach resulted in a loss of temporal accuracy on the fine mesh, it was argued and demonstrated that this can be effectively controlled through a suitable definition of the coarse mesh relative to the wavelength of the unsteady phenomenon. The method demonstrated good agreement with results of computations performed on the fine grid and a reduction in CPU time by a factor of 18 was achieved through the use of the two-grid acceleration for the calculation of a self-excited oscillating transonic flow.

Time-marching methods suffer a further disadvantage due to the level of sophistication required to implement phase shifted boundary conditions, which are required for single passage solutions of unsteady flows with blades vibrating at an interblade phase angle. At present, there are three established techniques to deal with this type of condition:

- Direct Store, Erdos (1977)
- Time Inclination, Giles (1987)
- Shape Correction, He (1990a)

In the Direct Store approach (Erdos, 1977), flow properties are stored throughout a period of unsteadiness at all phase shifted periodic boundaries and subsequently recalled as boundary conditions for the calculation of the following period. Although this technique is the most robust and flexible of the three options, it is rather intensive in terms of memory requirements. In the Time Inclination technique (Giles, 1987), the computational time plane is inclined in the pitchwise direction such that the phase shifted periodic boundaries are perceived by the solution procedure as the simple spatial kind. Time Inclination therefore removes the memory penalties incurred by Direct Store, and offers an additional benefit of an enhanced rate of convergence. Application of this approach is, however, severely limited, because the level of time inclination has to restricted in order to obey the characteristics of the governing equations. The third option, Shape Correction (He, 1990a), utilises Fourier coefficients to store the temporal variation of flow parameters at phase shifted periodic boundaries. Although this method vastly reduces the memory required and an increase in the rate of convergence can be expected compared to Direct Store, an increase in CPU time is incurred due to the extra calculations involved in determining the Fourier coefficients. This technique has since been developed for the treatment of phase shifted boundary conditions for single passage solutions of unsteady flows with multiple disturbances (He, 1992), which are likely to receive increasing attention in the very near future.

2.4 Closing Remarks

It is evident from the discussion of advances in the development of CFD methods for the prediction of oscillating blade flows, that fully three dimensional methods have been established which can be applied to realistic, 3D turbomachinery configurations. It is equally apparent, however, that experimental work has not kept pace with these developments and is somewhat deficient in respect to the demands of these advanced computational methods. To the authors knowledge there are no three dimensional test cases available in open literature that could be utilised to validate these methods and, through highlighting areas of deficiency, direct future developments. This data is also essential if basic understanding of these unsteady flows is to progress.

Serious attention must also be paid to the provision of test cases with clearly defined boundary conditions if experimental test data is to be exploited for CFD validation purposes. This has proved problematic in previous 2D oscillating cascade experiments, due to the difficulty involved in establishing unsteady periodic flow.

Chapter Three

The Low Speed Flutter Test Facility

A low speed flutter test facility has been commissioned in the Thermodynamics and Fluid Mechanics Laboratories of the School of Engineering, at the University of Durham. The test facility was designed to address the urgent need for detailed and reliable three dimensional test cases describing the behaviour of flow around oscillating turbomachinery blades, with the intent to enhance basic understanding and provide data for the validation of modern CFD methods. In this chapter the test facility is described, with special emphasis placed upon the philosophy behind the design.

3.1 Design Philosophy

Experimental work was performed in two parts during the course of this project. The principal objective of the first phase of experiments was to conduct a detailed investigation into the unsteady flow around a turbine blade oscillating in a three dimensional mode of vibration. In performing this task it was also intended that the first three dimensional test cases would be provided for open use, to assist the validation and future development of the sophisticated CFD methods described in section 2.3. The second phase of the experimental work, which is described in greater detail in Chapter 7x, was designed to investigate the influence of tip leakage upon the unsteady aerodynamic response of the oscillating turbine blade.

To ensure the design of a suitable test facility, the basic objectives of the present work were given careful consideration and some key issues identified. Specific objectives were subsequently formed, to direct the development of the test facility from concept through to completion. These are summarised by the following headings and the comments which

accompany them describe the relevant issues and some of the decisions which were enforced at the conceptual stage of design:

- *Ensure reliability of test data in terms of accuracy and repeatability* - This is obviously important for any experimental investigation and for the present work it was believed that this would be best achieved by constructing a large scale working section and operating at low speeds. This is because realistic reduced frequencies would be reproduced by low frequencies of blade vibration and therefore the difficulties involved in enforcing and controlling the frequency of blade vibration and the measurement of unsteady pressure would be greatly reduced.

- *Ensure high spatial and temporal resolution of measurements* - High spatial resolution of measurements was vital in the first phase of experiments in order to evaluate the three dimensional nature of the unsteady blade surface pressure response and in the second, to allow the influence of tip leakage upon the local unsteady flow to be examined. In terms of temporal resolution, it was considered necessary to resolve all low order harmonic components of the unsteady pressure response, but most especially the first and second harmonics, since the first determines aeroelastic stability and the second provides a good indication of nonlinear behaviour. The fulfilment of these objectives was largely assisted by the decision to use low operating speeds and a large scale working section. The large scale enabled detailed instrumentation and the low frequency of blade vibration permitted the use of externally mounted pressure transducers, which allowed unsteady pressure measurements to be acquired from any location that could be furnished with an ordinary static tapping. Operating at low frequencies of blade vibration further relieved the demands placed upon the instrumentation, since good levels of temporal resolution could be achieved with quite moderate sampling rates.

- *Provide and Maintain a clear specification of boundary conditions* - This was important to facilitate meaningful analysis of the test data, but moreover, it was required to enable comparison with solutions from CFD methods. Although problems were not envisaged in the definition of inlet and outlet conditions, previous work conducted with oscillating cascades had demonstrated considerable difficulty in defining the phase-shifted periodic boundary condition, due to problems associated with establishing a periodic unsteady flow. This problem had been especially evident in oscillating linear cascade experiments, e.g. Carta (1983) and Buffum & Fleeter (1993), and serious consideration was subsequently given to this objective in the detail design of the working section.

- *Establish a simple aero-mechanical environment* - This was primarily intended to prevent unnecessary ambiguity and thereby enable clear interpretation of the test data. It was also believed that attention to this matter would assist the precise specification of boundary conditions and generally ease the process of data acquisition. A preliminary decision to arise from consideration of this objective was to enforce a two dimensional steady flow in the working section and thereby ensure clear interpretation of the three dimensional unsteady test data in terms of the 3D mode of blade vibration.

- *Implement a realistic turbomachinery configuration* - This was important for the present work to retain some practical worth. In some respects, however, it was considered flexible, because the intention of the experimental work was not to evaluate performance of a particular design, but rather, assess the fundamental unsteady aerodynamic flow phenomenon induced by a three dimensional mode of blade vibration at subsonic speeds. To achieve this, some rudimentary features of a realistic configuration obviously had to be preserved, but not necessarily exactly reproduced.

- *Implement a cost-effective approach* - A modest budget was available for the commission of the test facility and whenever possible a cost-effective approach was adopted. The budget was not, however, inflexible and care was taken to ensure that the basic objectives of this project were not seriously prejudiced by the limited finance available.

As with most engineering projects, at several occasions during the design process the individual objectives described were observed to be in conflict. The design of the test facility subsequently developed through a continual process of compromise, most especially between the implementation of a realistic turbomachinery configuration and the realisation of simple and clearly defined aerodynamic and mechanical conditions.

3.2 The Test Facility

In this section the individual components of the low speed flutter test facility are described and discussed, with reference made to the objectives previously outlined. Through this, the process of compromise becomes apparent and the design of the facility is justified. Before this embarked upon, however, a brief overview of the facility is

provided to give the reader some understanding of general approach adopted and how the individual components combine.

3.2.1 Overview

The test facility employed a single, prismatic turbine blade extensively instrumented for steady and unsteady pressure measurements between 10% and 90% span. At the working section the blade was located within a profiled duct and driven at a sinusoidal rate in a three dimensional bending mode. The sidewalls of the working section were profiled in an attempt to simulate the adjacent blades in cascade, whilst ensuring a clear definition of boundary conditions through removing the phase shifted periodic boundary between adjacent blades. The flow through the working section was driven by a low speed wind tunnel and the tunnel boundary layers were bled in order to provide uniform inlet flow conditions. The facility was also equipped with externally mounted pressure transducers, which enabled detailed unsteady pressure measurements to be performed without prohibitive cost and a bilinear traverse gear for five-hole probe measurements of inlet and outlet flow conditions.

3.2.2 The Low Speed Wind Tunnel

A low speed wind tunnel was designed to deliver a uniform rectilinear flow at inlet to the working section. The tunnel, shown in figure 3.1, is a typical design for low speed applications, which was largely based upon existing wind tunnels in the Thermo-Fluids laboratories of the University of Durham. In this design, the non-uniform discharge from a centrifugal fan is diffused through a two stage, slatted diffuser into a large settling chamber. The pressure generated in this chamber then drives a flow through a shaped contraction, where it accelerates, into the working section and out to exhaust.

In wind tunnels of this kind, the quality of the flow delivered to the working section is largely dependant upon the contraction, most specifically its shape and the ratio of areas at inlet and exit. In the present design, a contraction ratio of 5:1 was achieved through shaping the top and bottom walls of the contraction, as shown in figure 3.1, which was further increased to 7:1 through the gentle profile applied to the sidewalls. An established design known as the Vitoshinskii nozzle, described by Gorlin & Slezinger (1966), was adopted for the shape of the endwalls in the contraction and a honeycomb was placed at

its exit to assist the development of a uniform rectilinear flow. The tunnel was designed for operation at variable speeds, with the flowrate delivered by the centrifugal fan being accurately controlled by a four kilowatt ac motor and a digital three phase invertor.
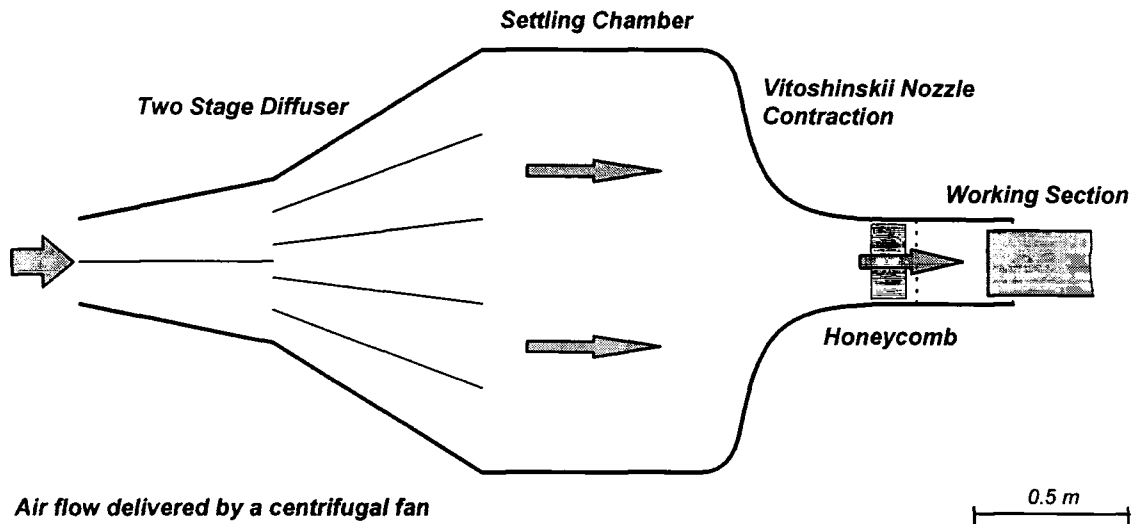
Figure 3.1: A cross section through the low speed wind tunnel

3.2.3 Specification of the Blade and Bending Mode

A large scale, prismatic turbine blade was utilised for the purposes of the present work. The blade section properties are summarised in table 3.1 and the profile is shown in figure 3.2. A co-ordinate specification of the blade section profile - a heavily modified version of a HP-IP nozzle guide blade which retains a realistic loading characteristic - is also provided in Appendix B.

Blade Section Properties	
Chord length, C	0.200 m
Aspect ratio, h/C	1
Solidity, C/S	1.35
Maximum thickness	0.175 C
Blade inlet angle, α'	25.0°
Blade exit angle, β'	73.4°

Table 3.1: Blade specification

35
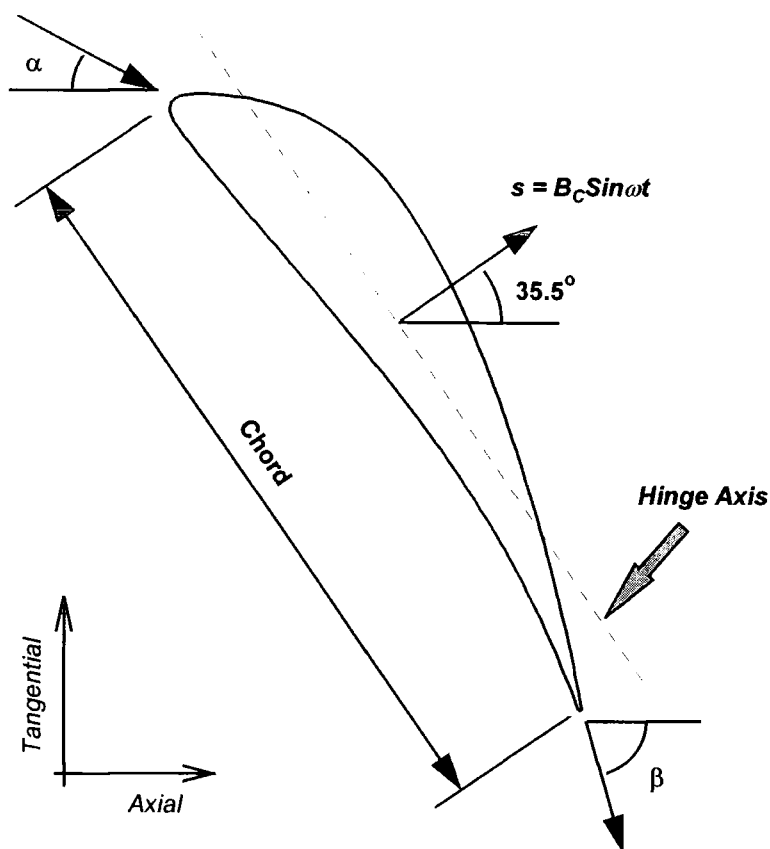
Figure 3.2: Blade profile and nomenclature

A constant section blade was employed in the present work to provide a two dimensional steady flow and therefore prevent ambiguity between unsteady effects associated with a spanwise variation in steady flow blade loading and those generated by a 3D mode of vibration. And a large scale (chord: 200 mm) was selected to enable detailed instrumentation of the blade surfaces. The blade aspect ratio, as described in table 3.1, was restricted to unity, largely for practical reasons associated with the large scale, but also to limit the length of tubing between the surface tappings and the externally mounted pressure transducers which were utilised for unsteady pressure measurements. Despite the limited aspect ratio, it was believed that a significant three dimensional effect would be introduced by a suitable definition of the bending mode. The blade camber and operational deflection, nominally specified at 40° (see table 3.2), were also restricted. This was intended to minimise the strength of the blade passage secondary flows and therefore prevent confusion between unsteady flow phenomenon influenced by the three dimensional secondary flow structure and those purely generated by the mode of blade vibration.
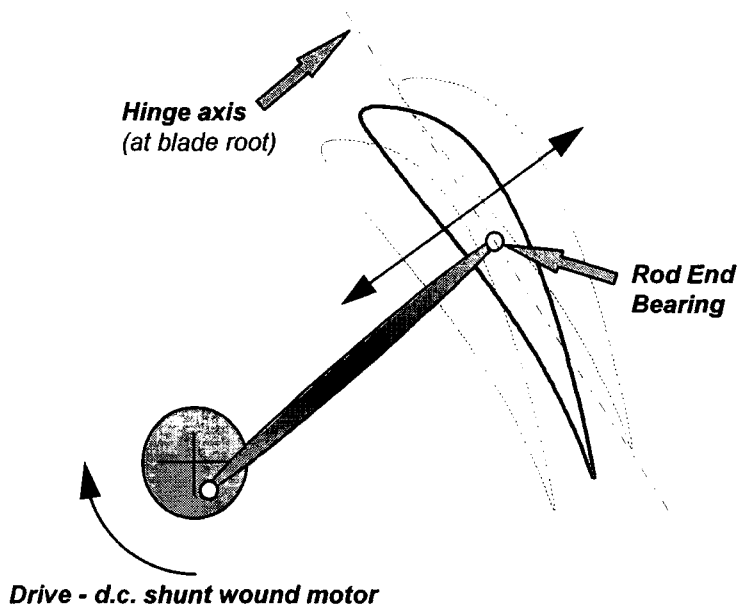
Figure 3.3: The blade drive mechanism (tip section)
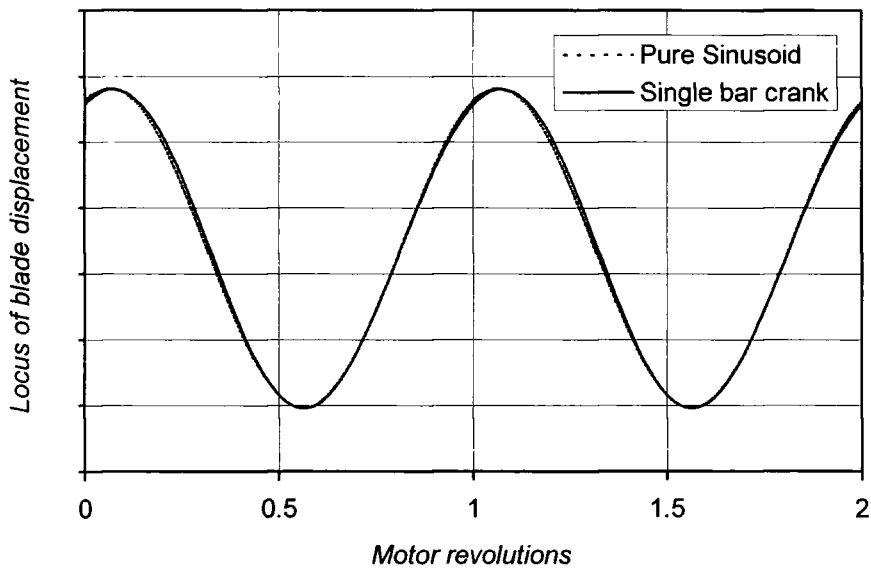
Figure 3.4: Locus of blade displacement delivered by the single bar crank

A three dimensional mode of blade vibration was obtained through hinging the blade at root and harmonically driving the tip section with a single bar crank type mechanism connected with a rod protruding from the blade tip, as shown in figure 3.3. This arrangement provided a linear variation in bending amplitude along the blade span, that increased towards the tip section: A bending amplitude of 5.5% chord was enforced at the

37

tip and an amplitude of 0.6% chord at the hub[†]. The direction of bending, as shown in figure 3.2, was nominally set at 35.5° relative to the axial direction. The single bar crank mechanism was powered by a thyristor controlled d.c. shunt wound motor which allowed accurate setting of the frequency of blade vibration.

Although the single bar crank mechanism described does not constitute a pure harmonic drive, with the length of the crank arm set much greater than the amplitude of blade vibration, a very good approximation to a pure sinusoidal drive was obtained in the present design, as indicated by figure 3.4.

3.2.4 The Working Section

The working section, shown in figure 3.4, was a self contained unit located within the exhaust of the low speed wind tunnel. This enabled the tunnel boundary layers to be bled and uniform flow conditions to be realised at its inlet. The sidewalls of the working section were made of fibreglass and profiled in an attempt to simulate the adjacent blades in cascade, whilst providing a clear definition of boundary conditions for both the steady and unsteady flow generated in the two blade passages. The profiled section of the left-hand sidewall was specified with the co-ordinates of the blade pressure surface and the right-hand wall with the suction surface, as shown in figure 3.5(i). These profiled regions of the sidewalls met plane sections which extended upstream to the inlet and one axial chord length downstream to the outlet of the working section. To prevent discontinuities at the intersection of the plane and profiled sections of the sidewalls, small cusps (5% chord in length) were incorporated at the locations corresponding to the leading and trailing edge position of the adjacent blades in cascade. The endwalls were planar and made out of perspex in order to provide good visual access to the working section.

The blade was centrally located within the working section and the root of the blade extended up through the hub endwall, where the hinge was attached. At this end wall, a foam gland was constructed to accommodate the small oscillation of the blade and to prevent leakage from the test section. A rubber gland was also incorporated at the tip endwall, in order to seal the channel which was cut to allow for the travel of the drive rod, which protruded from the blade tip and passed through this wall. A tip clearance of 1 mm (0.5% chord) was required at the tip endwall due to the motion of the blade.

[†] The non-zero value of bending amplitude at the hub was a practical consequence of mounting the hinge beneath the hub endwall of the working section.
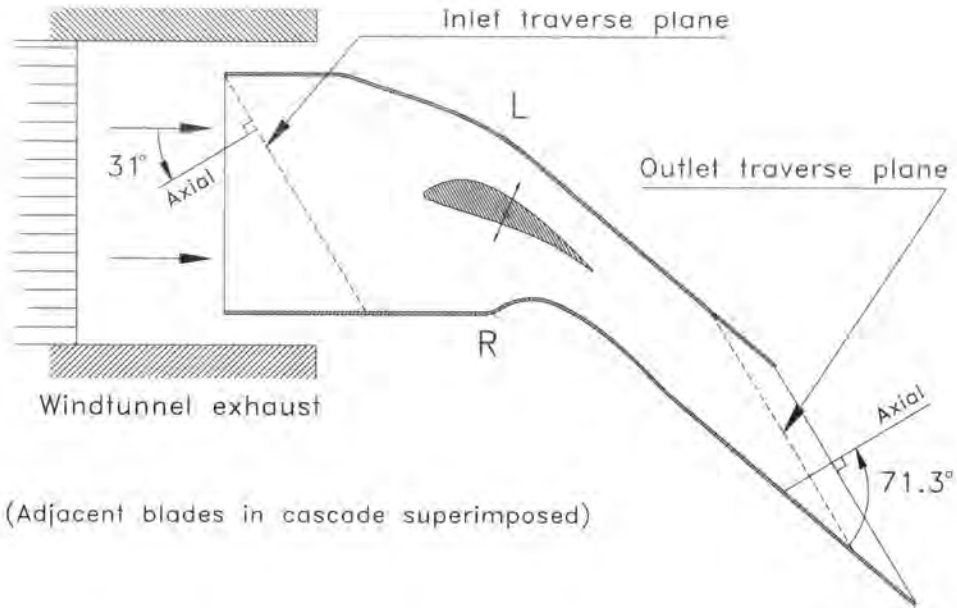
(i). The working section in plan view
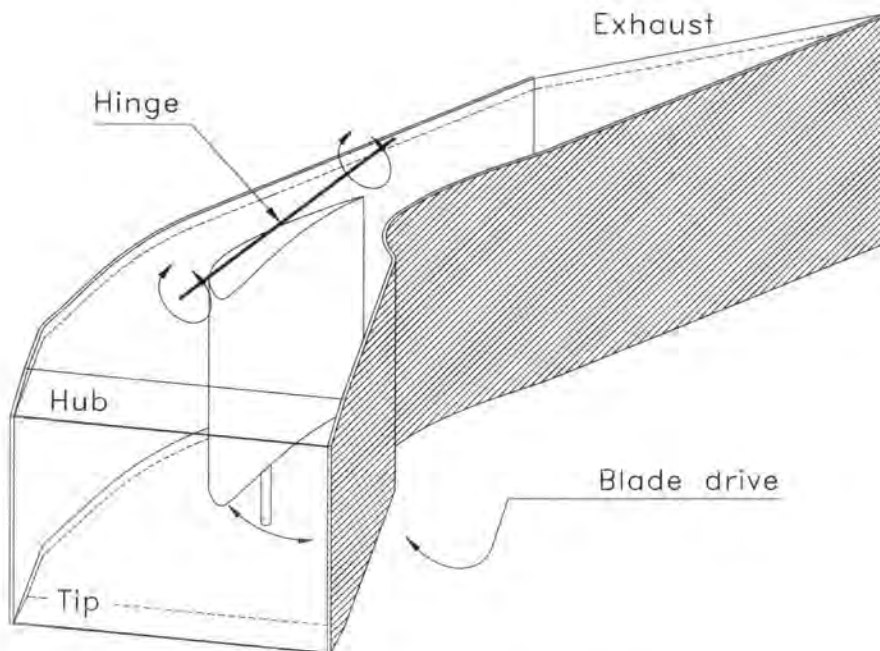
(ii). 3D schematic of the working section

Figure 3.5: The working section

Through bounding the flow around the oscillating turbine blade in the working section with the profiled sidewalls previously described, clearly defined boundary conditions were provided whilst an attempt was made to preserve some of the fundamental features of a normal blade passage flow, most especially a realistic blade loading and the provision of opposing surfaces for the reflection of pressure waves. The configuration of the working section also made for a simple and cost-effective facility, through removing the difficulty and expense involved in developing a synchronous multiple blade drive. And the use of a single blade enabled very detailed measurements to be acquired within a reasonable time scale.

It is accepted that the configuration of the working section is clearly deficient in modelling the infinite multiplicity of a realistic turbomachinery blade row and offers no mechanism to deal with a range of interblade phase angle or indeed simulate vibration at a realistic interblade phase angle. This is not, however, considered to be of vital importance when taken in context with the overall objectives of the present work. Indeed, it can be argued that although the present design does not represent the most realistic configuration, the fundamental unsteady aerodynamic response to a three dimensional mode of blade vibration can still be examined through oscillating the blade in an environment that simulates a normal blade passage flow at a very basic level. The design is therefore considered a reasonable compromise between the implementation of a realistic turbomachinery configuration and the provision of clearly defined boundary conditions.

It is also recognised that modifications would have to be made to a typical CFD method developed for turbomachinery applications, in order to make direct comparisons with test data generated by this facility. This inconvenience is, however, unequivocally offset by the clear definition of boundary conditions.

3.3 Operating Conditions

Table 3.2 describes the basic operating conditions for both phases of the experimental work performed in the low speed flutter test facility. The experiments were performed at very low speeds, with a typical exit Mach Number of 0.1, and realistic values of reduced frequency were reproduced. A constant Reynolds number was also imposed throughout testing, which is below normal operational values, but within a region of practicable interest where the viscous behaviour of the flow could be influential.

40

Experiment Conditions	
Inlet flow angle, α'	31.0°
Nominal exit flow angle, β'	71.3°
Reynolds number, *Re*	4.5×10^5
Typical exit Mach N°, M	0.1
Bending mode direction	35.5°
Bending amplitude at tip, B_C	0.055 *C*
Bending amplitude at hub	0.006 *C*
Reduced frequency, *k*	0.15, 0.25, 0.50, 0.75
Nominal frequencies, *f*	4.0, 6.7, 13.4, 20.1 Hz
(Nominal frequencies at ambient conditions of 1 atm. and 20 °C)	

Table 3.2: Summary of operational conditions

In the first phase of experiments, steady flow measurements were acquired at the conditions described in table 3.2 and detailed unsteady blade surface pressure measurements were performed with the blade vibrating in the three dimensional bending mode at four values of reduced frequency. In the second series of tests, designed to examine the influence of tip leakage upon the unsteady aerodynamic response, these conditions were matched at freestream, with unsteady measurements performed at three different settings of tip clearance.

3.4 Instrumentation

The blade surface was extensively instrumented with 110 static tappings, all of which were egressed through the root of the blade. The tappings were evenly distributed over five spanwise sections (10% (near hub), 30%, 50%, 70%, and 90% span), with ten tappings on the pressure surface and suction surface at each section. Additional tappings were also located at the leading and trailing edge of each section. The same tappings were used for both the steady and unsteady blade pressure measurements, and their positions are described in table 3.3 and the accompanying diagram.

The facility was also equipped with a bilinear traverse gear for five-hole probe measurements at two axial planes: the first located at inlet (one axial chord upstream of the blade leading edge); and the second located near exit (75% chord downstream of the blade trailing edge), as previously shown in figure 3.5(i).

41
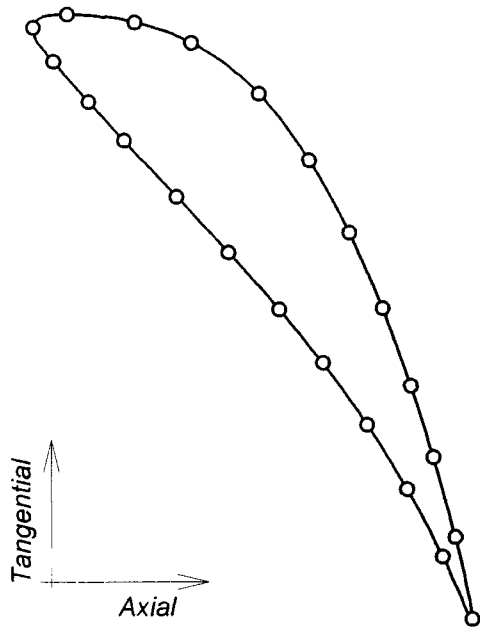
Chordwise location of tappings, x/C	
Pressure surface	Suction surface
0.058	0.016
0.130	0.077
0.201	0.143
0.304	0.251
0.406	0.363
0.508	0.475
0.600	0.585
0.703	0.694
0.805	0.790
0.907	0.985
Additional tappings at l.e. and t.e.	

Table 3.3: Distribution of blade surface pressure tappings

(Tappings located at five spanwise sections: 10%; 30%; 50%; 70% and 90% span)

Chapter Four

Data Acquisition and Processing

This chapter is concerned with the process of data acquisition and reduction. First, the apparatus and standard techniques employed for steady flow measurements are described, followed by a detailed discussion of the system developed for the acquisition and reduction of unsteady blade surface pressure data. In this discussion, particular attention is paid to the appropriateness of utilising externally mounted pressure transducers and the calibration procedure required to ensure acceptable accuracy of unsteady pressure measurements. Finally, the chapter concludes with an evaluation of experimental errors and repeatability, which provides further justification of the techniques adopted.

4.1 Steady Flow Measurements

The steady flow measurements obtained from the low speed test facility served two basic functions. The first was to provide the aerodynamic background for the unsteady experiments, i.e. capture any steady flow phenomenon which may influence the unsteady pressure response of the oscillating blade (including the tip leakage flow), and the second was to specify the inlet flow conditions and steady flow performance for CFD validation purposes. To achieve this, steady flow blade surface pressure measurements were recorded from all tappings between 10% and 90% span, using a tilted manometer bank, and five-hole probe traverses were performed at the inlet measurement plane (one axial chord length upstream of the leading edge) and the measurement plane located near exit (0.75 axial chord length downstream of the trailing edge).

A forward facing conical five-hole probe mounted on a precision, bilinear Unislide traverse was employed for the measurement of flow conditions at the two traverse planes.

The probe, which is shown in figure 4.1, was calibrated at representative Reynolds numbers (based on probe diameter) for the inlet and exit traverse measurements over a range of +/- 28° pitch and yaw angle, at 2° intervals. This procedure was performed in a dedicated facility following an established technique described by Treaster & Yocum (1979) which defines calibration coefficients for pitch angle, yaw angle, total pressure and static pressure. The coefficients used in the present work accompany figure 4.2, which describes the nomenclature for the numbering of the holes on the probe, and calibration charts obtained at a probe Reynolds number of 9×10^3 are presented in figures 4.3 to 4.5.

Probe diameter:	4.0 mm
Hole diameter (internal):	0.6 mm
Sting length:	10 probe diameters

Side Elevation
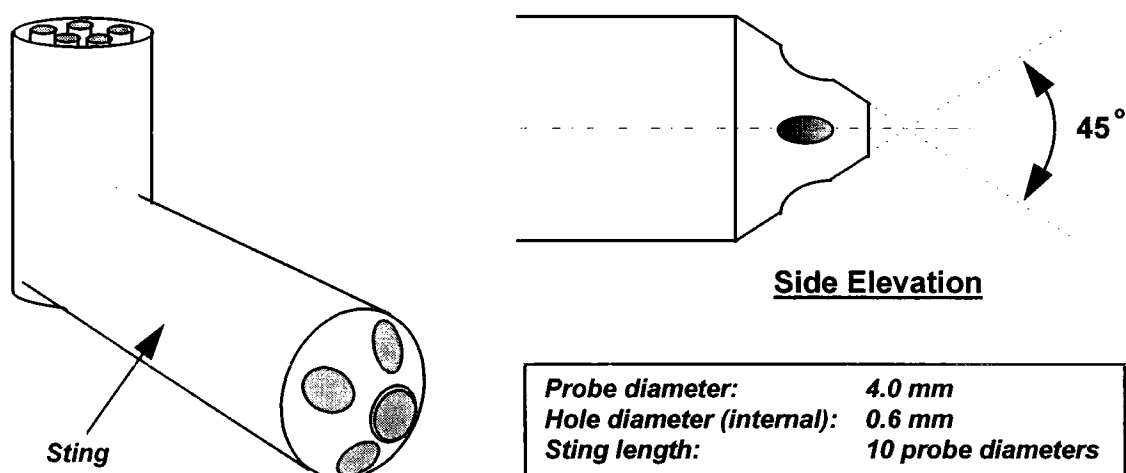
Figure 4.1: Forward facing conical five-hole probe
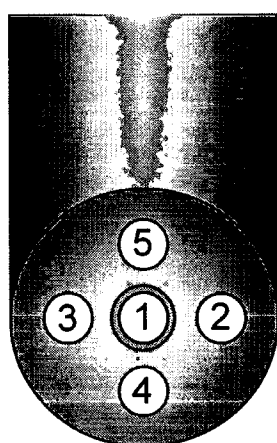
Yaw angle coefficient, $\quad k_y = \dfrac{P_2 - P_3}{P_1 - P_{av}}$ (4.1 i)

Pitch angle coefficient, $\quad k_p = \dfrac{P_4 - P_5}{P_1 - P_{av}}$ (4.1 ii)

Total pressure coefficient, $\quad k_T = \dfrac{P_1 - P_0}{P_1 - P_{av}}$ (4.1 iii)

Static pressure coefficient, $\quad k_S = \dfrac{P_{av} - P_S}{P_1 - P_{av}}$ (4.1 iv)

where, $\quad P_{av} = \dfrac{P_2 + P_3 + P_4 + P_5}{4}$

Figure 4.2: Five-hole probe nomenclature and calibration coefficients
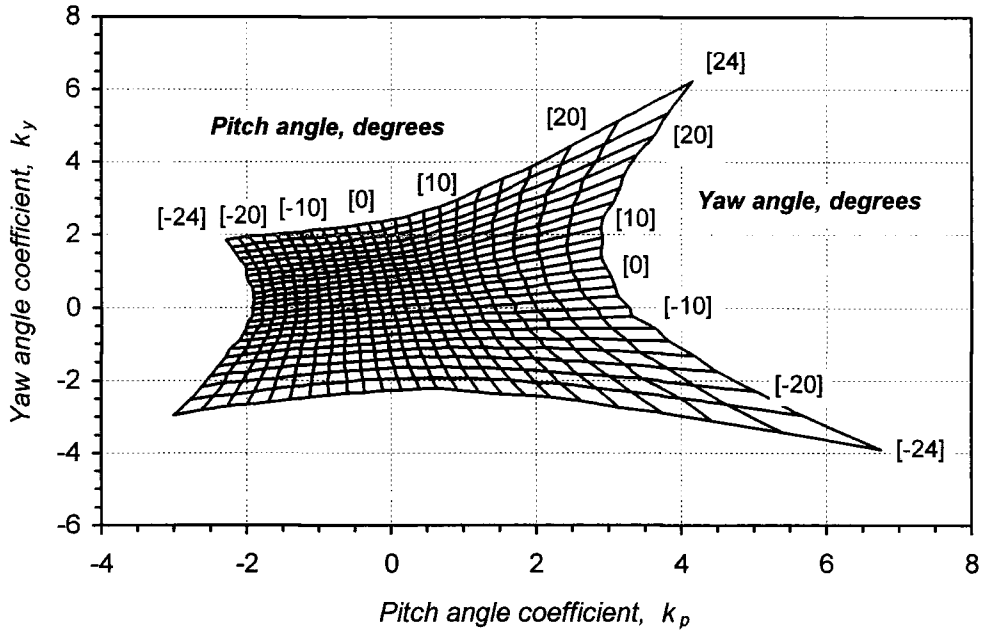
Figure 4.3: Five-hole probe calibration chart for pitch and yaw angle
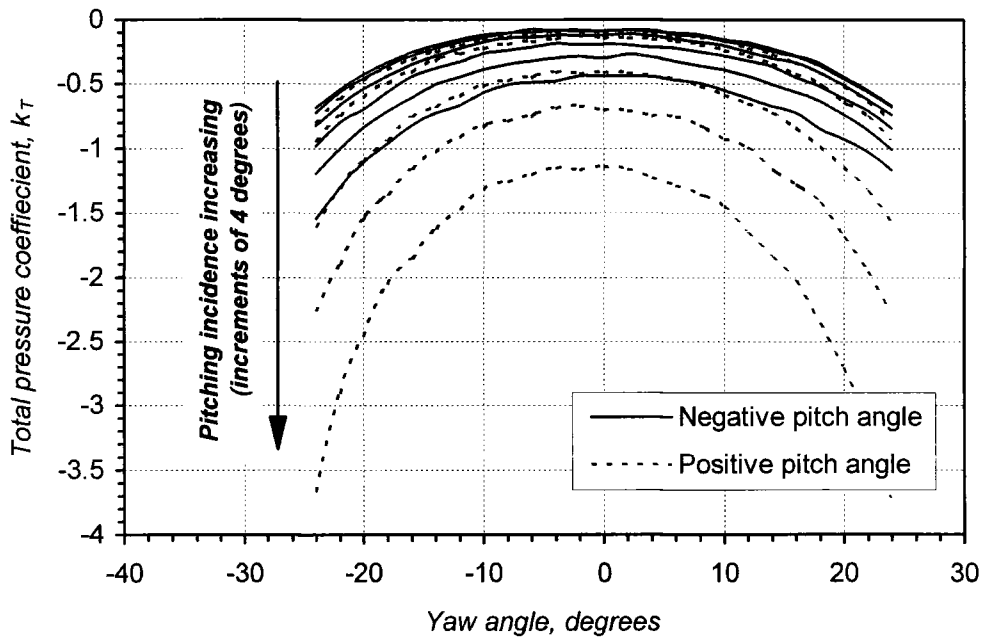
Figure 4.4: Five-Hole probe calibration chart for total pressure

Although the calibration charts for pitch and yaw angle coefficient, total pressure coefficient and static pressure coefficient, shown in figures 4.3 to 4.5 respectively, are smooth and continuous, the sensitivity of the probe notably increases for positive values of pitch angle and to a lesser extent for negative values of yaw angle. This was originally
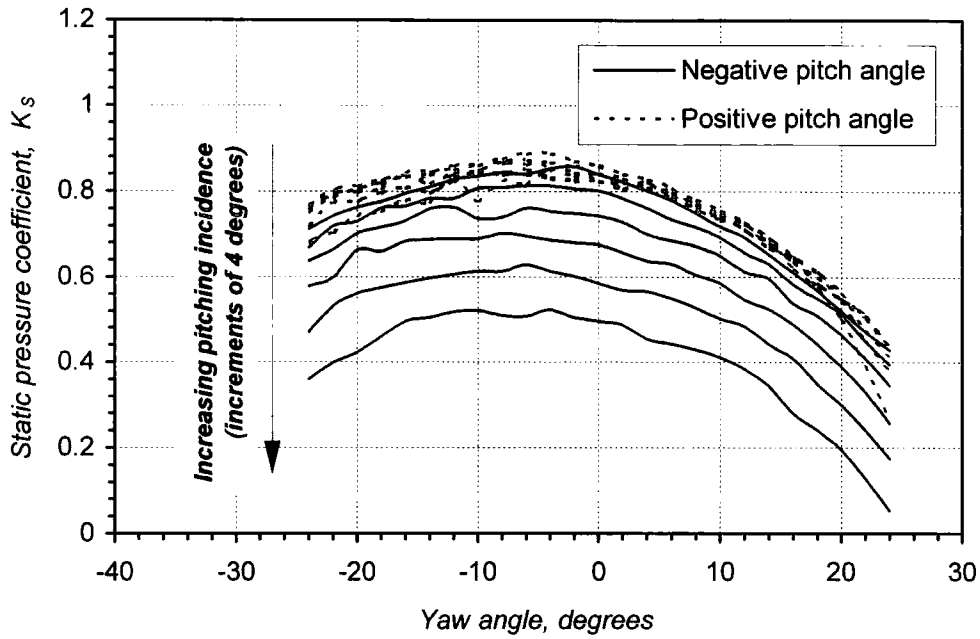
Figure 4.5: Five-hole probe calibration chart for static pressure
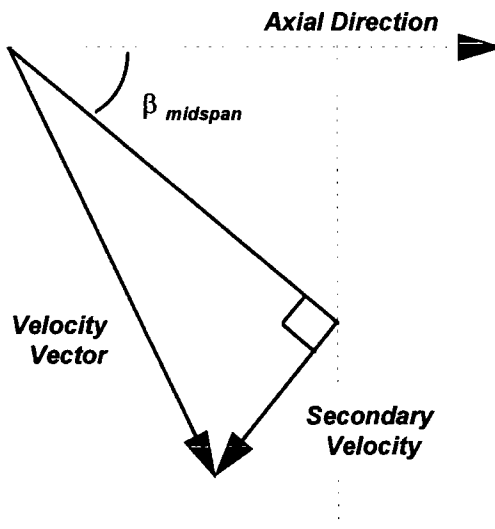
Figure 4.6: Definition of secondary velocity

presumed to be due to misalignment of the probe in the calibration facility, however, consistent repetition of this result suggested otherwise and close inspection of the probe tip revealed marked defects in the manufacture, with the holes being unequally spaced. Despite these imperfections, the performance of the probe was considered satisfactory since flow angles could be clearly resolved within an accuracy of $0.5°$ with suitable interpolation on the calibration map shown in figure 4.3.

During steady flow experiments in the low speed test facility, the pressures from the five-hole probe were measured with five calibrated pressure transducers and the data recorded on a p.c. using an Amplicon PC-74 data logging card. The acquisition of measurements was controlled by a software suite which logged the location of the probe, converted the raw data into pitch angle, yaw angles, total pressure and static pressure - through simple bilinear interpolation on the calibration maps - and calculated velocity through application of Bernoulli's equation.

The five-hole probe traverse measurements are presented in the following chapters as plots of normalised total pressure, total pressure loss and secondary velocity vectors, which were defined according to the convention shown in figure 4.6. In this convention, the secondary velocity at a given pitchwise location is defined relative, in the normal direction, to the velocity vector at midspan. In chapter 7, the measurements are also presented in pitch-averaged form, defined in the nomenclature, to analyse and compare the behaviour of the tip leakage flow over a range of tip clearance.

4.2 Unsteady Pressure Measurements

The low rates of blade vibration (4 - 21 Hz) employed in the test facility to match realistic reduced frequencies permitted the use of externally mounted pressure transducers for the measurement of blade surface unsteady pressure - a technique previously adopted in the work of Kobayashi (1989) and He (1990b). Although this approach offered an important benefit over the use of miniature surface mounted pressure transducers, through allowing detailed measurements to be performed with a limited number of transducers and at reasonable cost, some additional complications were introduced. The most significant of these was the correction required to account for phase shift and attenuation of pressure waves along the tubes connecting the surface tappings and the external pressure transducers. Additional care was also required to ensure and evaluate the repeatability of measurements, because a series of tests would be required to obtain the response of the full blade surface. A simple and robust system was therefore developed to assure the accuracy and repeatability of these measurements. This system performed three basic functions: (1). the acquisition of synchronised unsteady pressure signals; (2). the process of data reduction and (3). the correction of unsteady pressure signals for phase shift and attenuation along the tapping tubes.

4.2.1 Data Acquisition

Five temperature compensated pressure transducers (type: Sensym 142C01D, 0-1 psi range) were employed for unsteady pressure measurements, which meant that a set of twenty measurements were required to cover the 100 pressure tappings located on the blade suction and pressure surfaces. The transducers delivered an output voltage signal which was directly proportional to the applied pressure, as demonstrated by the linear calibration plot shown in figure 4.7.
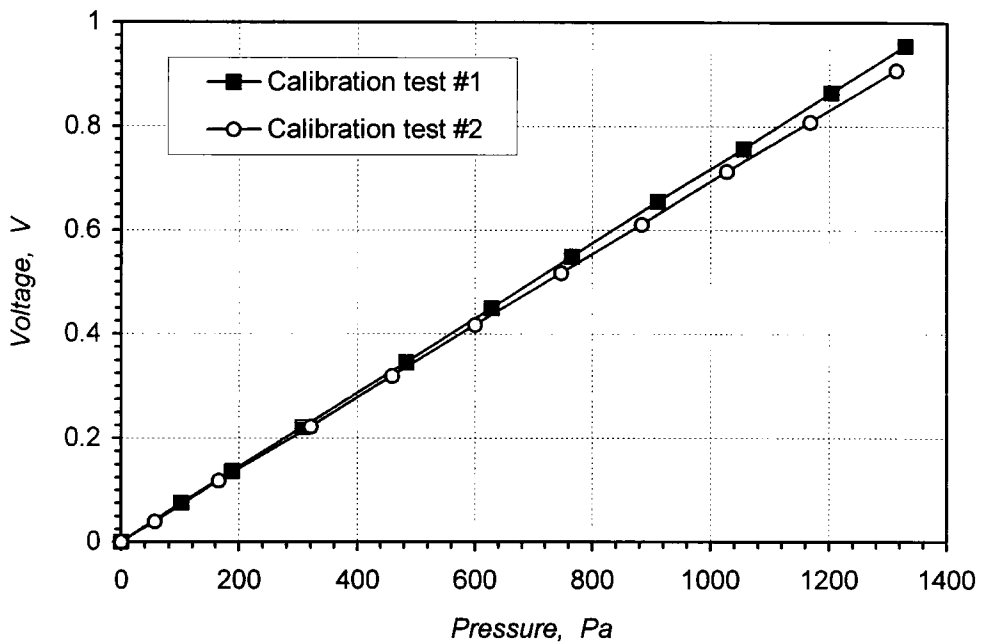
Figure 4.7: Sample pressure transducer response

Despite temperature compensation and a regulated voltage supply (8.000 volts +/- 0.001 volts), a series of calibration tests performed over a period of two weeks during the commission of the facility revealed a slight, but marked, variation in the gradient and offset which defined the response of each transducer. The variation in the gradient of response is demonstrated for an extreme case by two calibration plots in figure 4.7, which were obtained for the same pressure transducer on different days. To prevent errors being introduced by this variation, a two-point calibration procedure was performed before each set of unsteady pressure measurements. In this calibration procedure, the voltage offset of each transducer was recorded as well as the voltage response to an arbitrary pressure load, which was simultaneously imposed on each transducer and a micro-manometer. These

two measurements allowed the linear response of each transducer to be accurately defined for each set of measurements. Furthermore, because the calibration procedure was performed with the data logging card used throughout the unsteady experiments, any deviation in the linear response of each data channel of the card was also inherently accounted for.

Figure 4.8 shows a schematic representation of the principal hardware components employed in the system developed for the acquisition of synchronised unsteady pressure signals. In this system, the unsteady pressure signals, or rather voltages, from the five pressure transducers were discretised and logged on a personal computer using an Amplicon PC-74 data logging card, with the acquisition of measurements being triggered at a fixed phase in the blade motion. The trigger signal was provided by a transmissive optical Schmitt sensor which delivered a high voltage output when a slot, cut into a plate installed on the blade drive, passed through its sensitive aperture. This signal was monitored on the high frequency response external trigger channel of the data logging card and data acquisition was initiated on the trailing edge of a TTL voltage pulse, which corresponded to the passing of the trailing edge of the blade drive slot. The trigger pulse was also utilised to monitor the frequency of the blade vibration on a digital tachometer, to provide a quick visual reference, and on the data logging card as a secondary measure which provided an accessible record of frequency for each set of unsteady pressure data.
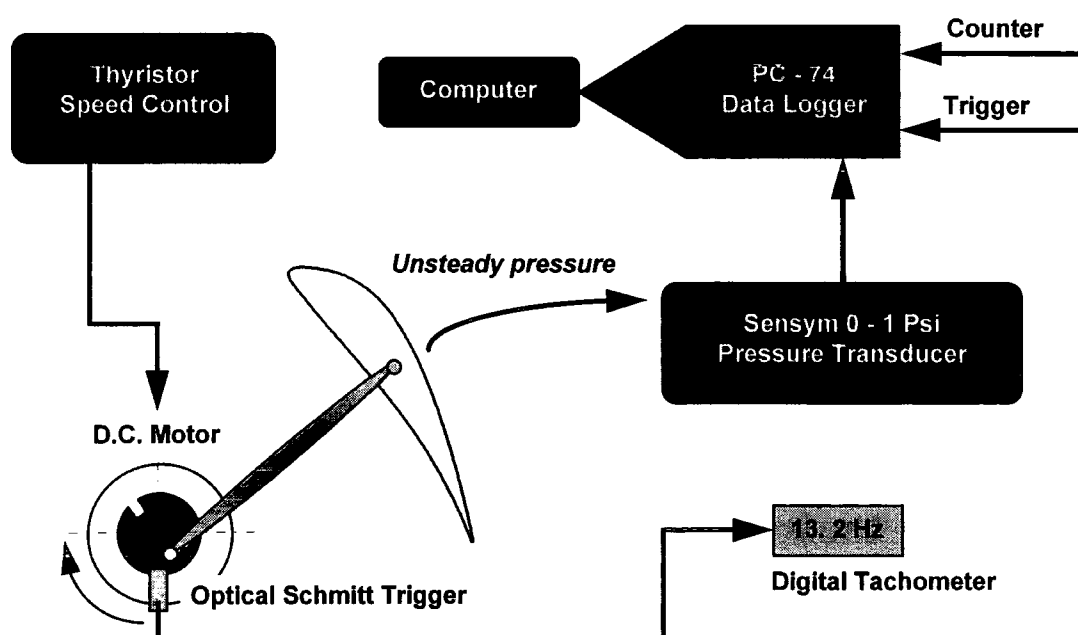
Figure 4.8: Schematic of data acquisition hardware

Sampling of the unsteady voltage signals, delivered by the pressure transducers, was performed with a 12-bit analogue-to-digital converter (ADC) onboard the PC-74 data acquisition card. The 12-bit accuracy of the ADC provided 4096 quantisation levels, equally distributed over an input voltage range of 0 to 5 volts which was equivalent to the full scale range of the transducer signal output. The sampling procedure, as with any form of discretisation, introduced a maximum error of half a quantisation level, which represented an accuracy of +/- 0.8 Pa on a typical pressure transducer response previously shown in figure 4.7.

To ensure a comparable level of temporal resolution and accuracy of measurements throughout the range of unsteady experiments, the rate of sampling was prescribed according to the test case reduced frequency. These rates, described in table 4.1, were specified to ensure a minimum of 200 sampled points per period of the first harmonic pressure response, which according to Shannon's Sampling Theorem (described by Lynn & Fuerst, 1996), is sufficient to capture frequency components up to the 100th harmonic. This is obviously far beyond practicable interest, which as previously described was considered to be confined to the low order harmonic components. These high sampling rates were therefore not intended to resolve high order harmonic components, but rather, were taken as a measure to increase accuracy. Although changing the sampling rate does not influence the accuracy of an individual sampled point, through increasing the number of sampled points in the period of vibration, the statistical correctness of the data set is enhanced. This is because a closer approximation to a normal (Gaussian) distribution of errors, which arise through both discretisation and signal noise, is obtained. An increase in accuracy was therefore expected in the evaluation of Fourier coefficients of the low order harmonic components, compared to a data set with relatively few sampled points. The minimum number of 200 sampled points in a period of the first harmonic response and 100 in the second were considered adequate for this purpose, whilst not presenting any serious problem in terms of data storage.

The sampling of data channels on the PC-74 data acquisition card was performed sequentially, with the time between sampling of consecutive channels defined by the overall sampling rate, i.e. the sampling rate multiplied by the number of channels being sampled. This meant that whilst the sampling of channel 1 (pressure transducer 1) was initiated by the trigger signal, the sampling of other channels were initiated slightly later, with the response of the fifth transducer triggered latest of all. To prevent a consistent phase error being introduced by this process (within the range $0° - 1.5°$), a simple

correction was subsequently introduced during post processing to maintain accurate phase reference to the blade motion.

| | Test case reduced frequency, k | | | |
	0.15	0.25	0.50	0.75
Nominal frequency, Hz:	4.0	6.7	13.4	20.1
Sampling rate, Hz:	1000	2000	3330	5000
No. samples / period:	249	299	248	249

Table 4.1: Sampling rates

(Nominal frequencies based on ambient conditions of 1 atmosphere and 20°C)

The measurement of blade vibration frequency on the data acquisition card was achieved through sampling the trigger signal, provided by the transmissive optical Schmitt sensor, on an additional data channel at the rates described in table 4.1. This introduced a maximum discretisation error of +/- 0.25% in the measurement of the specified frequency value, which was prescribed in order to match the test case reduced frequency and Reynolds number.

During preliminary testing, the high frequency response trigger channel on the data acquisition card was observed to function erratically and this hardware trigger mechanism was replaced by a software procedure which operated on the sampled trigger response (labelled as the counter input on figure 4.8). In this arrangement, data acquisition was arbitrarily triggered by keyboard input on the p.c. and continued for a duration corresponding to approximately 3.5 periods. The sampled data from the trigger signal was then searched for the trailing edge of the trigger pulse, which provided the phase reference for the unsteady pressure data, and the data was stored for a two period interval beginning at this point. This procedure, unfortunately, introduced an additional discretisation error in referencing a fixed phase in the vibration of the blade which had a maximum value of +/- 0.75° and increased the error in frequency measurement to +/- 0.5% of the specified value. Although this situation is not ideal, it allowed a further check to be enforced, through replacing the single slotted plate on the blade drive with a plate cut with eight, equally spaced slots which functioned as a crude encoder. During testing, the time interval between the trailing edge signal from consecutive slots was displayed to provide a

qualitative indication of smooth rotation of the blade drive throughout the sampling interval. To ensure consistent phase reference to the blade motion during measurements with this eight slot arrangement, one of the slots was cut considerably wider than the others to provide a unique signal from the optical sensor which could be distinguished by the software as the trigger pulse.

In a further effort to improve the signal to noise ratio and remove the contribution from turbulent fluctuations, the unsteady pressure signals from each tapping were ensemble-averaged, the process of which is described by Eq. (4.2).

$$P(x,z,t) = \frac{1}{N} \sum_{n=1}^{N} P(x,z,t + nT) \qquad (4.2)$$

where N represents the number of periods averaged and T the time period.

It is important to note at this juncture that the process of ensemble-averaging acts to reduce the contribution from any random event which disguises the true signal. This includes the error contribution from discretisation, which has been discussed at length, as well as turbulence and electrical signal noise. And the errors previously described due to discretisation of a sampled pressure, and phase reference to the blade motion, are considerably diminished by the averaging over a number of periods. In addition to this measure, shielded, twisted pair wiring was employed throughout the data acquisition hardware to reduce the component of electrical noise.

During the first series of measurements it was found that ensemble-averaging over 40 periods was sufficient to capture a clearly defined periodic signal as indicated by figure 4.9, which shows a representative sample of raw and ensemble-averaged unsteady pressure measurements. This figure also provides qualitative justification of the procedures adopted for data acquisition, demonstrating the high level of temporal resolution achieved in both the raw data measurements and the final ensemble-averaged response, despite the low magnitude of unsteady pressure generated at the low speed operating conditions.

The procedures described in this section were co-ordinated and controlled by a dedicated software suite which interfaced with the Amplicon PC-74 data acquisition card. The software, named FLogger (Flutter Logger), performed several functions including the setting of flow conditions to match the prescribed test conditions, the calibration of
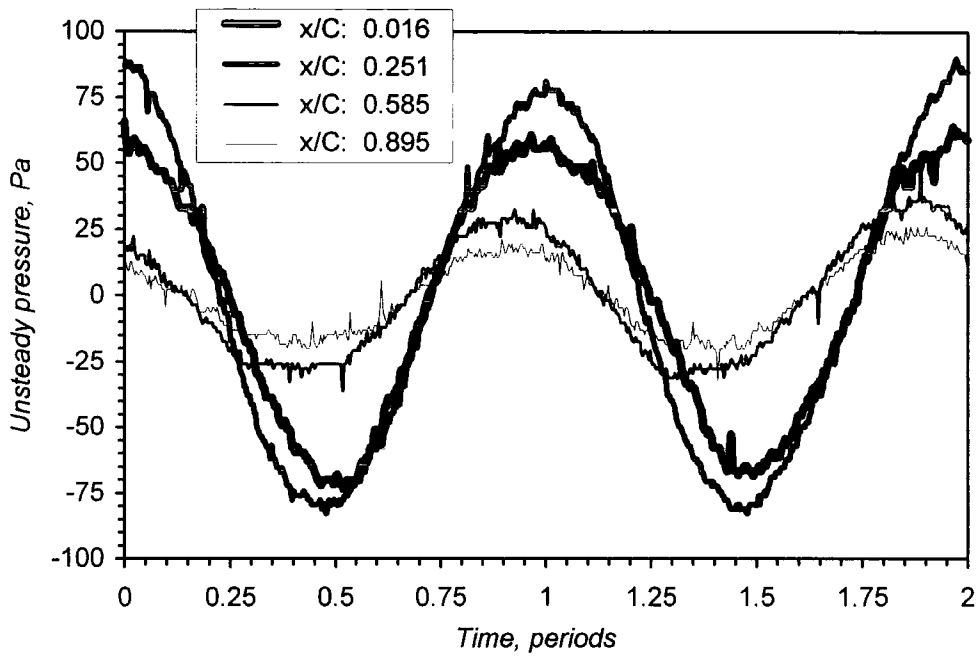
(i). Raw pressure response
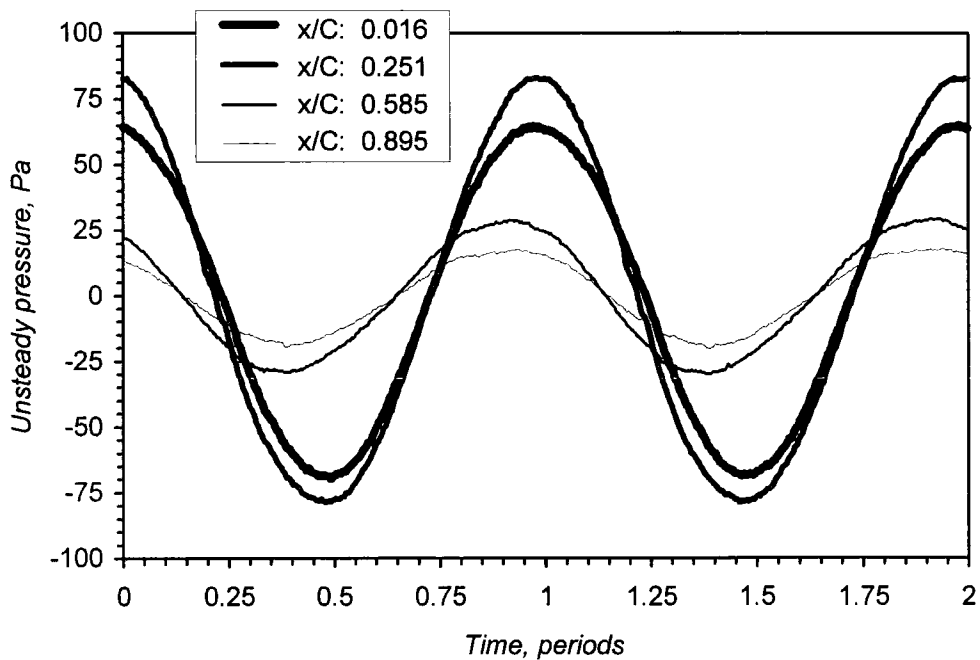
(ii). Ensemble-averaged pressure response (40 periods)

Figure 4.9: The acquisition of unsteady pressure signals and noise reduction (sample results at 70% span, suction surface, k: 0.25)

pressure transducers, the setting of sampling rates, the acquisition of synchronised raw pressure measurements, and the process of ensemble-averaging. The software also provided a visual display of measurements at each stage of the acquisition procedure which allowed errors and erroneous measurements to be readily identified.

4.2.2 Data Reduction

The ensemble-averaged pressure measurements were reduced into their harmonic components through evaluating the coefficients of the Fourier series for a periodic signal with application of Eq. 4.3 using the trapezium rule.

$$P(t) = \frac{1}{2}a_0 + \sum_{n=1}^{\infty}(a_n Cos(n\omega t) + b_n Sin(n\omega t)) \qquad \text{(4.3 i)}$$

$$a_n = \frac{2}{T}\int_0^T P(t)Cos(n\omega t)\,dt \qquad where\ n = 0, 1, 2, 3 ..... \qquad \text{(4.3 ii)}$$

$$b_n = \frac{2}{T}\int_0^T P(t)Sin(n\omega t)\,dt \qquad where\ n = 1, 2, 3 ..... \qquad \text{(4.3 iii)}$$

This allowed the fluctuating component unsteady pressure response (P') to be expressed as a summation of harmonic components, with each harmonic defined by a pressure amplitude (Ap_n) and a phase angle relative to the blade motion (ϕ_n), described by Eq. 4.4.

$$P'(x,z,t) = \sum_{n=1}^{\infty} Ap_n(x,z)Sin(n\omega t + \phi_n(x,z)) \qquad \text{(4.4)}$$

$$where \quad Ap_n = \sqrt{a_n^2 + b_n^2} \quad and \quad \phi_n = ArcTan\left(a_n/b_n\right)$$

Following this procedure, the amplitude of the first and second harmonic components and the phase angle of the first harmonic were corrected by the calibration procedure described in section 4.2.3, for attenuation and phase shift along the tubes which separated the blade surface tapping points and the pressure transducers.

To enable meaningful analysis of the test data, the amplitude of the harmonic components of the unsteady pressure are presented in the following chapters in the non-dimensional form described by Eq. 4.5. It is important to note here that the non-dimensional bending amplitude at the tip is introduced, rather than the local bending amplitude, to enable direct comparison of the amplitude of unsteady pressure at any of the spanwise sections.

$$|Cp_n| = \frac{Ap_n}{(\overline{P_{01}} - \overline{P_2})B_C} \tag{4.5}$$

To evaluate the work done, we first consider an arbitrary point on the blade surface vibrating at a local bending amplitude, B_L. In the present configuration, the displacement (s) of this point during vibration is described by,

$$s = B_L Sin(\omega t) \tag{4.6}$$

and the vibration velocity by,

$$V_{blade} = B_L \omega Cos(\omega t) \tag{4.7}$$

The instantaneous aerodynamic force at this point, resulting from the unsteadiness, in the direction of bending is given by,

$$F_1 = Ap_1 Sin(\omega t + \phi_1) \tag{4.8}$$

Where F_1 defines the force per unit area projected normal to the direction of bending. It is important to note here, that consideration is confined to the contribution from the first harmonic pressure response, because the contribution to work done from the higher harmonics integrates to zero through a period of blade vibration.

Now, since the rate at which work is done to the blade is defined,

$$\dot{W} = F_1 V_{blade} \tag{4.9}$$

then the work done over a period of blade vibration is therefore given by,

$$W_{cycle} = \int_T Ap_1 Sin(\omega t + \phi_1) B_L \omega Cos(\omega t) \ dt \tag{4.10}$$

55

which reduces to,

$$W_{cycle} = \pi \, B_L \, Ap_1 \, Sin\phi_1 \tag{4.11}$$

The work done (per unit blade span) at a given spanwise section in the present configuration is then obtained by integrating Eq. 4.11 over the blade surface,

$$W = \int_C \pi B_L \, Ap_1 \, Sin\phi_1 \, dA \tag{4.12}$$

where dA is the projected area, normal to the direction of bending

This can then be expressed in non-dimensional form as the local aerodynamic damping (ξ_C), described by Eq. 4.13, to enable global comparison of the extensive data generated by this type of work. The minus sign is introduced in Eq. 4.13 to ensure that positive work done corresponds with negative aerodynamic damping, i.e. a positive coefficient of local aerodynamic damping indicates a stable condition.

$$\xi_C = \int_C \frac{-\pi B_L \, |Cp_1| Sin\phi_1}{CB_C} \, dA \tag{4.13}$$

The overall aerodynamic damping (ξ) is then obtained through integrating the local aerodynamic damping over the blade span (Eq. 4.14), which indicates the aeroelastic stability of the full blade during the three dimensional mode of vibration.

$$\xi = \frac{1}{h} \int_h \xi_C \, dz \tag{4.14}$$

4.2.3 Calibration of Unsteady Pressure Signals

A calibration procedure was developed to correct the unsteady pressure measurements for phase shift and attenuation along the lengths of tubing which separated the blade surface tapping points and the pressure transducers. The purpose of this procedure was to

determine the rate of attenuation and phase velocity[†] of the first and second harmonic components of the unsteady pressure signals within the tubing, and thereby enable the true pressure response to be extrapolated from that recorded by the external pressure transducers. The validity of the calibration procedure, described in this section, was reliant upon four basic assumptions which are summarised below:

- A harmonic pressure signal attenuates at a constant rate and propagates at a constant velocity within all the tapping tubes.

- A pressure signal containing multiple frequency components obeys the principle of linear superposition, with the attenuation and phase velocity of each component being uniquely defined.

- End effects can be neglected.

- Resonance can be neglected.

These assumptions were considered reasonable, since a constant radius was maintained throughout the tubing, the tubes were of significant length (0.35 - 0.51 m) compared to the radius (4 $\times 10^{-4}$ m), but considerably lower than the wavelengths of the pressure waves under scrutiny, and the amplitude of the pressure waves was low.

The calibration procedure was performed within the confines of the test facility previously described, prior to the acquisition of set of unsteady pressure measurements, with the blade vibrating at the prescribed frequency for that particular test case. Under these conditions, the rates of attenuation and phase velocity of the first and second harmonic pressure signals were determined through the acquisition of the Fourier decomposed pressure response from two tappings[‡], for separate cases with increasing tube lengths (in the range 0.4 to 1.2 m). A typical result of this calibration procedure is presented in figure 4.10, which shows the phase shift and attenuation of the first harmonic component of the pressure signal at a blade vibration frequency of 13.2 Hz (k: 0.50).

[†] The phase velocity describes the propagation velocity of the pressure wave, which is expressed in non-dimensional form relative to the undisturbed speed of sound.

[‡] The two tappings were selected to provide a representative range of amplitude of the first harmonic pressure response.

57
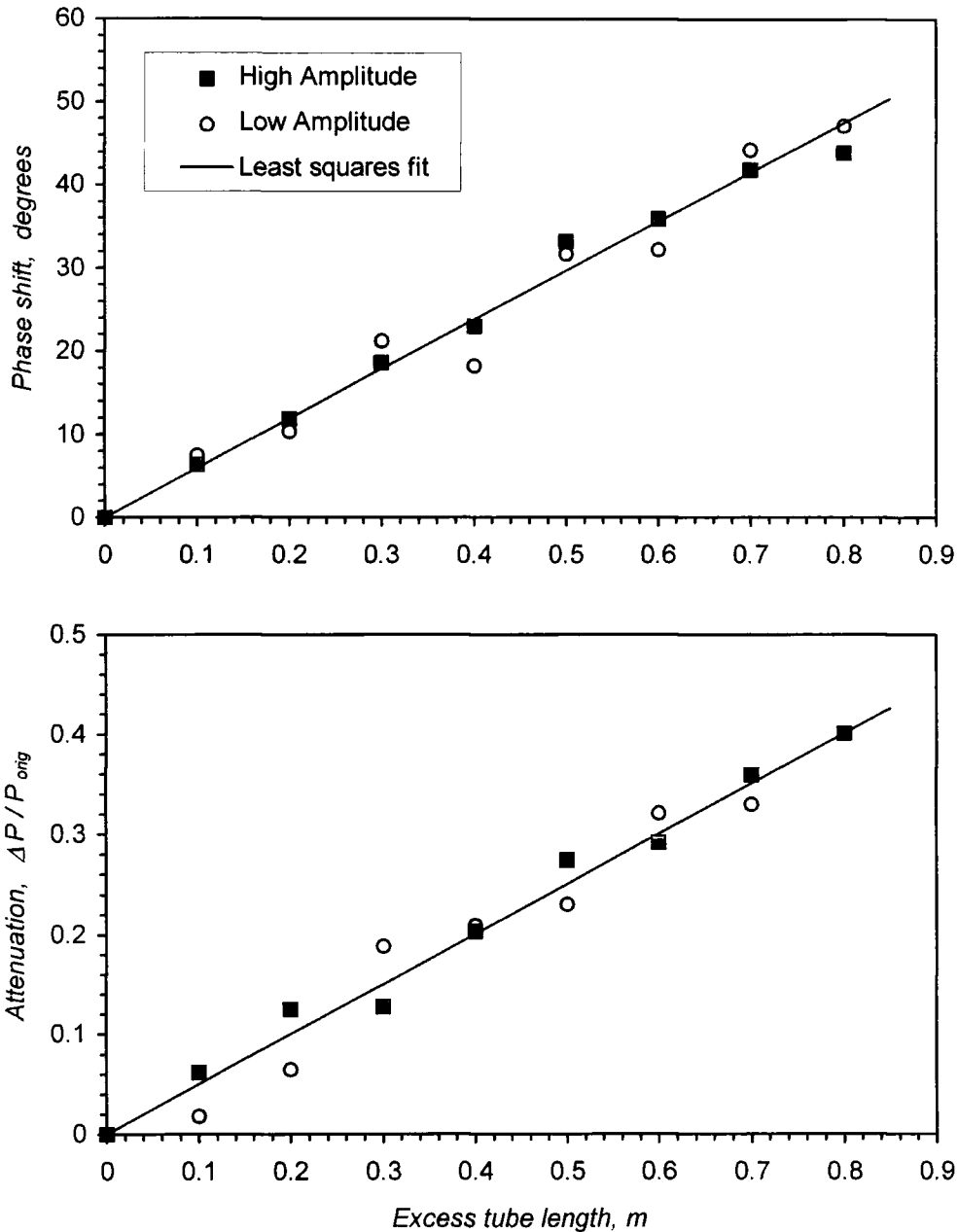
Figure 4.10: Correction for phase shift and attenuation of unsteady pressure signals (Calibration plot - first harmonic component at 13.2 Hz; orig. tube length: 0.45 m)

The plots shown in figure 4.10 clearly demonstrate phase shift and attenuation to have a linear relation with tube length, which was defined for the purpose of the calibration by the least squares best fit line also shown. The gradient of the best fit line on the phase shift calibration plot described the phase shift per unit length of tubing, which was simply exploited to correct the phase angle of the first harmonic pressure response measured by the pressure transducers. Similarly, the gradient of the best fit line in the attenuation

58

calibration plot - when extrapolated to zero tube length - defined the attenuation of the first harmonic component of the pressure signal per unit length of tubing, which was subsequently employed to correct the amplitude of this harmonic component.

The results of the calibration procedure for first harmonic pressure measurements in the first phase of unsteady pressure measurements are summarised in table 4.2. The table describes the attenuation and phase shift (also expressed as non-dimensional phase velocity) per unit length of tubing for each test case.

Test case k	frequency (Hz)	Attenuation (dP / P) per m	Phase shift degrees per m	Phase velocity (a/V_{phase})
0.15	4.04	0.130	27.8	6.50
0.25	6.8	0.245	44.6	6.20
0.50	13.2	0.406	59.3	4.24
0.75	20.4	0.582	60.7	2.81

Table 4.2: Summary of results for calibration of unsteady pressure measurements (Attenuation and phase shift defines the correction of 1st harmonic pressure)

It is apparent from table 4.2, that the pressure waves decay rapidly, especially at the higher frequencies, through the tubing and propagate at a fraction of the speed of sound, with the lower frequencies propagating at the lowest rate. This marked decay of the unsteady pressure waves within the tubing and the low rate of propagation meant that considerable correction was made to the first harmonic pressure measurements. In the worst case this corresponded to an amplitude correction of 29.7% and a phase shift correction of 31.0° (k: 0.75; frequency: 20.4 Hz; tube length: 0.51 m). This significant level of correction clearly indicated the accuracy of measurements to be dependant upon the validity of the calibration procedure, and verification of the results presented in table 4.2 was sought to instil confidence in the approach adopted.

The study of the behaviour of pressure waves propagating in cylindrical tubes dates back to the nineteenth century, occupying the likes of Kirchoff and Rayleigh. Some of the most notable contributions to the understanding of this problem are summarised by Tijdeman (1975). The analytical and numerical solutions presented in his work demonstrate the rate of propagation and attenuation of pressure waves in long cylindrical tubes to be

predominantly governed by the reduced frequency $(k = \omega R / a)$ and shear wave or Stokes number $(s = R\sqrt{\rho\omega / \mu})$. Furthermore, under satisfaction of the conditions $k \ll 1$, i.e. low reduced frequency, and $k/s \ll 1$ in long tubes, Tijdeman shows the attenuation and rate of propagation to be predominantly determined by the shear wave number alone. In the present case - for a tube with radius 0.4 mm and conditions in described in table 4.2 - the reduced frequency falls into the range 3.0×10^{-5} to 1.5×10^{-4} and the shear wave number varies between 0.5 and 1.25, which clearly satisfies the criteria described.
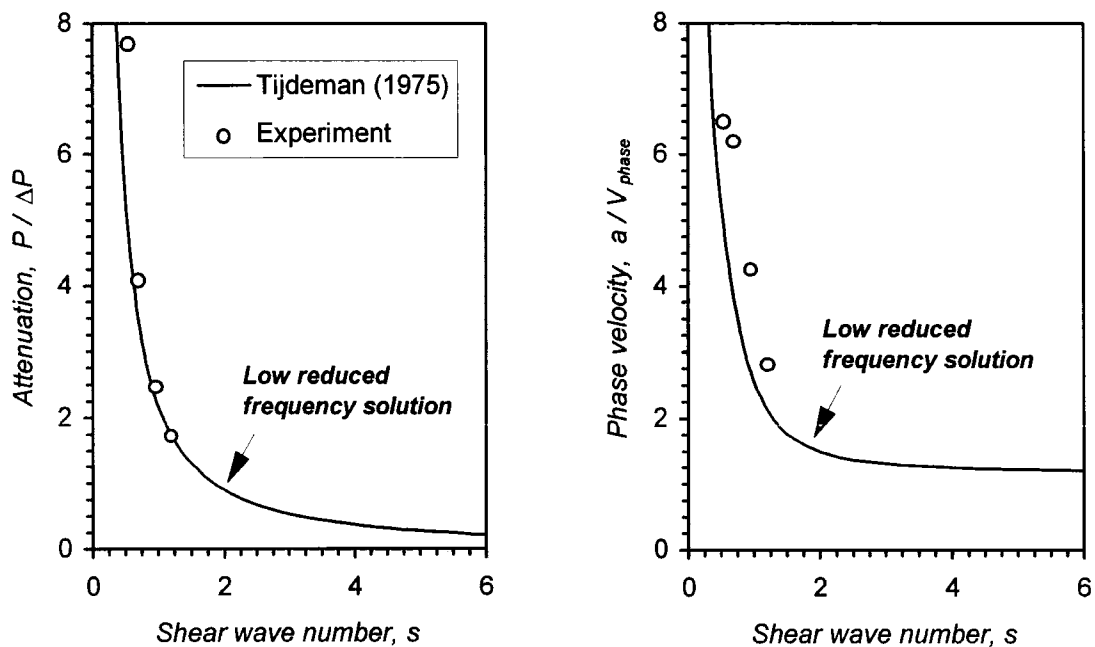
Figure 4.11: Attenuation and phase velocity of pressure waves in the tapping tubes (Experimental measurements are provided by the calibration procedure and the 'low reduced frequency' solution is taken from Tijdeman, 1975)

The plots in figure 4.11 show the analytical 'low reduced frequency' solution, presented by Tijdeman (1975)[§], for the rate of propagation and attenuation of pressure waves in cylindrical tubes as a function of shear wave number. The plots also shows the response of the tubing measured during the calibration procedure previously outlined and summarised in table 4.2. The excellent agreement between the measured response and

---

[§] The analytical 'low reduced frequency' solution presented by Tijdeman was taken from contributions by various authors, and validated against a complete numerical solution under the criteria $k \ll 1$ and $k/s \ll 1$.

that predicted by the 'low reduced frequency' solution provides strong evidence in support of the calibration procedure, demonstrating the correction introduced to be comparable to that predicted by analysis with sound physical basis.

As previously described, it was originally intended to correct the second harmonic component[**] of the unsteady pressure measurements by the same means as the first. The amplitude of the uncorrected second harmonic component was, however, extremely weak with a typical value an order of magnitude lower than the first harmonic. It was, therefore, not considered appropriate to perform the calibration procedure described and the maximum frequency of blade vibration in the test facility (25 Hz) precluded calibration at blade frequencies representative of the second harmonic component for test case reduced frequencies k: 0.50 and 0.75. It was, however, considered desirable to correct the second harmonic signals even though the purpose of these measurements was to provide a qualitative indication of non-linearity, and this was achieved through defining the rate of attenuation for each case from the 'low reduced frequency' solution presented in figure 4.11. Although it could be argued that this introduces some uncertainty regarding the accuracy of the corrected second harmonic, it meant that correction was consistently applied throughout the measurements. Higher order harmonic components were not corrected due to the lack of an appreciable signal in the ensemble-averaged measurements and calibration for the acceleration of the tapping tubes was not required due to the low rates of blade vibration.

4.3 Evaluation of Experimental Errors and Repeatability

Whilst the small errors associated with steady flow measurements can be simply defined by the accuracy of the individual instruments, the overall error introduced by the complex procedure for unsteady pressure measurements is far less clear. A series of tests were therefore performed to provide a quantitative indication of errors and repeatability, in order to define the accuracy of measurements presented in subsequent chapters and evaluate the performance of the test facility. This series of tests comprised of 40 sets of measurements, performed at a mid range reduced frequency (k: 0.35), from five tappings which were selected to provide a representative range of amplitude of unsteady pressure. In each set of measurements, the procedures described in sections 4.2.1 and 4.2.2 were

---

[**] The second harmonic component of the unsteady pressure response required correction for attenuation only, since the phase angle is of no practical importance.

61
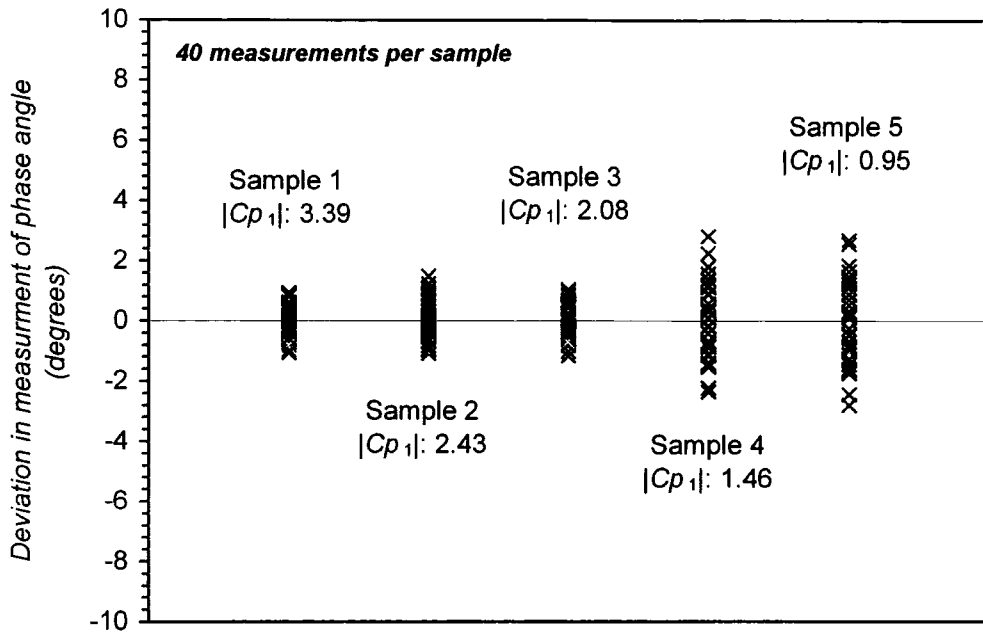
Figure 4.12: Repeatability and errors in the measurement of phase angle of the first harmonic pressure response
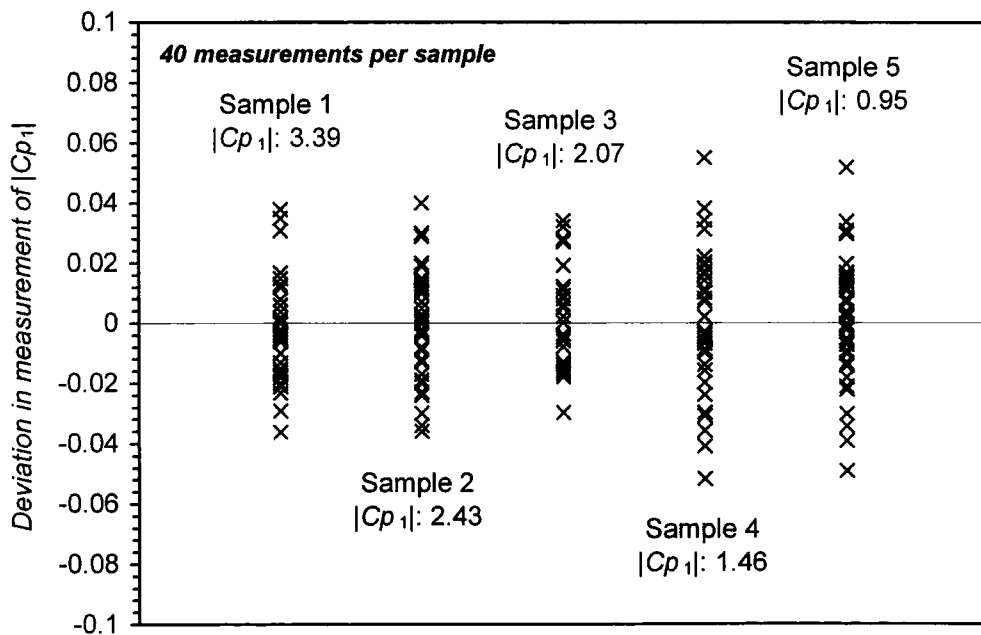
Figure 4.13: Repeatability and errors in the measurement of amplitude of the first harmonic pressure response

followed to acquire the amplitude and phase angle of the first harmonic pressure response from each tapping, which were then corrected for phase shift and attenuation as described in section 4.2.3. The results of these tests are presented in figures 4.12 and 4.13, which

show the deviation from the mean in the measured value of phase angle (ϕ_1) and amplitude ($|Cp_1|$) for each of the tappings.

Figures 4.12 and 4.13 demonstrate an excellent level of repeatability, which accounts for the contribution of random errors, with all deviations in the measurement of phase angle falling within the range +/- 4° and within +/- 0.06 for the non-dimensional amplitude of the first harmonic pressure. The plots therefore indicate an exceptional level of accuracy with an overall standard deviation of 0.93° in measurement of phase angle and 0.018 in the measurement of $|Cp_1|$.

Although the standard deviations expressed above are representative indications of the influence of random errors, which include inaccuracies in the setting of operating conditions for each case, the accuracy of the pressure transducers and the process of discretisation, they do not account for systematic errors, i.e. those which consistently shift the measurements. The most significant source of such error was perceived to be the correction for phase shift and attenuation in the tapping tubes, which was consistently applied to the measurements presented in figures 4.12 and 4.13. In order to evaluate the accuracy of this correction, the deviation of measurements from the best fit lines, shown in figure 4.10, was recorded for the calibration of first harmonic signals at each test case reduced frequency. The standard deviation of these calibration measurements was 2.45° in phase angle and 0.042 in $|Cp_1|$. Again, this demonstrates a good level of accuracy, which combined with the results presented in figures 4.12 and 4.13 allows an overall error band to be confidently established that envelopes the standard deviation of measurements. This error band was conservatively estimated as +/- 6° in the measurement of the true phase angle (ϕ_1) and +/- 0.1 in the measurement of the true pressure amplitude ($|Cp_1|$). This represents a high level of accuracy for this type of experimental work and clearly demonstrates the ability of the test facility to provide reliable and accurate unsteady pressure measurements.

Chapter Five

The Experimental Results and Discussion

An extensive set of steady flow and unsteady pressure measurements, obtained at the conditions previously outlined in chapter 3, are presented and discussed. The chapter opens with five-hole probe measurements performed at the inlet and exit traverse planes and blade surface pressure measurements, which define the steady flow conditions for the oscillating blade experiments. The unsteady test data comprises of a detailed set of blade surface unsteady pressure measurements from five spanwise sections of tappings between 10% and 90% span, which were acquired with the turbine blade oscillating in a three dimensional bending mode over a range of reduced frequency between 0.15 and 0.75.

The steady flow measurements demonstrate the realisation of uniform inlet flow conditions in the test facility and a predominant two dimensional flow structure throughout the working section. Whilst the unsteady pressure measurements indicate a significant three dimensional behaviour of the unsteady flow around the oscillating turbine blade. And the results of an experimental evaluation of linearity, also included, indicate a predominant linear behaviour of the unsteady flow.

To the authors knowledge the results provide the first three dimensional test data of its kind, which may be freely exploited towards the validation of advanced three dimensional methods for blade flutter prediction.

5.1 Steady Flow Results

Figures 5.1 to 5.6 show the results of the steady flow measurements obtained at the flow conditions described in table 3.2. Figures 5.1 and 5.2 describe the inlet flow conditions, figure 5.3 the blade pressure distribution and figures 5.4 to 5.6 the exit flow conditions.

The five-hole probe measurements performed at the inlet traverse plane, presented as normalised total pressure distribution and velocity vectors in figures 5.4 and 5.5 respectively, demonstrate the realisation of reasonably uniform steady flow conditions. Only slight deviation is evident in the total pressure contours shown in figure 5.1, with the total pressure coefficient (which is normalised with the isentropic exit dynamic pressure) remaining within 2% of the mass-averaged value over the majority of the inlet traverse plane. Towards the endwalls in the right hand side of the traverse plane - as viewed in figure 5.1 - the deviation in total pressure exceeds this +/- 2% band, with the total pressure coefficient dropping below 0.97. This is most likely to be caused by boundary layer growth on the endwalls which extend upstream of the traverse location in these regions, as previously shown in figure 3.5(i), and losses incurred at the inlet to the working section. The deficit in total pressure is, however, clearly restricted to the near endwall region. Indeed, all measurements taken between the 2.5% and 97.5% spanwise locations fall into the +/- 2% deviation band. The inlet velocity vectors shown in figure 5.2 (plotted on a plane normal to the sidewalls at inlet to the working section) also demonstrate limited variation in the flow conditions when taken in context with the sensitive scale. Apart from the near wall regions, the velocity vectors indicate a rectilinear flow to be established at the inlet traverse location with a band of +/- 1° covering the variation in pitch and yaw angle and a standard deviation below 0.5°. Towards the test section sidewalls the measured deviation in flow angle is notably more significant, most especially near the left sidewall where the traverse location coincides with the inlet of the working section. Although there is some uncertainty regarding the accuracy of the five-hole probe measurements performed in the near wall regions, due to a lack of calibration for wall effects, the marked deviation in flow angle towards the left sidewall is believed to be a true indication of the flow structure, because it far exceeds the deviation measured in other near wall regions. The deviation in velocity vectors at the left sidewall, especially near the hub and tip spanwise locations, is indicative of a flow separation at inlet to the working section. This again, however, appears to be a localised phenomenon and flow visualisation performed with a mesh of cotton threads 0.1 axial chord lengths downstream of the inlet traverse plane showed a rectilinear flow structure in the near wall regions, indicating the reattachment of the separated flow.

The spanwise variation in blade surface pressure distribution measured between 10% and 90% span is shown in figure 5.3. The plot indicates uniform loading over the majority of the blade surface, at least between 10% and 90% span. Towards the tip section, at the
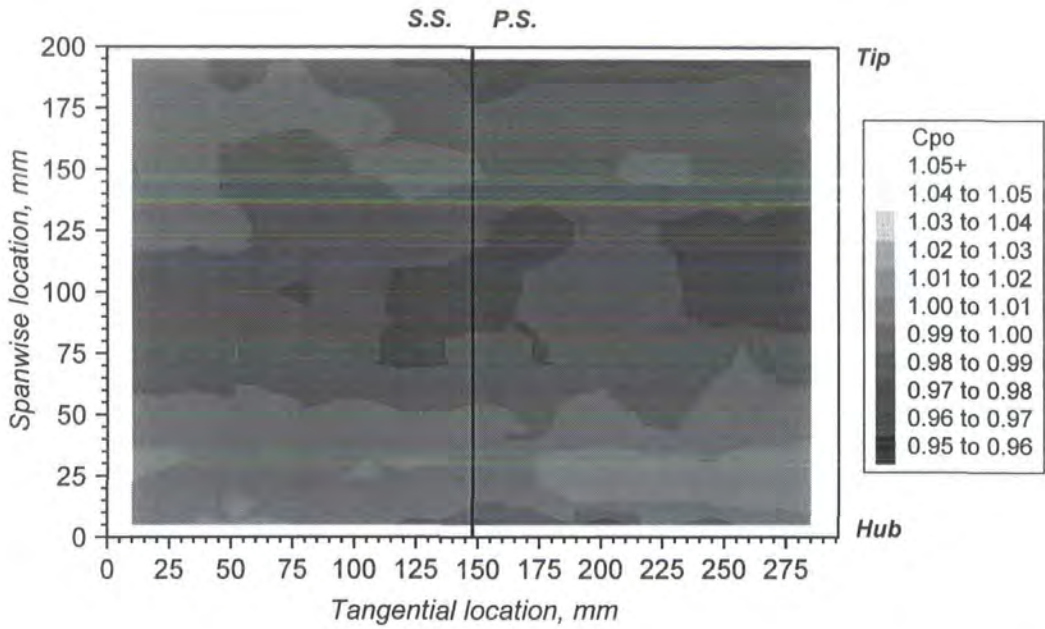
Figure 5.1: Normalised total pressure (Cp_0) distribution at the inlet traverse plane

$$where, \quad Cp_0 = (P_0 - \overline{P_2})/(\overline{P_{01}} - \overline{P_2})$$
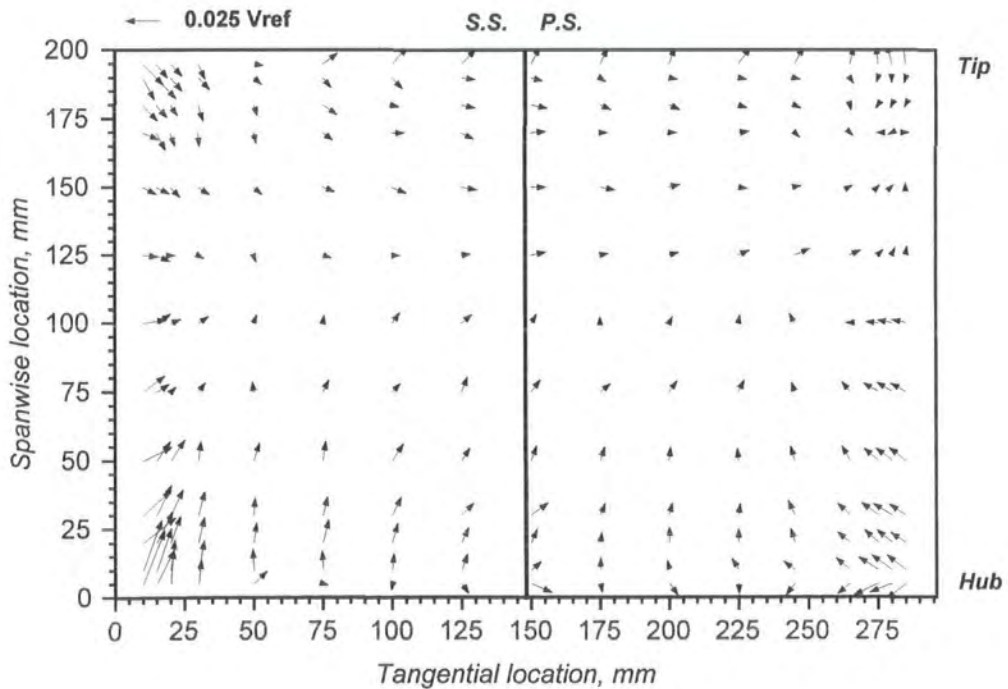
Figure 5.2: Velocity vectors at the inlet traverse plane

(Vectors are projected on to a plane normal to the direction of the inlet sidewalls)
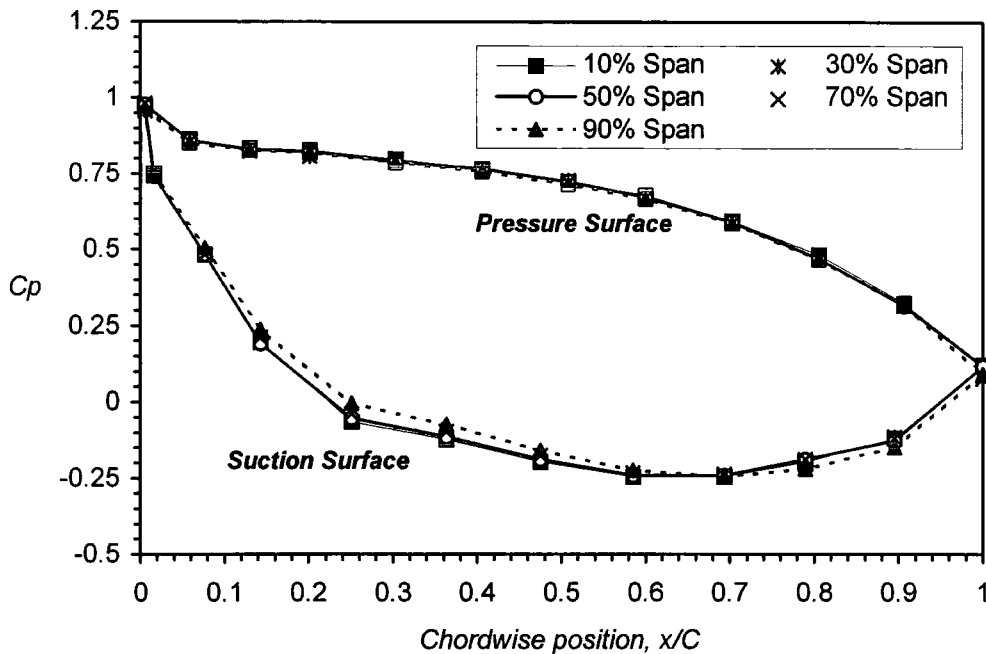
Figure 5.3: Steady flow blade surface pressure distribution

90% span location there is, however, some deviation evident in pressure distribution over the suction surface, with slight unloading between 10% and 50% chord and a small increase in suction aft of 70% chord, when compared to the measurements at other spanwise locations. These deviations are consistent with the development of a tip leakage flow, which is supported by the fact that they are not evident at the 10% span location, i.e. near the hub endwall. Overall, the blade surface pressure response is predominantly two dimensional though, with the deviations described over the suction surface at 90% span merely discernible in figure 5.3.

Figures 5.4 to 5.6 show the results of the five-hole probe measurements performed at the outlet traverse plane which is located 0.75 axial chord lengths downstream of the trailing edge. The distribution of total pressure loss (figures 5.4 and 5.6) and the secondary velocity vectors (figure 5.5) indicate a predominant two dimensional flow structure between 15% and 85% span, although the flow is clearly not periodic. Within this region the principal sources of loss are clearly associated with formation of a wake and the boundary layer growth over the test section sidewalls. The total pressure loss is, however, notably greater toward the right sidewall than the left, due to the higher velocities induced over the right sidewall which is contoured by the suction surface profile, the left sidewall being profiled with the pressure surface profile.
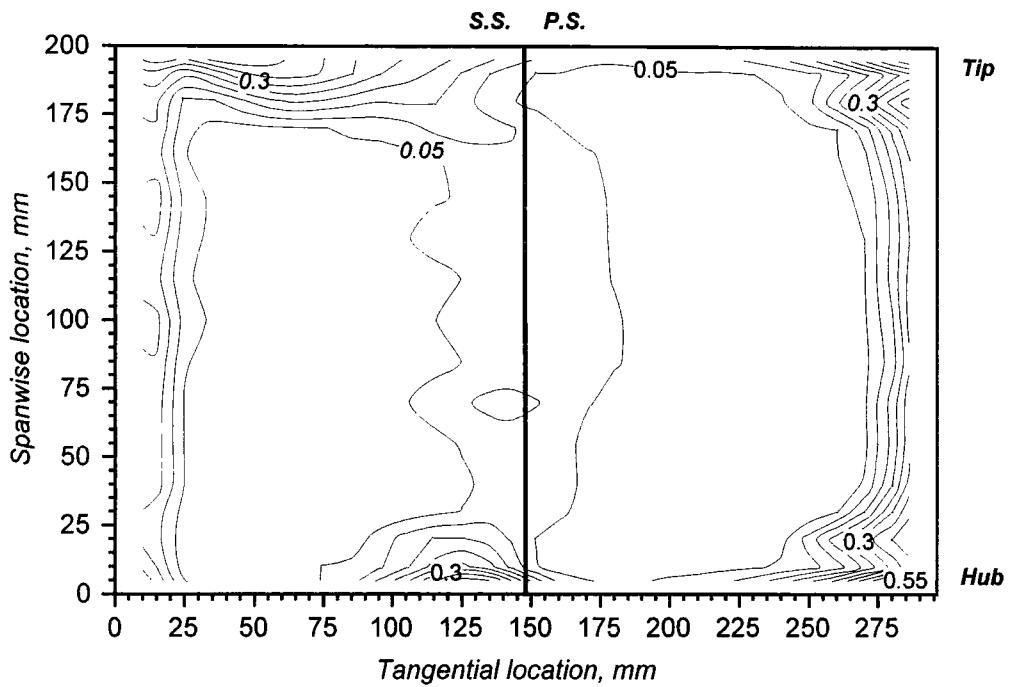
Figure 5.4: Total pressure loss coefficient (*Y*) measured at the exit traverse plane (Contour intervals set at increments of 0.05)
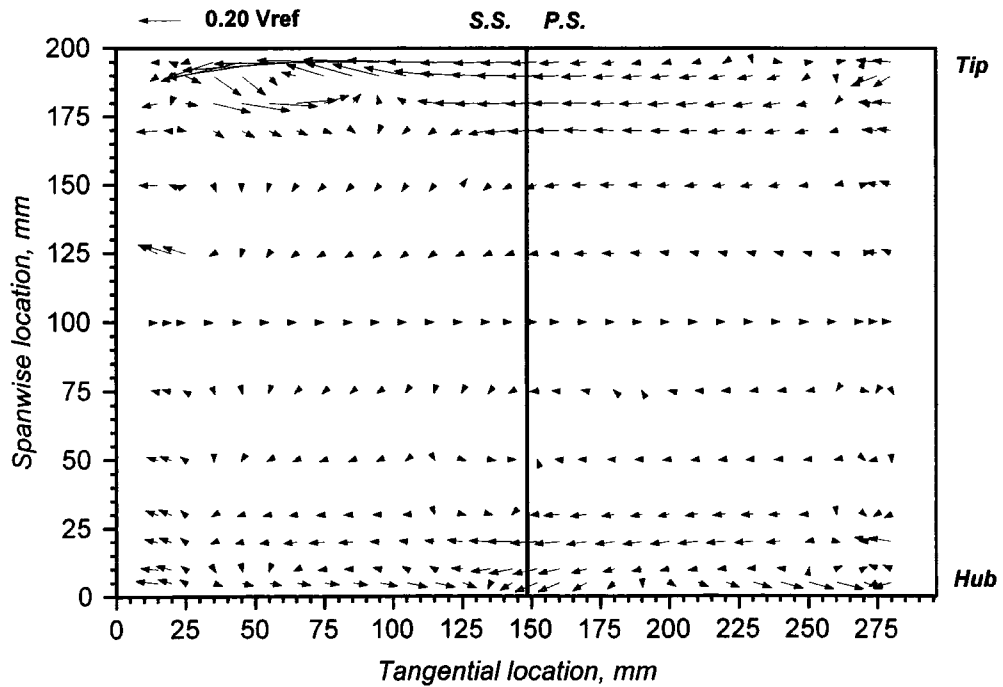
Figure 5.5: Secondary velocity vectors at the exit traverse plane
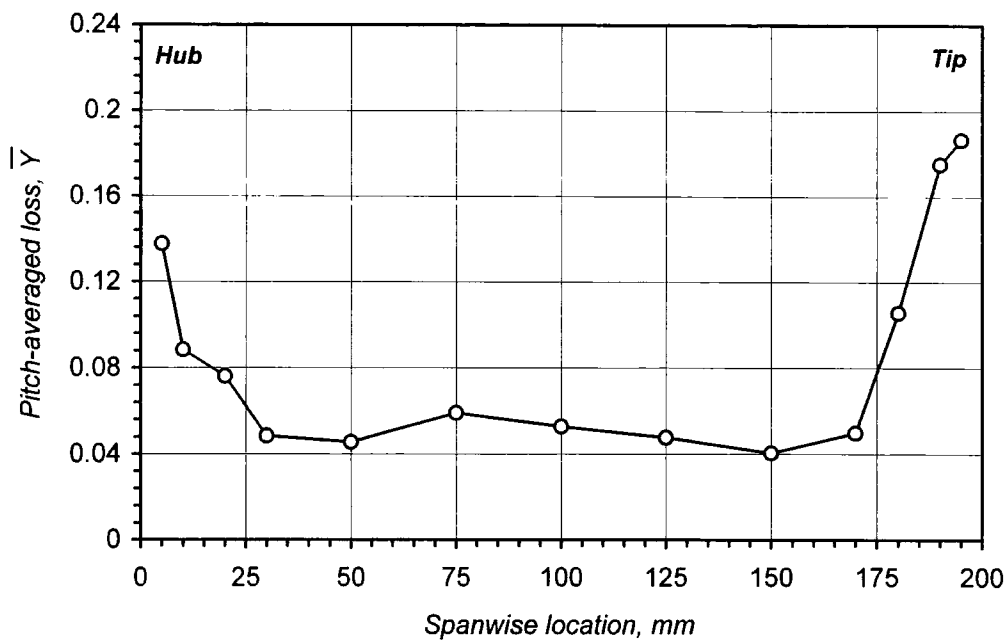
Figure 5.6: Spanwise variation in pitch-averaged total pressure loss coefficient at the exit traverse plane

In the near endwall regions of the exit traverse plane, the two dimensional flow structure breaks done with greater deviation evident in the secondary velocity vectors and a marked increase in total pressure loss shown in both the contour plot (figure 5.4) and the pitch-averaged measurements (figure 5.6). Towards the hub endwall, the distribution of total pressure loss shown in figure 5.4 is dominated by two distinct loss cores: the first located at the downstream pitchwise location corresponding to root of the blade suction surface and the second at the corner of the hub and the left sidewall. The location and structure of these loss cores are consistent with the development of blade passage secondary flow, although this cannot be fully corroborated due to the inability to resolve a passage vortex with secondary velocity vectors at these locations. Towards the tip endwall the total pressure loss is notably higher, as indicated by the spanwise distribution of pitch-averaged loss shown in figure 5.6. This increased loss is clearly associated with the vortex structure captured by the five-hole probe measurements in the downstream region corresponding with the left blade passage, which extends over approximately 15% span in the tip endwall region and is evident in both figure 5.4 and 5.5. The vortex structure described was established to be due to the development of a tip leakage flow which emerges from the tip gap on the suction surface side of the blade and convects high loss fluid in the near endwall region from the right hand passage into the left. This explains the comparatively

69

low level of loss experienced towards the tip endwall in the downstream region corresponding to the right blade passage. The prominence of the tip leakage vortex in the tip endwall region provides additional evidence to support the premise that the subtle deviations in blade surface pressure at 90% span are induced by formation of this secondary flow structure.

In addition to loss associated with the tip leakage vortex there is a smaller loss core towards the tip endwall, located near the right side wall. Like the distribution of total pressure loss observed in the hub endwall region, this is also consistent with the formation of a blade passage secondary flow, although the secondary velocity vectors at the traverse plane do not indicate the presence of a passage vortex.

In the closure of this discussion it is important to note that the spanwise extent of the three dimensional endwall flow structures described increases downstream of the blade due to the mixing out process. It may therefore be reasonably assumed that within the immediate vicinity of the blade, the region of three dimensional flow is confined to a region nearer the endwalls than that observed at the exit traverse plane.

5.2. Unsteady pressure Measurements

In this section a detailed set of blade surface unsteady pressure measurements are presented. The results were obtained with the blade vibrating in a three dimensional bending mode (B_C: 5.5% chord unless otherwise stated) at four different values of reduced frequency (k: 0.15, 0.25, 0.50 & 0.75), and at an operating Reynolds number of 4.5 x 10^5. A specification of other operating conditions is provided in table 3.2. At each setting of reduced frequency, unsteady pressure measurements were acquired at five equally spaced spanwise sections between 10% and 90% span to allow an evaluation of the three dimensional nature of the unsteady aerodynamics.

The discussion and presentation of results is divided into two parts. The first is entirely concerned with the first harmonic blade surface pressure response recorded at each test case reduced frequency, which is responsible for work done to the oscillating blade. Particular attention is given here to the three dimensional nature the unsteady flow and information provided by the measurements which indicate the predominant flow physics. The second part is concerned with an experimental investigation into the linearity of the unsteady aerodynamics.

5.2.1 First Harmonic Pressure Measurements

Figures 5.7 to 5.14 show the first harmonic pressure measurements obtained at each of the four test case reduced frequencies. There are two figures provided for each test case, the first describing the variation in the normalised amplitude of first harmonic pressure ($|Cp_1|$) over the blade surfaces and the second the variation in phase angle (ϕ_1) relative to the blade motion. The following eight figures therefore cover the full set of measurements.

Upon inspection of the set of first harmonic pressure measurements, there appears to be a well defined pattern to the results, with few exceptions, which is governed according to the chordwise position, spanwise location and reduced frequency. To clarify this comprehensive observation, we will first consider the first harmonic pressure measurements obtained at a reduced frequency of 0.15, which are presented in figures 5.7 and 5.8. These figures clearly show that, regardless of the spanwise location, there is a consistent shape to the distribution of amplitude and phase angle of first harmonic pressure over the blade chord on both the pressure surface and suction surface. In addition to this, there is a consistent trend evident in the results depending upon the spanwise location, the extent of which varies according to the chordwise location. Comparison of these measurements with those obtained at the other reduced frequencies reveal very similar patterns, with some trends becoming more or less pronounced and a general shift in the response, as shown in figures 5.9 to 5.14.

Such generalised observations may not at first appear helpful, since they do not give any indication about the exact nature of the unsteady flow. They do, however, highlight some factors which have a marked influence upon the unsteady pressure response and demonstrate the existence of some important unsteady flow effects. The chordwise trends in the results indicate the influence of the aerodynamic loading over the blade and the passage geometry upon the unsteady pressure generation, and the variation with reduced frequency equally demonstrates its influence. Most importantly, in terms of the present work, the nature of the spanwise trends in the results indicates a significant three dimensional behaviour of the unsteady aerodynamics.

The preliminary observations described here, form the basis of the detailed discussion which follows. First, the chordwise variation in measurements are described and explained, followed by the three dimensional effects associated with the spanwise variation in bending amplitude and finally, the influence of reduced frequency.
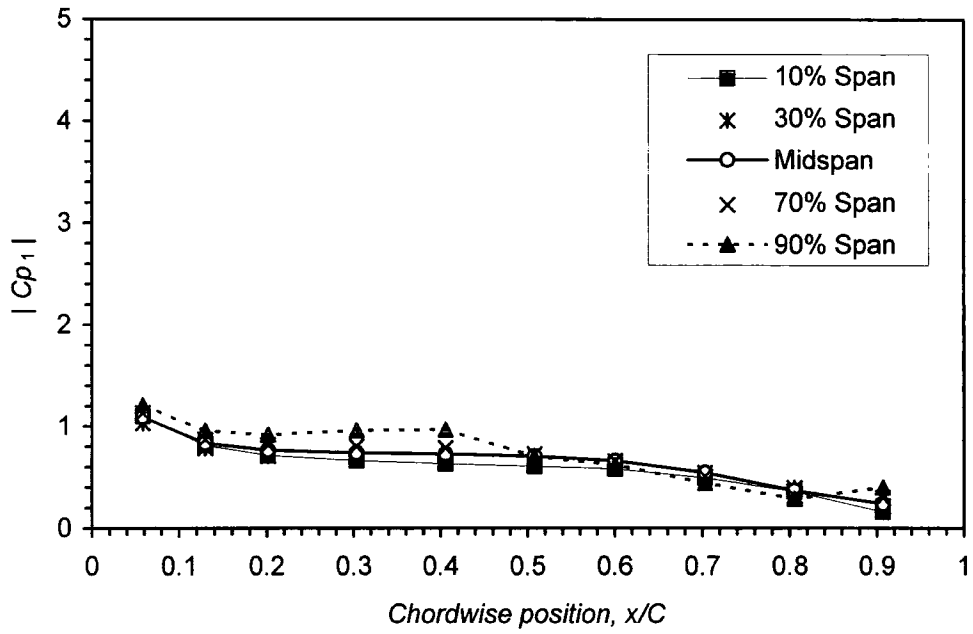
(i). Pressure surface response
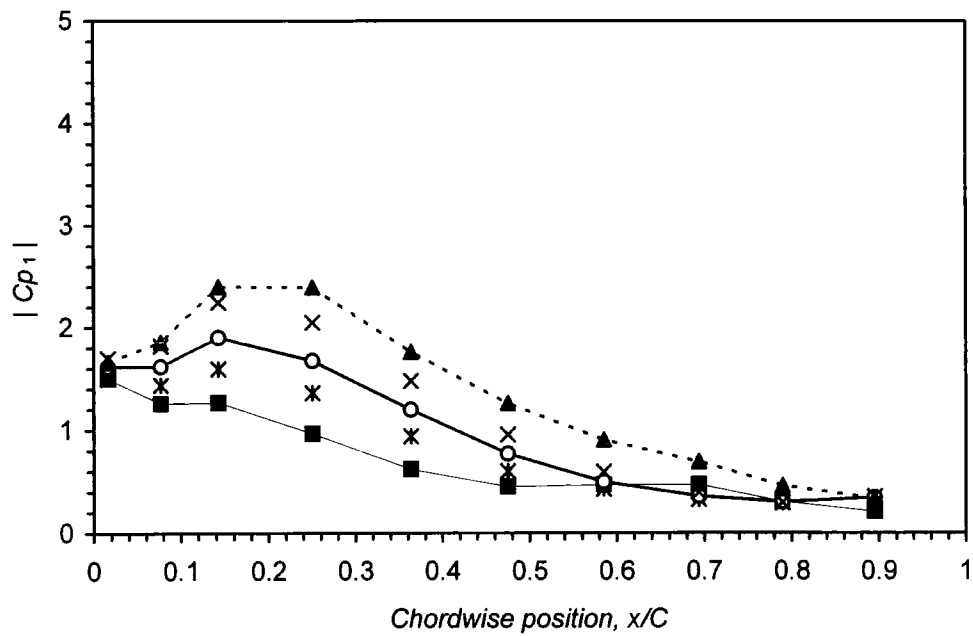
(ii). Suction surface response

Figure 5.7: Variation in amplitude of first harmonic pressure over the blade surface, *k*: 0.15
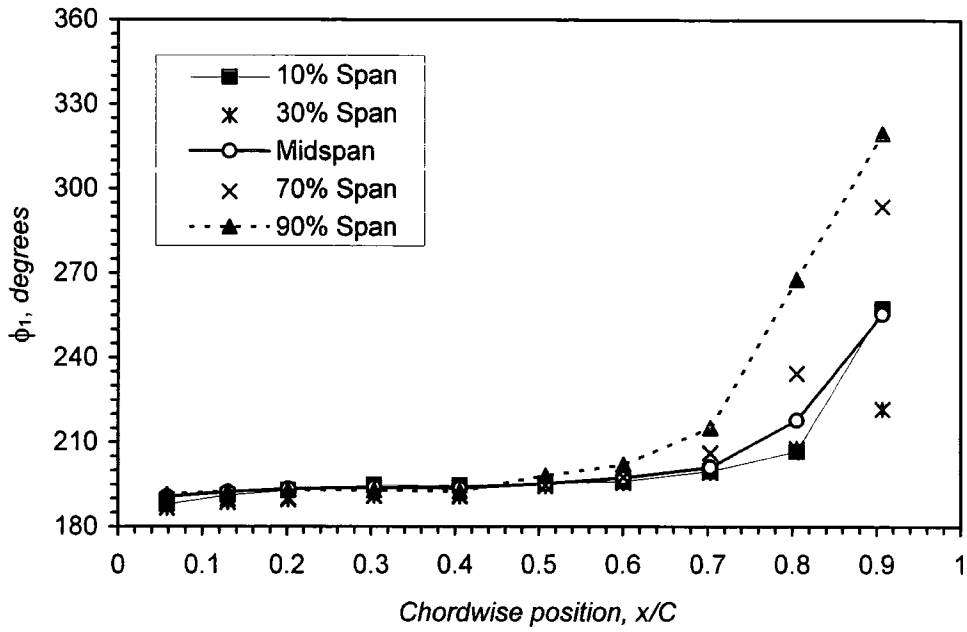
(i). Pressure surface response
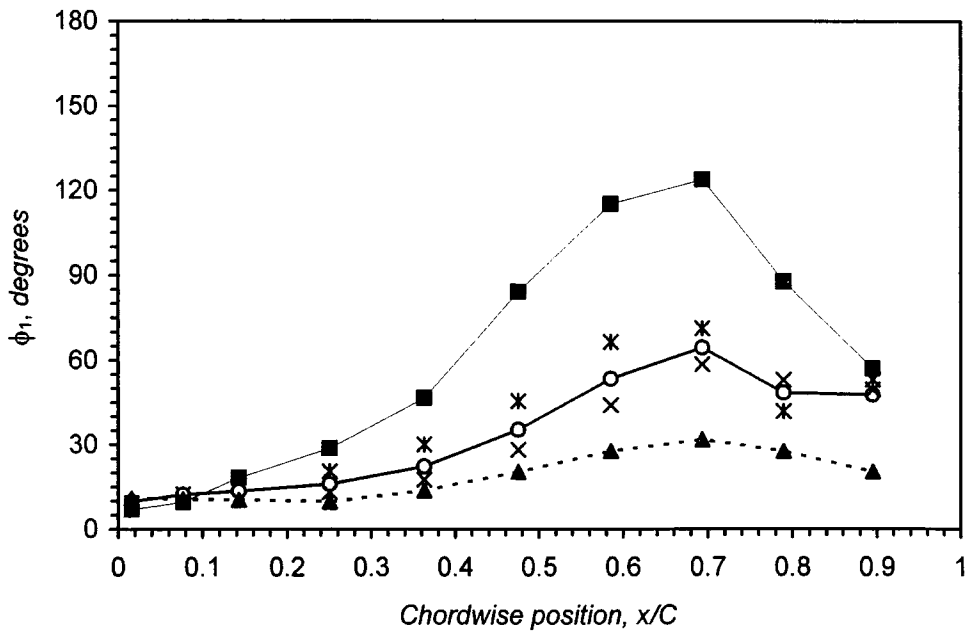
(ii). Suction surface response

**Figure 5.8: Variation in phase angle of first harmonic pressure
over the blade surface, *k*: 0.15**
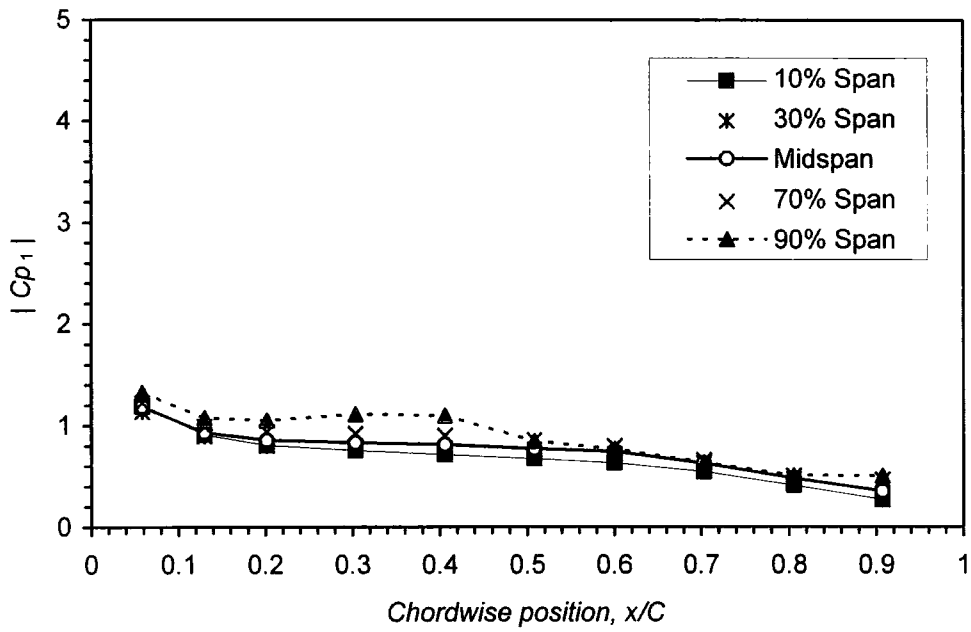
(i). Pressure surface response
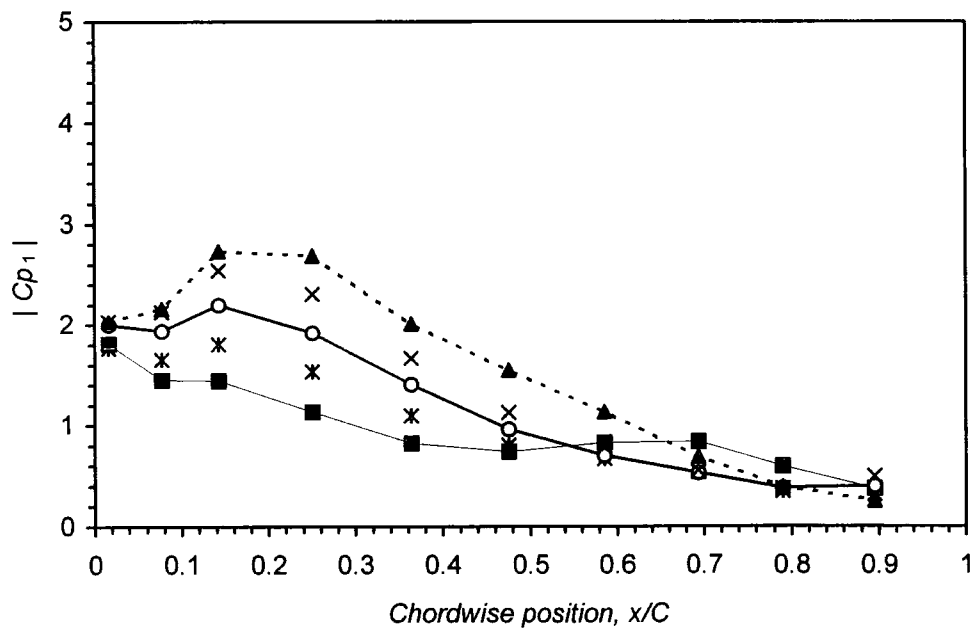
(ii). Suction surface response

**Figure 5.9: Variation in amplitude of first harmonic pressure
over the blade surface, *k*: 0.25**
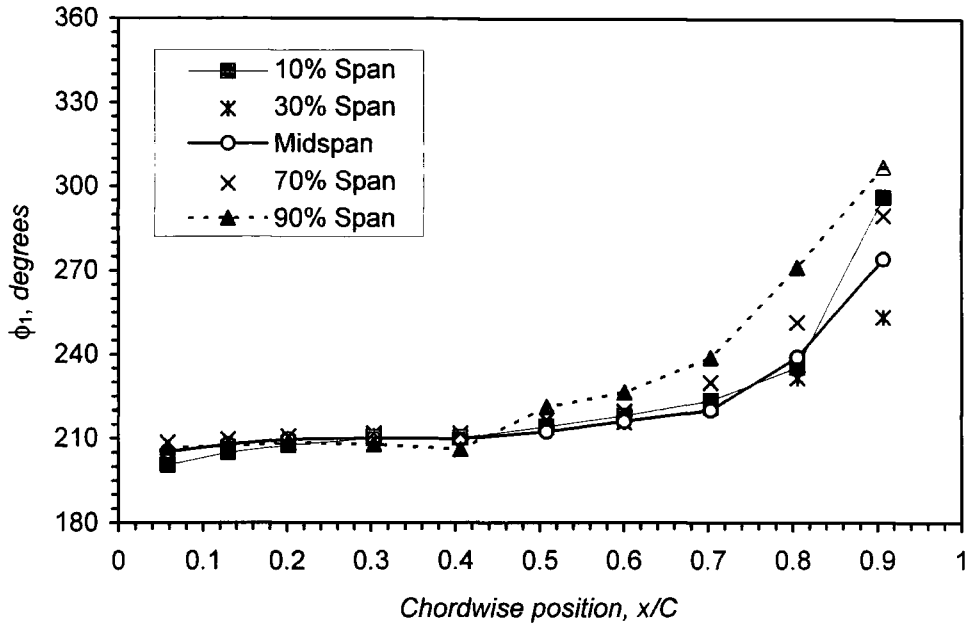
(i). Pressure surface response
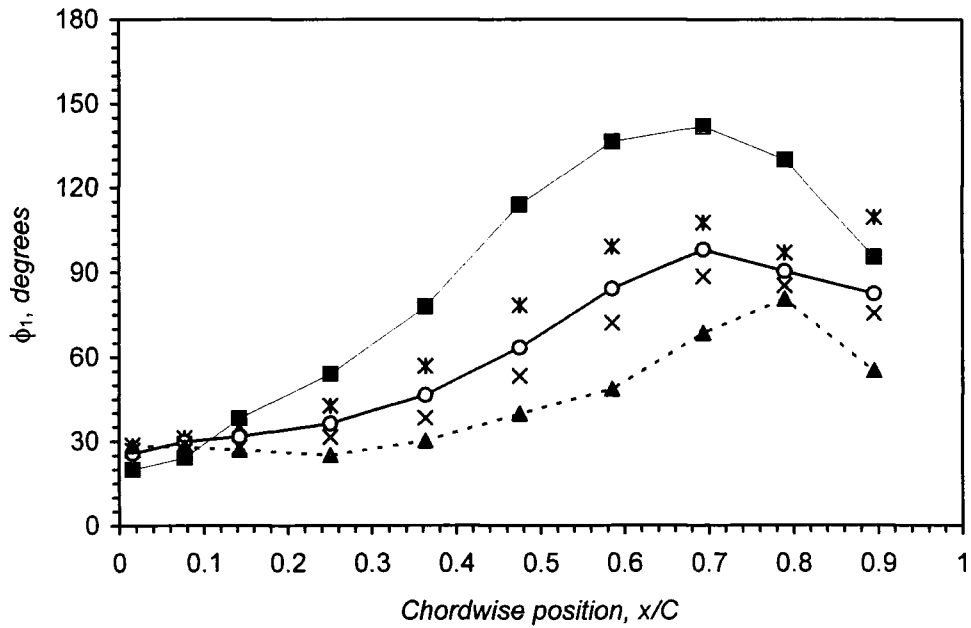
(ii). Suction surface response

**Figure 5.10: Variation in phase angle of first harmonic pressure
over the blade surface, *k*: 0.25**
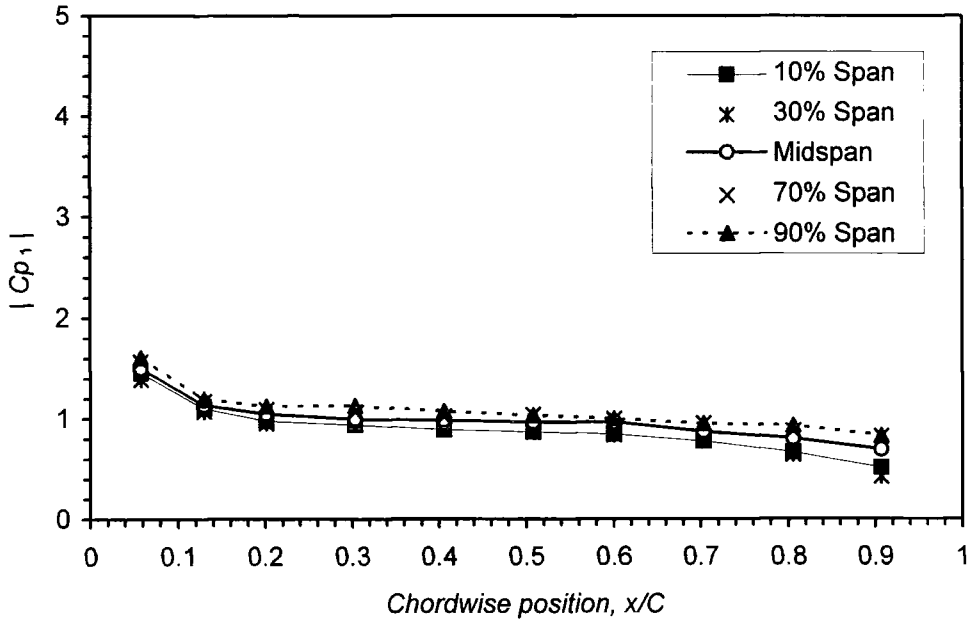
(i). Pressure surface response
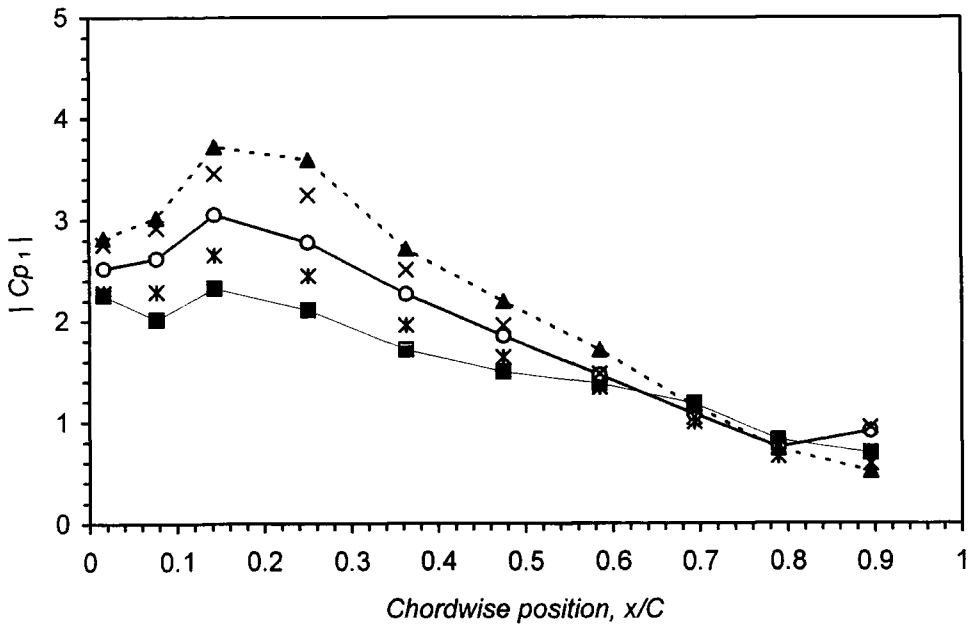
(ii). Suction surface response

**Figure 5.11: Variation in amplitude of first harmonic pressure
over the blade surface, k: 0.50**
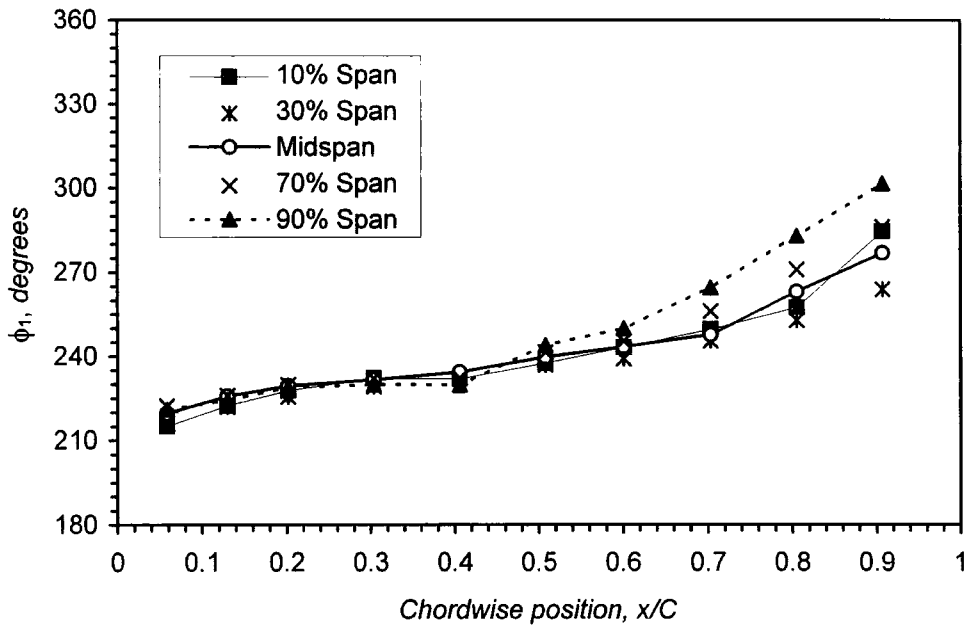
(i). Pressure surface response
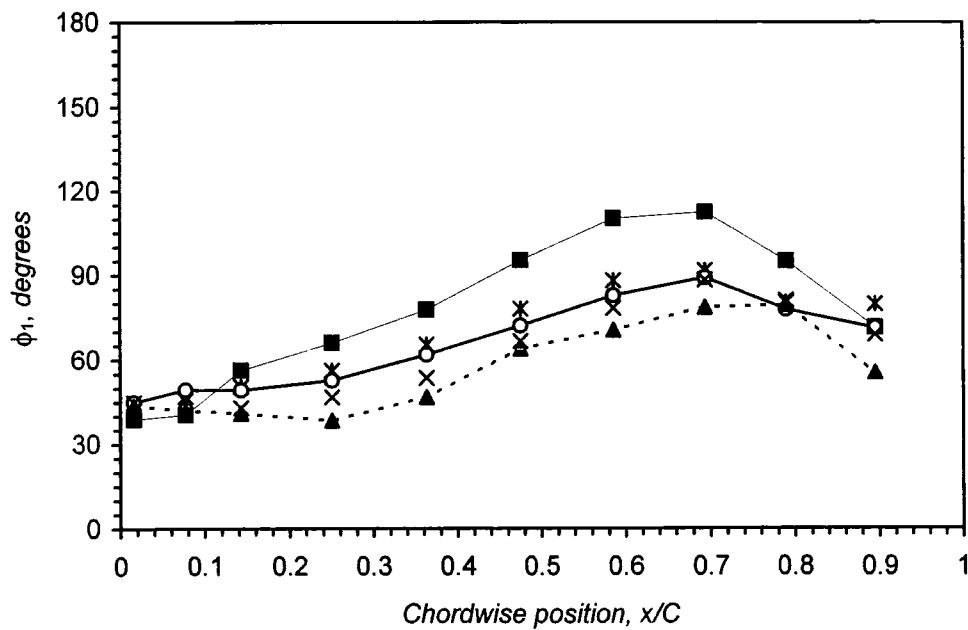
(ii). Suction surface response

Figure 5.12: Variation in phase angle of first harmonic pressure over the blade surface, *k*: 0.50
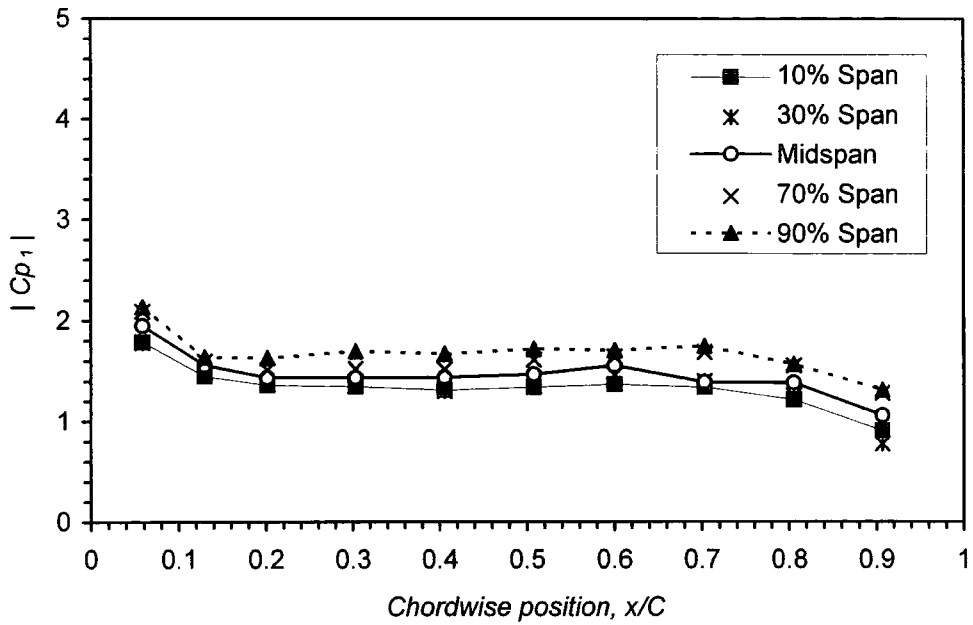
(i). Pressure surface response
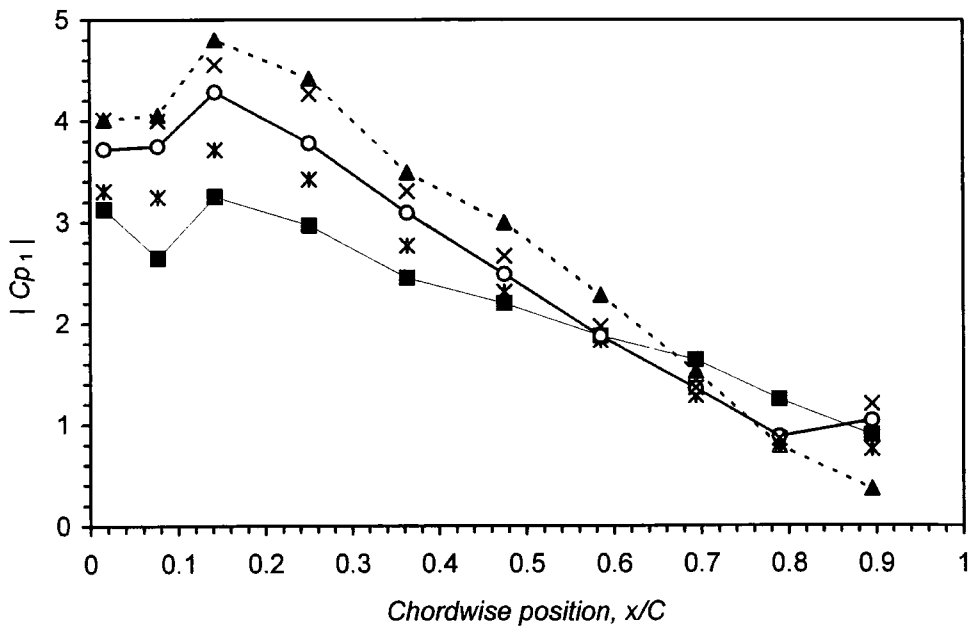
(ii). Suction surface response

Figure 5.13: Variation in amplitude of first harmonic pressure over the blade surface, *k*: 0.75
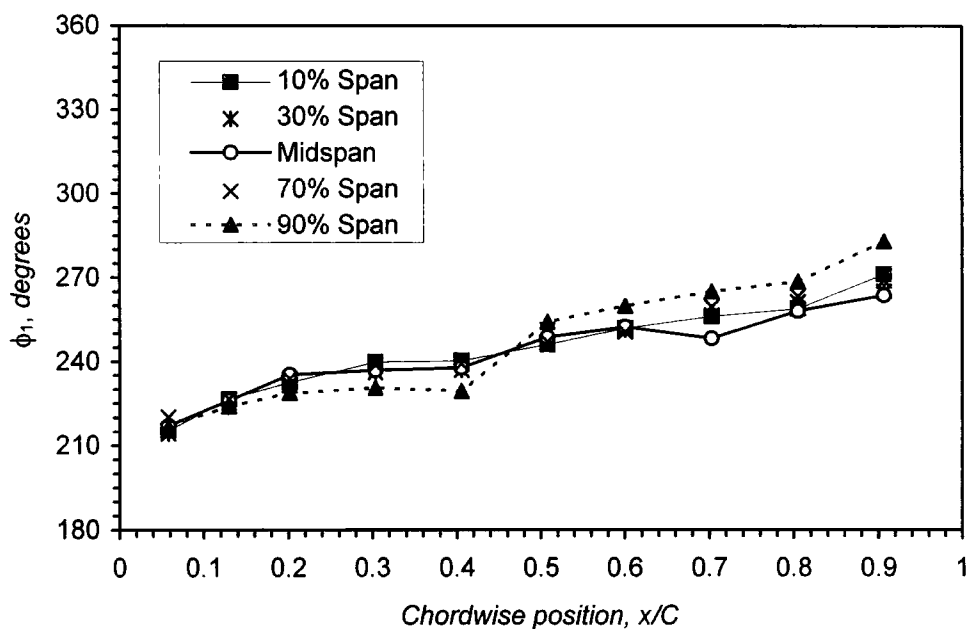
(i). Pressure surface response
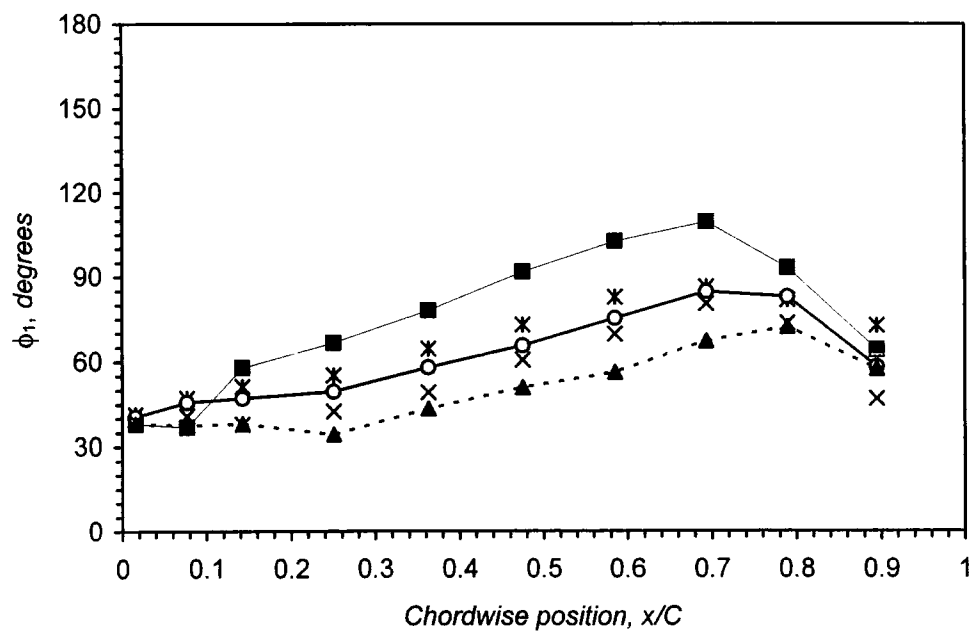
(ii). Suction surface response

Figure 5.14: Variation in phase angle of first harmonic pressure over the blade surface, *k*: 0.75

Throughout the range of reduced frequency, the amplitude of unsteady pressure is generally higher on the suction surface (figures 5.7, 5.9, 5.11 and 5.13), with a peak evident somewhere between 0% and 30% chord depending upon the spanwise location - the peak moving towards the leading edge for spanwise locations nearer the hub. Downstream of the peak amplitude of unsteady pressure on the suction surface, the amplitude decreases with a minimum value usually recorded at the 90% chord location, which corresponds with the tapping located nearest the trailing edge. Over the pressure surface, the amplitude is generally lower with a uniform distribution between 15% and 70% chord. Upstream of the 15% chord location, the amplitude increases slightly towards the leading edge, whilst downstream of 70% chord there is a gradual decrease towards the trailing edge, with the lowest amplitude also recorded at the 90% chord location on the pressure surface. These chordwise trends in amplitude of unsteady pressure exhibit a strong resemblance to the steady flow blade surface pressure distribution, shown previously in figure 5.3, with regions of highest unsteady pressure activity coinciding with regions of strong acceleration. This is most especially evident in the first 30% chord on the suction surface, where both the steady flow acceleration and amplitude of unsteady pressure are greatest.

The concentration of unsteady pressure activity in the forward 30% chord of the suction surface and towards the leading edge of the pressure surface suggests the unsteady pressure generation to be largely driven by an incidence effect, induced by the motion of the blade. Although the presence of the peak amplitude of unsteady pressure aft of the leading edge region on the suction surface (normally between 20% and 30% chord), indicates the change in passage area to be equally, if not more so, important in terms of the generation of unsteady pressure, since around this location the change is quite considerable.

The measured phase angle of the first harmonic pressure indicates a stable aeroelastic condition throughout the entire set of measurements, with a phase lead to the blade motion evident at all tapping locations on the suction surface and a phase lag over the pressure surface, as shown in figures 5.8, 5.10, 5.12 and 5.14. The distribution of phase angle over the pressure surface also follows a general trend, whereby it increases towards the trailing edge, although the gradient of this increase varies with reduced frequency and aft of 50% chord with spanwise location too. This variation in phase angle indicates that the unsteady pressure response over the pressure surface is lead by the trailing edge, with a pressure wave propagating upstream from this location. Over the suction surface the

variation in phase angle is somewhat different, with an increase in phase observed up to approximately 70% chord, typically followed by a drop in phase towards the trailing edge. This indicates that the unsteady pressure response near the trailing edge lags that directly upstream on suction surface. It is notable though, that this region coincides with an area of quite strong diffusion where viscous effects are likely to be influential.

To understand the influence of viscous effects upon the unsteady flow within the region of diffusion towards the trailing edge of the suction surface, it is important to consider the nature of the boundary layer - which may be transitional, entirely laminar or subject to a laminar separation bubble at the operating Reynolds number (4.5 $\times10^5$). The gradual changes in phase angle recorded along the blade chord within the region of diffusion does not, however, seem to indicate the presence of an unsteady laminar separation bubble given the previous experience of this unsteady phenomenon described by He (1998a). His work indicated, through measurements supported by a quasi-steady analysis, that an abrupt change in phase angle in the order of 180° could be expected in the unsteady pressure response around the point of reattachment of a laminar separation bubble, which does not fit the pattern of the present results. Under conditions of a laminar boundary layer, the flow may also be prone to an unsteady open type separation, whilst the likelihood of this behaviour would be greatly reduced for a turbulent boundary layer. A set of measurements was therefore repeated with a boundary layer trip[†] located on the suction surface, to force transition to a turbulent state and thereby highlight any unsteady flow effects attributable to laminar boundary layer over the suction surface and / or transitional effects.

The unsteady pressure measurements obtained with the boundary layer trip, at a test case reduced frequency of 0.25, are presented in figures 5.15 and 5.16 as the amplitude and phase of the first harmonic pressure response respectively. The measurements are plotted against those obtained at identical conditions without the boundary layer trip for three spanwise sections: 10% span, midspan and 90% span. Figure 5.15, clearly shows the amplitude of unsteady pressure to be unaffected by the boundary layer trip, although some discrepancies can be observed in the measured amplitude towards the trailing edge of the

---

[†] A conservative boundary layer trip design, provided by Kuk (1995) and based upon the criteria presented by Schlichting (1979) and Walker (1992), was adopted in the present work to ensure transition and prevent relaminarisation. The trip was located at a fractional surface distance (*l/C*) of 0.32 measured from the leading edge, and set with a height of 0.45 mm.

suction surface at 10% span. These discrepancies are, however, believed to be associated with leakage flow through a faulty gland at the root of the suction surface, which was replaced when the blade was removed for the fitting of the boundary layer trip, rather than an unsteady phenomenon induced by the state of the boundary layer. This point of view is supported somewhat by the fact that equivalent discrepancies are not evident towards the trailing edge of the suction surface at the midspan or the 90% span location.

In terms of the phase angle of the first harmonic pressure, figure 5.16 shows the response of the pressure surface to be largely unaffected by the introduction of the boundary layer trip, as might reasonably be expected. There are, however, some marked quantitative differences in the phase angle of the suction surface response between the measurements performed with and without the boundary layer trip. Aft of 15% chord, the phase angle of the unsteady pressure response with the boundary layer trip is consistently lower than that obtained without it, with the difference between the two sets of measurements becoming progressively more pronounced further downstream the blade chord. When considered in a qualitative sense, the measured phase angle over the suction surface for both cases is, however, very similar, with an increase in phase still observed along the blade chord up to approximately 70% chord, followed by a consistent drop in phase towards the trailing edge. This would suggest that the fundamental mechanism determining the nature of the unsteady pressure response is unchanged by the introduction of the boundary layer trip.

Although the set of measurements performed with and without the boundary layer trip do not explicitly indicate the important viscous effects in terms of the unsteady pressure response, some tentative conclusions can be drawn. First, the set of measurements combined with the observations of He (1998a) seem to indicate the absence of an unsteady laminar separation bubble. It also seems unlikely that the unsteady flow is characterised by an open type separation towards the trailing edge of the suction surface, given the excellent comparison between the amplitude of unsteady pressure and the good qualitative comparison in the measured phase angle. The quantitative difference in the measured phase angle with and without the boundary layer trip does, however, indicate the viscous effects to have some bearing upon the unsteady pressure response. These are most likely to be associated with the unsteady boundary layer thickness aft of 70% chord on the suction surface and the sensitivity of this boundary layer to information convected downstream, which may explain the drop in phase observed towards the trailing edge. In this respect, the behaviour of a laminar and turbulent boundary layer is only expected to be quantitatively different.
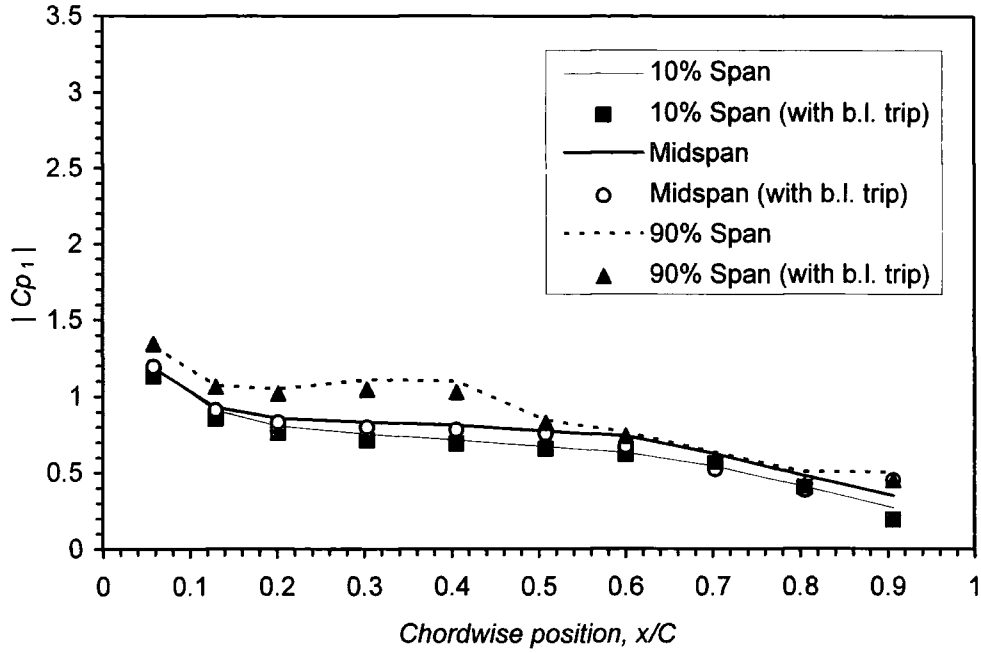
(i). Pressure surface response
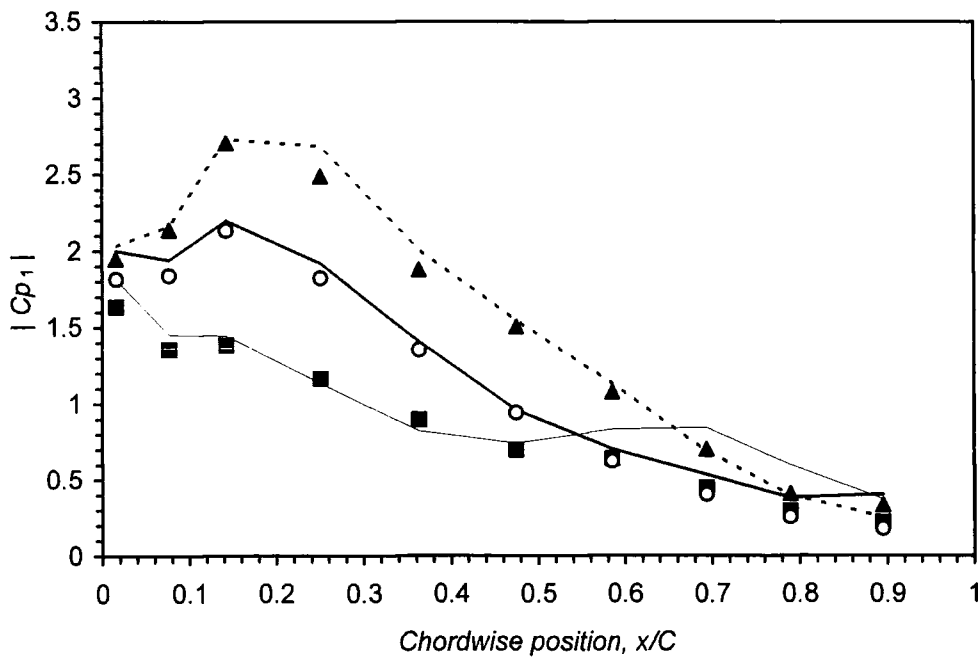
(ii). Suction surface response

Figure 5.15: Amplitude of the first harmonic pressure response with and without a boundary layer trip, *k*: 0.25
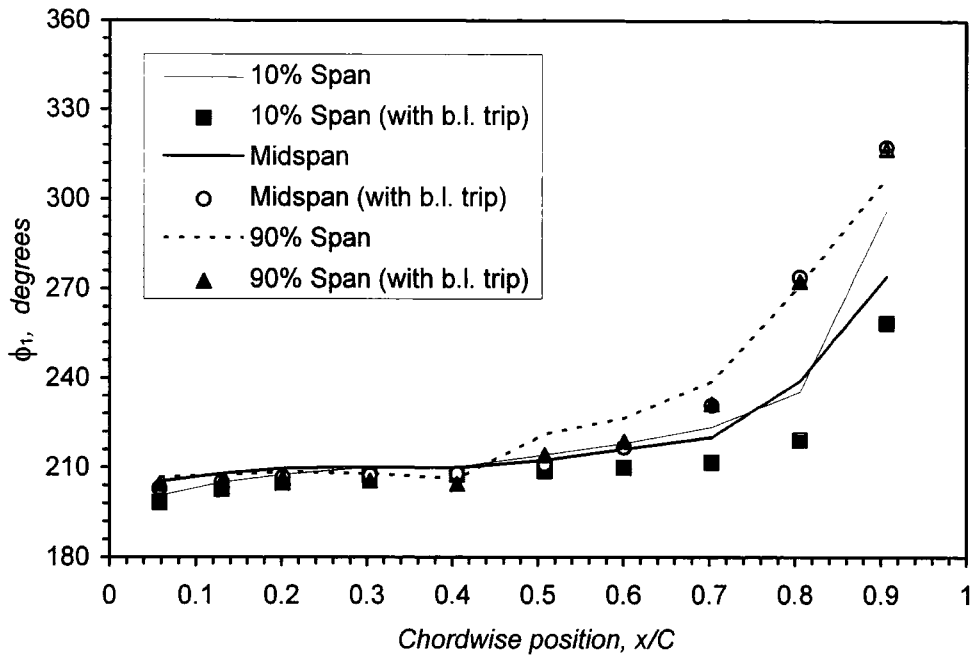
(i). Pressure surface response
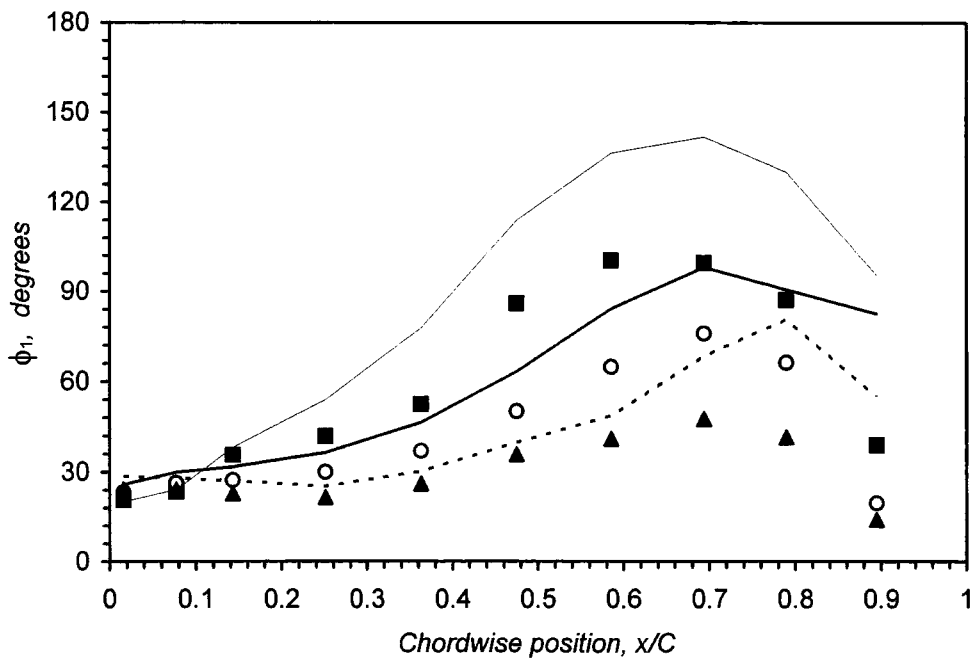
(ii). Suction surface response

Figure 5.16: Phase angle of the first harmonic pressure response, with and without a boundary layer trip, *k*: 0.25

In terms of the spanwise variation of the unsteady pressure response, there are several consistent trends in the results that indicate a strong three dimensional behaviour of the unsteady aerodynamics. These manifest most predominantly in the measured amplitude of unsteady pressure over the blade surfaces, previously shown in figures 5.7, 5.9, 5.11 and 5.13. At all values of reduced frequency, there is an almost uniform amplitude of unsteady pressure at any given chordwise location between 10% and 90% span, although fractional increases can be observed between these spanwise sections of measurements. In contrast to previous observations from two dimensional oscillating cascade experiments and computations, this demonstrates that the generation of unsteady pressure is almost entirely insensitive to the local bending amplitude, which increases by a factor of five between the 10% and 90% spanwise locations. The measurements therefore indicate a strong communication within the unsteady flow field between spanwise sections, with pressure waves propagating over the blade span to counteract the gradients that one might expect, given the variation in bending amplitude. In addition, the results clearly demonstrate the possibility of significant unsteady pressure generation at spanwise sections under very low, or even negligible, amplitudes of blade vibration.

The variation in amplitude of unsteady pressure over the suction surface also displays an insensitivity to the local bending amplitude, although to a lesser degree than that observed for the pressure surface. At chordwise locations between approximately 10% and 60% chord, there is a marked and fairly consistent increase in amplitude of unsteady pressure along the blade span which reflects the increase in local bending amplitude. The rate at which the amplitude of unsteady pressure increases along the blade span is, however, considerably lower than the corresponding increase in bending amplitude. Indeed, even in the most extreme case (25% chord on the suction surface at a reduced frequency of 0.25, shown in figure 5.9), the amplitude at 90% span is just one and half times greater than that recorded at 10% span, whilst as previously stated the bending amplitude increases by a factor of five. This limited variation in the amplitude of unsteady pressure along the blade span again indicates the presence of strong communication between spanwise sections through the propagation of pressure waves, which attempts to impose a uniform spanwise distribution of unsteady pressure.

Although the three dimensional nature of the amplitude of the unsteady pressure response, observed in the discussion above, can be explained through quite basic flow mechanisms, it is important to note that this behaviour seemingly challenges the validity of conventional quasi-3D strip method approach to the prediction of unsteady flows of this kind.

The spanwise variation in phase angle of the first harmonic pressure response, shown in figures 5.8, 5.10, 5.12 and 5.14, provides further evidence of three dimensional behaviour of the unsteady flow, most especially in terms of the suction surface response. Over the majority of the suction surface a reasonably consistent decrease in phase angle can be observed between the 10% and 90% spanwise locations, which cannot be explained with a simple two dimensional analysis of the unsteady aerodynamics. From 30% to 70% span there is a quite uniform shift in the phase angle between consecutive spanwise sections, of around 0° to 15° depending upon chordwise location and reduced frequency. Towards the hub endwall, i.e. between 30% and 10% span, the shift in phase angle becomes far more pronounced, especially at the lower reduced frequencies (k: 0.15 and 0.25). This pattern is not, however, repeated with any consistency towards the tip endwall, and the marked shift in phase at 10% span may quite conceivably be associated the localised hub leakage flow previously described.

At chordwise locations within the forward 50% chord of the pressure surface there is a limited variation in the measured phase angle between 10% and 90% span, with a band of +/- 5° enveloping the variation in most cases. This lies within the specified standard deviation of 6°. Aft of 50% chord, however, a deviation in phase angle becomes evident along the blade span, the extent of which generally increases towards the trailing edge. In this region the measured unsteady pressure response is led by the 10% span location, with an increase in phase generally observed towards 90% span of up to 80° (90% chord location, k: 0.15). It is clearly apparent, through comparison of the plots over the range of reduced frequency, that this variation in phase angle along the blade span is most pronounced in the two cases of lowest reduced frequency, i.e. k: 0.15 and 0.25 - shown in figures 5.8(i) and 5.10(i) respectively. At these low frequencies the amplitude of unsteady pressure is especially low towards the trailing edge of the pressure surface ($|Cp_1| < 0.5$) and as such the measurements are subject to the greatest degree of error. It is therefore difficult to determine whether the significant spanwise variation in phase angle observed in these instances is an accurate indication of three dimensional behaviour of the unsteady aerodynamics. In any case, it is of minor significance in terms of the aeroelastic stability of the present configuration, due to the very fact that it coincides with the region of lowest unsteady pressure activity on the blade surface.

The variation in the first harmonic pressure response with changes in reduced frequency is most clearly evident in the measured amplitude of unsteady pressure, through comparison of figures 5.7, 5.9, 5.11 and 5.13. These figures show a consistent and marked increase in

the amplitude of unsteady pressure at all locations on the blade surfaces for cases of increased reduced frequency, at least within the range tested. This could be explained in a quasi-steady sense by the increasing influence of the incidence effect, induced by the motion of the blade, as the frequency of blade vibration increases.

The variation in phase angle of first harmonic pressure with reduced frequency is less clear, due to the complexities introduced by a change in the relative time scales of convection and unsteady disturbance. Figures 5.8, 5.10, 5.12 and 5.14 do however indicate a general, albeit slight, increase in phase angle over the pressure surface, and the forward 50% chord of the suction surface, for increases in reduced frequency between 0.15 and 0.50. Above this value of reduced frequency, i.e. from 0.5 to 0.75, this trend is no longer apparent, with the phase angle of the first harmonic pressure response almost identical at the two highest values of reduced frequency tested.

To allow direct comparison of the variation in the unsteady pressure response with reduced frequency, and give an indication of aeroelastic stability, the results are presented as plots of aerodynamic damping in figures 5.17 and 5.18. Figure 5.17 shows the span-wise variation in local aerodynamic damping for each test case reduced frequency, whilst figure 5.18 shows the variation in overall aerodynamic damping with reduced frequency.

Figures 5.17 and 5.18 indicate a stable aeroelastic condition at all spanwise locations on the blade surface throughout the range of reduced frequency. The plots also show a consistent increase in aerodynamic damping with reduced frequency, which is associated with both the increase in amplitude of unsteady pressure and the shift in phase angle of the first harmonic pressure response previously described. In addition to the trends induced by the variation in reduced frequency, the spanwise distribution in local aerodynamic damping, shown in figure 5.17, indicates that the contribution to aerodynamic damping increases in a predominantly linear manner along the blade span. It is also apparent from this plot, that the contribution from the 90% span location is approximately five times that observed at 10% span, as seen in figure 5.17. This simply reflects the linear variation in local bending amplitude along the blade span which, it should be noted, is utilised to evaluate the local aerodynamic damping, and further demonstrates the quite uniform unsteady aerodynamic response observed along the blade span. It most especially highlights the insensitivity of the amplitude of the first harmonic pressure response to the local bending amplitude.
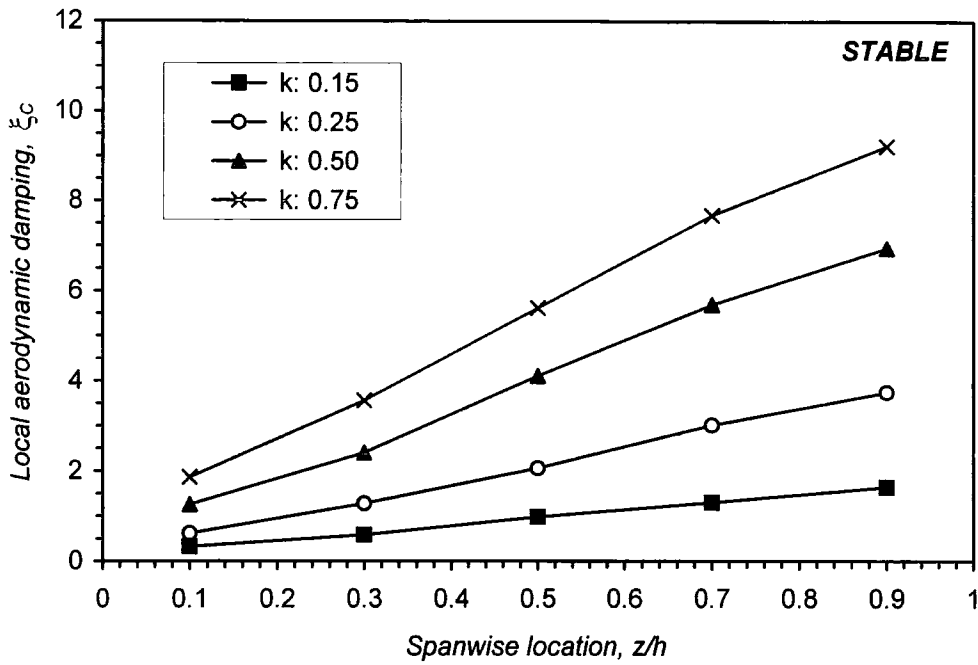
Figure 5.17: Spanwise variation in local aerodynamic damping[**], *k*: 0.15 - 0.75

[**] **Note the inclusion of local bending amplitude, B_L, in the definition of local aerodynamic damping,**

$$\xi_C = \int_C \frac{-\pi B_L |Cp_1| Sin\phi_1}{CB_C} dA$$
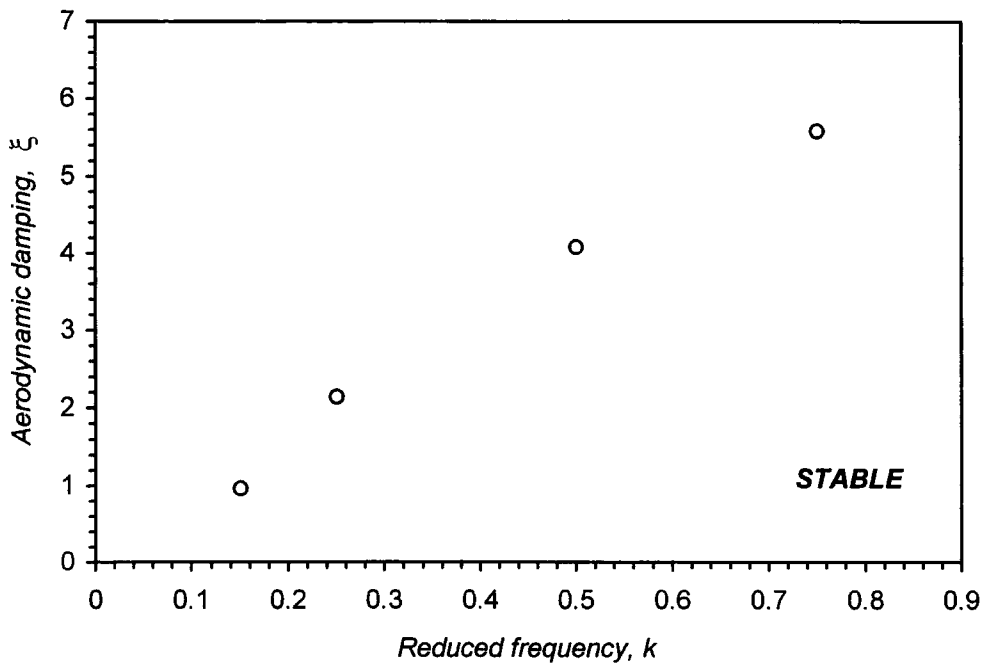
Figure 5.18: Variation in overall aerodynamic damping with reduced frequency

5.2.2 Evaluation of Linearity

The linearity of the unsteady aerodynamic response is of general interest in terms of the behaviour of the unsteady flow, it is also important, however, in order to gauge the appropriateness of the time-linearised assumption for the general computation and modelling of oscillating blade flows. Moreover, for the purposes of the present work it was important to determine linearity, since the computations were performed with the blade vibrating at half the actual amplitude of vibration due to problems experienced in obtaining a converged solution with the blade vibrating at the full bending amplitude, as described later, in chapter 6.

Two sets of measurements are presented here, in order to assess the linearity of the test configuration. The first set of results, shown in figures 5.19 to 5.23, utilise the relative amplitude of the second harmonic pressure response recorded at each test case reduced frequency (k: 0.15, 0.25, 0.50 and 0.75) as an indicator of linearity. These figures seem to demonstrate a predominant linear response of the unsteady aerodynamics throughout the range of reduced frequency, with the measured amplitude of second harmonic pressure an order of magnitude lower than the first at most locations on the blade surface. There are, however, some notable instances of relatively high amplitude of second harmonic pressure aft of 40% chord on the suction surface, which indicate a nonlinear behaviour of the unsteady aerodynamics. These are most especially evident at the 10% span location, and to a lesser extent at 30% span, when the blade vibrates at lower values of reduced frequency. In the extreme, at 75% chord and 10% span on the suction surface, the amplitude of second harmonic pressure rises to 60% of the local amplitude of first harmonic pressure, as shown in figure 5.19. This clearly indicates the presence of a significant second harmonic component, although it notably coincides with a region of low unsteady pressure activity.

The instances of moderate to high relative amplitude of second harmonic pressure described here may not necessarily indicate a non-linear unsteady aerodynamic response to the blade vibration, indeed, it is quite conceivable that it has arisen through a non-linear behaviour of a leakage flow through a faulty hub seal gland. This point of view is somewhat supported by the concentration of the high relative second harmonic pressure response at spanwise sections located nearest the hub section, whilst other spanwise sections further along the blade span (where the bending amplitude is much higher) do not exhibit similar behaviour.
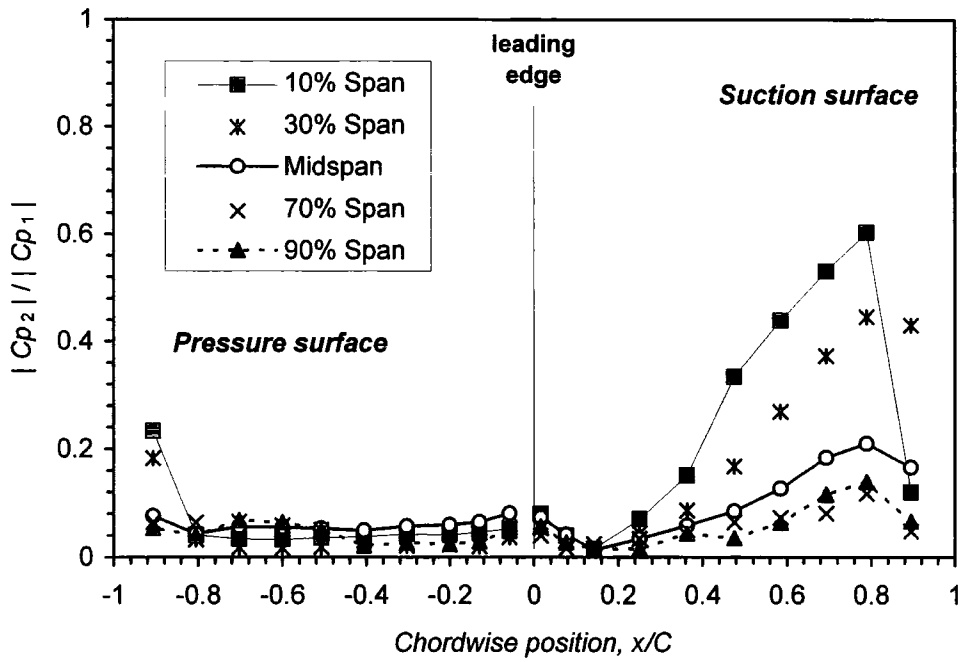
Figure 5.19: Relative amplitude of the second harmonic pressure response, *k*: 0.15
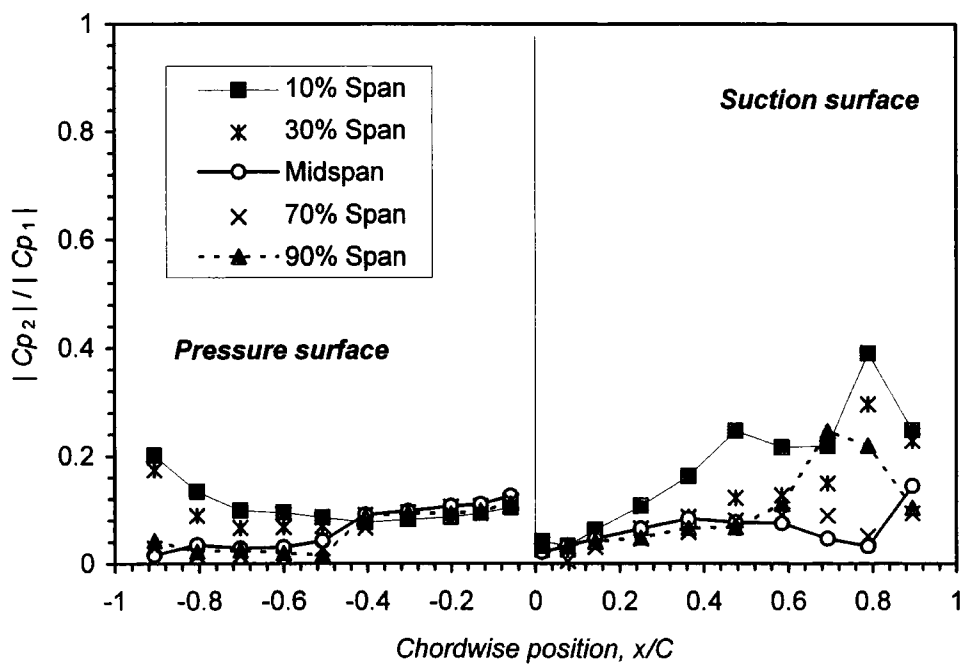
Figure 5.20: Relative amplitude of the second harmonic pressure response, *k*: 0.25
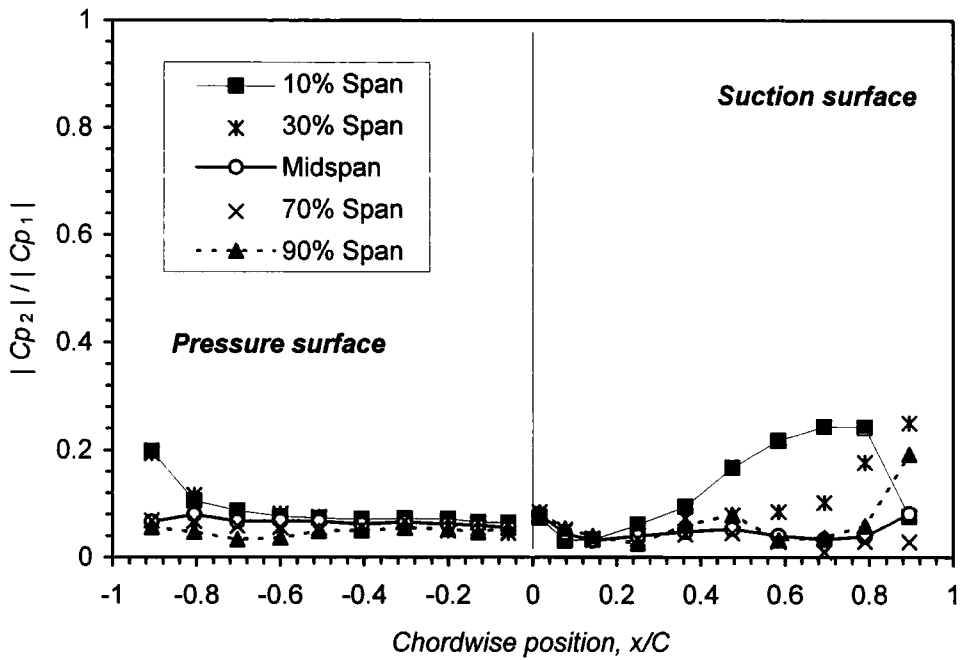
Figure 5.21: Relative amplitude of the second harmonic pressure response, *k*: 0.50
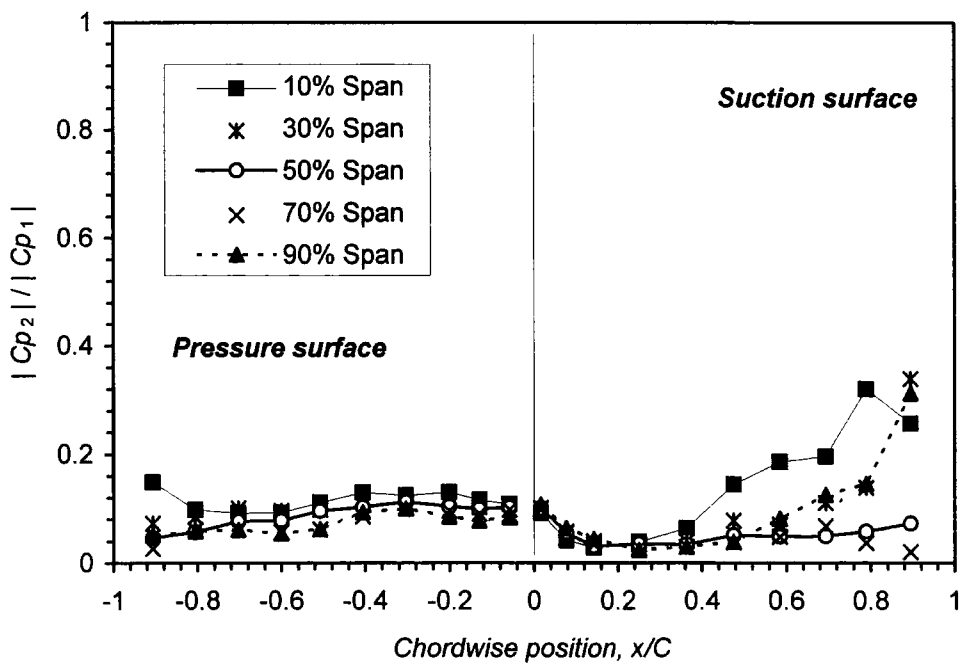
Figure 5.22: Relative amplitude of the second harmonic pressure response, *k*: 0.75
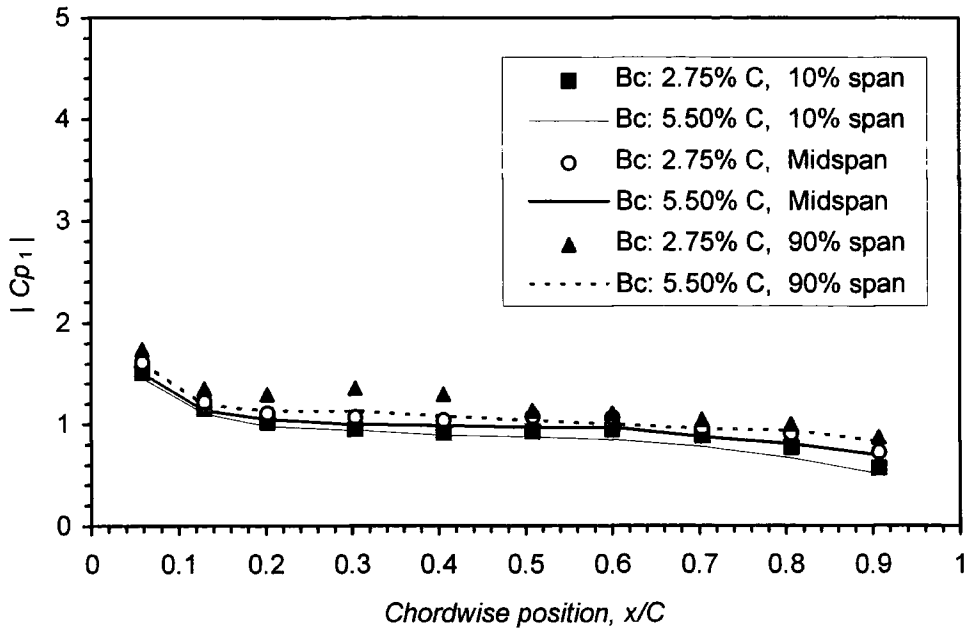
(i). Pressure surface response
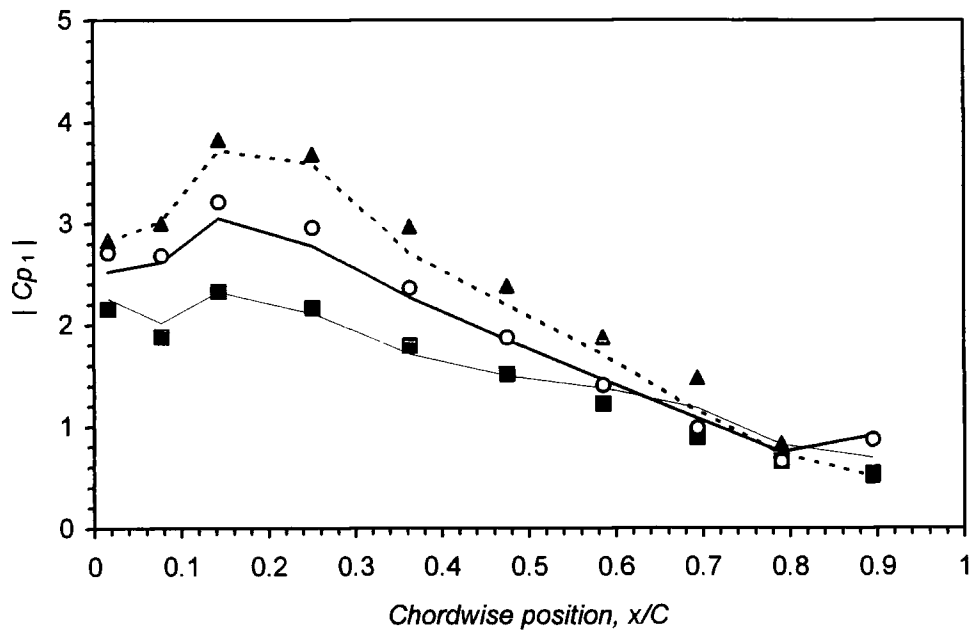
(ii). Suction surface response

Figure 5.23: **Experimental test for linearity - Amplitude of first harmonic pressure at different bending amplitudes** (*B_C*: 0.055 C and 0.0275 C at *k*: 0.50)
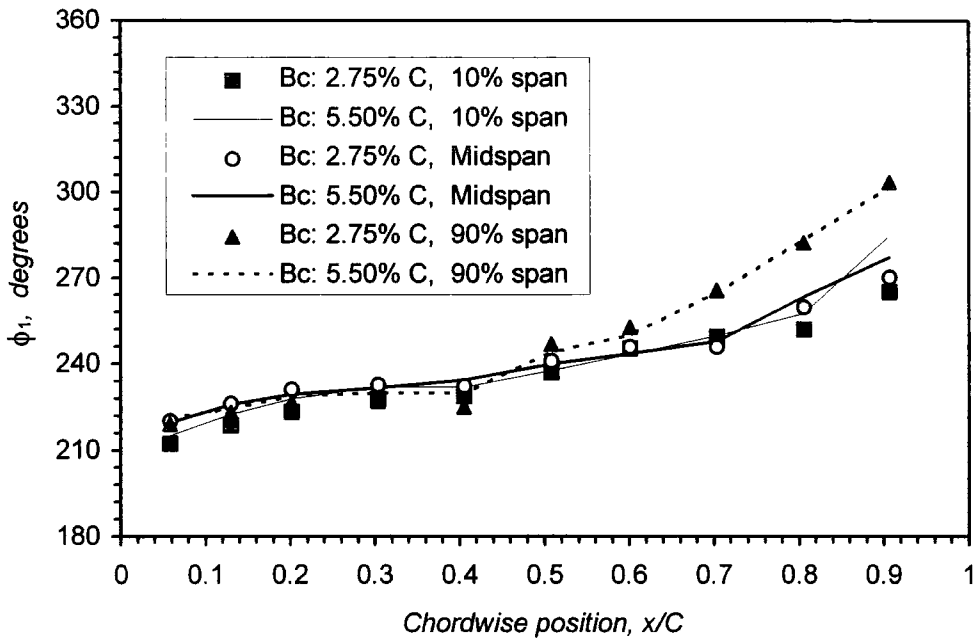
(i). Pressure surface response
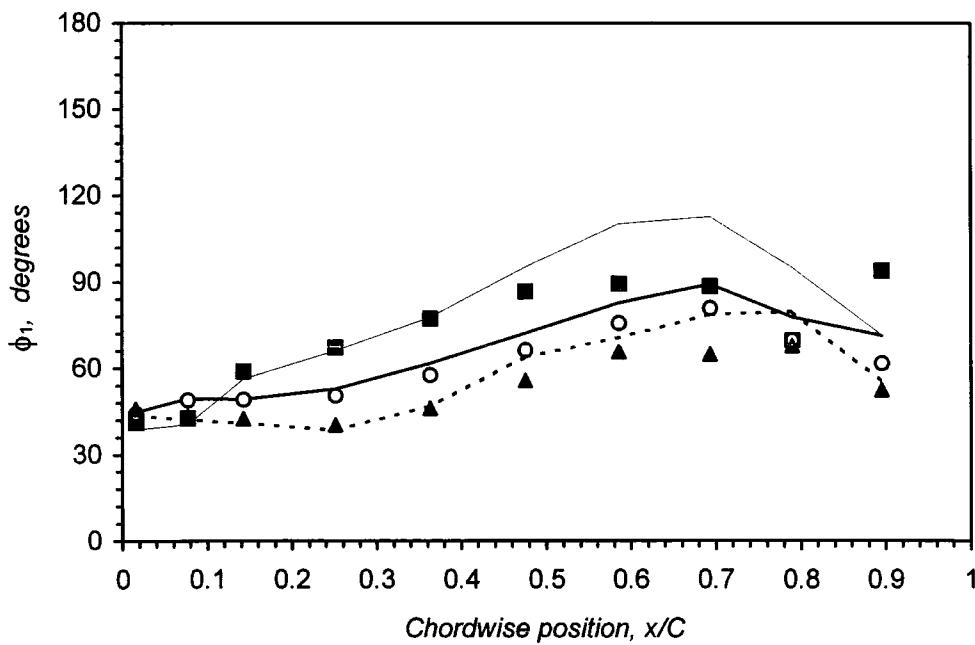
(ii). Suction surface response

Figure 5.24: Experimental test for linearity - Phase angle of first harmonic pressure at different bending amplitudes (B_C: 0.055 C and 0.0275 C at k: 0.50)

In addition to the second harmonic pressure measurements, a set of unsteady pressure measurements were repeated at a reduced frequency of 0.5 with the blade vibrating at half the bending amplitude (B_C: 2.75% chord), to give a more rigorous indication of linearity, albeit for a single test case. The blade surface unsteady pressure response obtained at this reduced bending amplitude is compared to that previously obtained at the full bending amplitude in figures 5.23 and 5.24, which shows the variation in amplitude and phase angle of first harmonic pressure respectively. In the interests of clarity, the results are provided for just three spanwise sections: 10% span, midspan and 90% span. The measurements presented in these figures also demonstrate a predominantly linear behaviour of the unsteady aerodynamic pressure response, with an almost identical amplitude of unsteady pressure coefficient obtained at the two bending amplitudes and a very good comparison in the phase angle recorded for the two cases. There are, however, slight discrepancies evident in the measured phase angle of first harmonic pressure over the suction surface between the measurements obtained at different bending amplitudes. These are most evident aft of 50% span on the suction surface at the 10% span location, suggesting a nonlinear behaviour of the unsteady aerodynamics in this region. This is entirely consistent with the observations of the second harmonic pressure response, and is presumed to be associated with the hub leakage flow previously referred to.

5.3 Summary

An extensive set of steady flow measurements and unsteady pressure measurements - obtained with the turbine blade driven in a three dimensional bending mode - have been presented and discussed. The steady flow measurements, which described the steady flow blade loading and inlet and exit flow conditions, indicated a predominant two dimensional steady flow structure through the working section, although a localised tip leakage vortex was captured in the tip endwall region by five-hole probe measurements performed at the exit traverse plane. Whilst the unsteady pressure measurements, which were obtained from five spanwise sections of tappings between 10% and 90% span, indicated a strong three dimensional behaviour of the unsteady aerodynamics. This was most manifestly present in the amplitude of the unsteady blade surface pressure response, which displayed a large degree of insensitivity to the local bending amplitude. It was also noted, that the observed three dimensional behaviour challenges the validity of the conventional quasi-

3D strip method approach to the prediction of unsteady flows of the present kind. An additional set of unsteady pressure measurements, performed at a reduced bending amplitude, indicated a predominantly linear behaviour of the unsteady aerodynamics.

The experimental results presented in this chapter provide the first three dimensional test data for aeroelastic applications in turbomachinery.

Chapter Six

The Computational Method, Results and Discussion

This chapter is concerned with the computational phase of the present work, which was performed with an extended three dimensional time-marching Euler solution method for oscillating blade flows. The principal objective here is to evaluate the capability of this method to predict the relevant 3D unsteady aerodynamic phenomenon exhibited by the oscillating turbine blade flow experiment. Although, the computational results and accompanying discussion are also intended to provide further insight into the behaviour of the unsteady flow previously discussed in chapter 5.

In the first part of this chapter, the computational method is presented with particular attention given to the modifications required for simulation of the experimental test configuration. Following this, computational solutions of the experimental test cases, previously provided in chapter 5, are presented and discussed. These results are most encouraging, with good qualitative and quantitative agreement obtained with the experimental test data throughout.

Quasi-3D solutions, obtained through operating the computational method in the strip method approach, are also presented. And comparison of these solutions with both the full 3D predictions and the experimental test data, highlights the strong three dimensional behaviour of the unsteady aerodynamic response as well as the inadequacies of the conventional quasi-3D approach for the prediction of this type of unsteady flow.

6.1 The Computational Method

The computational solutions to be presented, were obtained from a modified version of a single-passage, three dimensional time-marching Euler method for oscillating blade

flows, which was originally provided by Dr. L. He. In this method, the flow is assumed to be governed by the unsteady 3D Euler equations for inviscid, compressible flow. The equations are discretised in space with a cell-vertex finite volume scheme, Denton (1983), and temporally integrated using the explicit multi-step Runge-Kutta method following Jameson *et al* (1981). To ensure numerical stability, the second and fourth order adaptive smoothing proposed by Jameson *et al* (1981) is adopted in the streamwise direction with simple linear smoothing applied in the pitchwise and radial directions. The method is implemented over a simple 'h-type' mesh with a zonal moving grid defined around the blade to account for its oscillation, as described by He (1990a). The original code dealt with the phase shifted periodic boundary condition, for blade vibration at non-zero interblade phase angle, using the Shape correction technique developed by He, (1990a). This function was not, however, required for the purposes of the present work, since the sidewalls of the experimental working section removed the periodic blade to blade boundary condition.

6.1.1 Basic discretisation and Treatment of Far-Field Boundaries

The flow in the computational model is governed by the unsteady three dimensional inviscid Euler equations for compressible flows, which are written below in the conservative form.

$$\frac{\partial U}{\partial t} + \frac{\partial F}{\partial x} + \frac{\partial G}{\partial y} + \frac{\partial H}{\partial z} = 0 \tag{6.1}$$

where

$$U = \begin{pmatrix} \rho \\ \rho u \\ \rho v \\ \rho w \\ \rho e \end{pmatrix} \quad F = \begin{pmatrix} \rho u \\ \rho uu + p \\ \rho uv \\ \rho uw \\ u(\rho e + p) \end{pmatrix} \quad G = \begin{pmatrix} \rho v \\ \rho uv \\ \rho vv + p \\ \rho vw \\ v(\rho e + p) \end{pmatrix} \quad H = \begin{pmatrix} \rho w \\ \rho uw \\ \rho vw \\ \rho ww + p \\ w(\rho e + p) \end{pmatrix}$$

To allow discretisation in the physical co-ordinate system, the equations are then formulated in an integral form over a dynamic finite volume, as described in Eq. 6.2. This makes for a simple and efficient method compared to a finite difference approach which requires a Jacobian matrix transformation at each time step for such applications.

$$\frac{\partial}{\partial t}\iiint U\,dxdydz + \left[\iint (F - U\frac{\partial x}{\partial t})\,dydz + \iint (G - U\frac{\partial y}{\partial t})\,dxdz + \iint (H - U\frac{\partial z}{\partial t})\,dxdy\right] = 0$$

where $\dfrac{\partial x}{\partial t}$, $\dfrac{\partial y}{\partial t}$ and $\dfrac{\partial z}{\partial t}$ are the velocity components of the finite volume (6.2)

The additional fluxes $U\dfrac{\partial x}{\partial t}$, $U\dfrac{\partial y}{\partial t}$ and $U\dfrac{\partial z}{\partial t}$ are introduced in Eq. 6.2 to account for the temporal movement of the finite volume, through simple correction of the flux U for the prescribed deformation of the volume in time. The integral form of the Euler equations presented here is discretised in the present method with a cell-vertex scheme, in which the fluxes through each cell boundary surface are evaluated from the flow properties stored at the mesh vertices, and the calculated change in U within each cell is equally distributed to its vertices.

The temporal integration is performed with a five step, second order accurate, Runge Kutta scheme which offers enhanced computational efficiency compared to the two-step method, most especially at the low reduced frequencies which are of interest here, see He & Denton (1993). The exact procedure is described below in its discretised form.

$$U^{n+i} = U^n \frac{\Delta V}{\Delta V^{n+1/4}} - \frac{1}{4}\frac{\Delta t}{\Delta V^{n+1/4}}\left(R^n - D^n\right)$$ (6.3 i)

$$U^{n+ii} = U^n \frac{\Delta V}{\Delta V^{n+1/6}} - \frac{1}{6}\frac{\Delta t}{\Delta V^{n+1/6}}\left(R^{n+i} - D^n\right)$$ (6.3 ii)

$$U^{n+iii} = U^n \frac{\Delta V}{\Delta V^{n+3/8}} - \frac{3}{8}\frac{\Delta t}{\Delta V^{n+3/8}}\left(R^{n+ii} - D^n\right)$$ (6.3 iii)

$$U^{n+iv} = U^n \frac{\Delta V}{\Delta V^{n+1/2}} - \frac{1}{2}\frac{\Delta t}{\Delta V^{n+1/2}}\left(R^{n+iii} - D^n\right)$$ (6.3 iv)

$$U^{n+v} = U^n \frac{\Delta V}{\Delta V^{n+1}} - \frac{\Delta t}{\Delta V^{n+1}}\left(R^{n+iv} - D^n\right)$$ (6.3 v)

$$U^{n+1} = U^{n+v}$$ (6.3 vi)

$$\text{where, } R = \sum_{ijk}\left[\left(F - U\frac{\partial x}{\partial t}\right)\Delta A_x + \left(G - U\frac{\partial y}{\partial t}\right)\Delta A_y + \left(H - U\frac{\partial z}{\partial t}\right)\Delta A_z\right]$$

In equations 6.3 D^n represents an artificial damping term, which is introduced to maintain numerical stability. This dissipative term is updated at the beginning of each five step sequence and evaluated using the second and fourth order adaptive smoothing function proposed by Jameson *et al* (1981) in the streamwise direction and simple linear smoothing in the pitchwise and radial directions.

The inlet far field boundary is specified with a prescribed total temperature, total pressure and flow direction and the flow properties are calculated by extrapolating pressure from the interior domain and assuming isentropic flow from the inlet stagnation conditions. The outlet far field boundary is specified with a reflecting fixed back pressure condition, which corresponds with the exhaust to atmosphere in the experimental test configuration. Other flow properties are upwinded here.

6.1.2 Zonal Moving Grid

As previously described, by adopting a finite volume approach, the oscillation of the blade can be handled in the physical co-ordinate system with a dynamic mesh which is defined according to the motion of the blade.

In the interests of computational efficiency, the zonal moving grid technique described by He (1990a) is adopted in the present method. This methodology allows a user specified region to be established around the blade in which the mesh nodes are free to move, as shown for a single passage computational domain in figure 6.1. Within this region the velocity components of each mesh node are evaluated at the beginning of each time step to allow solution of the discrete form of the Euler equations presented in Eq. 6.3. Whilst outside this region, the additional flux terms $U\frac{\partial x}{\partial t}$, $U\frac{\partial y}{\partial t}$ and $U\frac{\partial z}{\partial t}$ are discarded.

For most practical applications, a moving grid enveloping just two or three cells adjacent to the blade surfaces is sufficient, at least for inviscid computational meshes. In the present case, however, a much larger moving grid region was required to handle the large amplitude of vibration at the tip section in the experimental test configuration.

The formulation described allows very simple treatment of the blade surface boundary condition, through the stipulation of zero flow flux across the cell boundaries on the blade surface, with pressure terms preserved to account for work done in the energy equation.
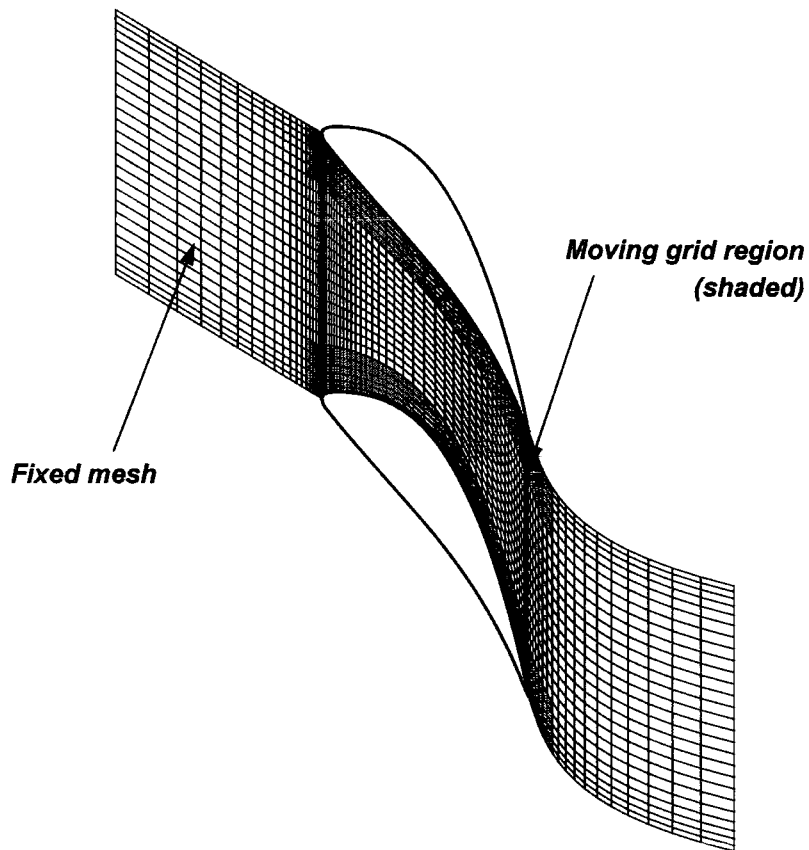
Figure 6.1: The zonal moving grid

6.2   The Computation of Experimental Test Cases

In order to model the experimental test configuration, the source code of the original, single passage version of the computational method was modified to generate a double blade passage computational domain. This extended domain, shown in figure 6.2, was a discretised reproduction of the experimental working section, extending one axial chord length upstream of the blade leading edge which corresponds to the location of the inlet traverse plane, and one axial chord length downstream of the trailing edge which corresponds with the exhaust to atmosphere. The working section sidewalls, highlighted in bold in figure 6.2, were also modelled in this modified version of the computational method, through the implementation of a zero flow flux boundary condition.

In addition to these basic modifications, further effort was required to ensure correct implementation of the discretised equations and smoothing functions within the near wall regions of this somewhat unusual computational domain.

100
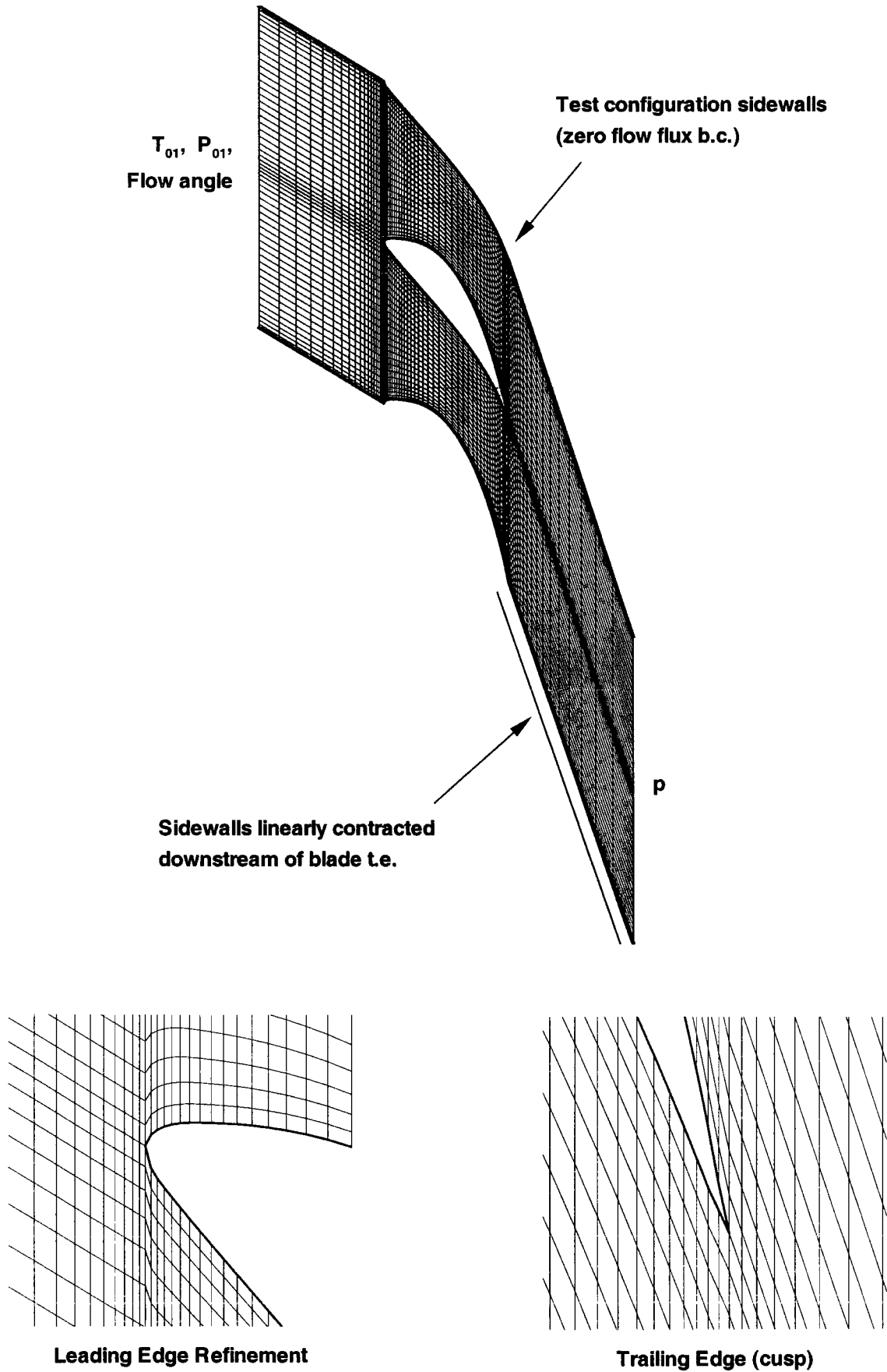
Figure 6.2: The computational domain (54x81x11)
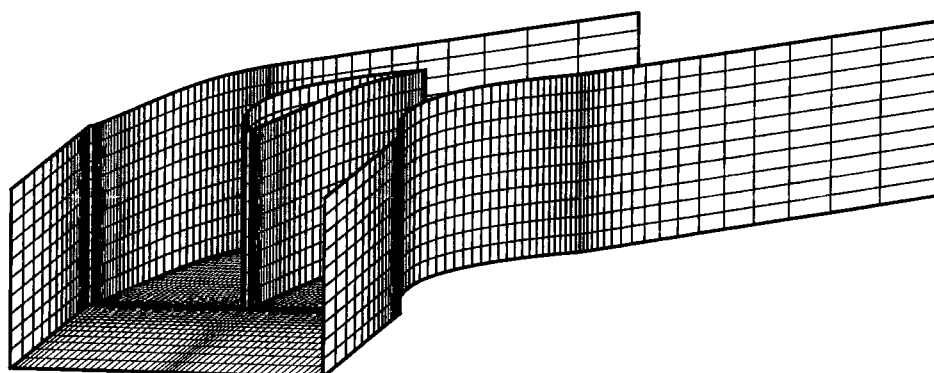
Figure 6.3: 3D view of computational domain

(solid surfaces are meshed, except for the tip endwall)

Figures 6.2 and 6.3 show the mesh employed to generate the steady and unsteady flow solutions presented later in this chapter. This consisted of 81 nodes distributed in the axial direction, 54 nodes in the circumferential direction and 11 nodes in the radial direction, which was found to be sufficient to obtain a reasonably mesh independent solution for both the steady and unsteady flow calculations. The mesh was refined in the axial and circumferential directions to resolve the leading and trailing edge regions, and a single node cusp was appended to the trailing edge. An extensive moving grid was also defined to cope with the large amplitude of vibration at the blade tip section. The zonal moving grid extended 14 nodes in the pitchwise direction adjacent to the blade surfaces and 10 nodes up and downstream of the blade leading and trailing edge respectively. The tip clearance in the experimental configuration was not, however, included in the computational domain.

Downstream of the blade trailing edge, the sidewalls of the computational domain were linearly contracted compared to experimental set-up, as indicated in figure 6.2. The extent of this contraction was determined by an approximate evaluation of boundary layer displacement thickness based upon five-hole probe measurements performed at exit from the working section. At the downstream far field boundary each sidewall was contracted by 3.0% chord in the pitchwise direction, and the endwalls, which were similarly contracted, by 0.75% chord. The purpose of this contraction, which is discussed at greater depth in section 6.3.1, was to simulate the blockage introduced by the boundary layer growth over the experimental test section sidewalls and thereby correct the mass flow to more realistic levels in the inviscid computations.

The inlet and exit far-field boundaries were specified with uniform conditions provided by the experimental measurements presented in section 5.1, although the inlet stagnation conditions were scaled to increase the isentropic exit Mach number to 0.3. This increase in operating Mach number was required to obtain a converged solution from the density based time-marching method, but should not introduce any significant compressibility effects into the computations.

For the computation of each unsteady test case, the reduced frequency was matched. The bending amplitude was, however, limited to half the value imposed in the experiments, i.e. B_C = 2.75% chord. This situation was enforced due to problems encountered in obtaining a converged solution with the blade vibrating at the full bending amplitude. This is thought to be associated with the direction of bending and the large amplitude at the tip causing excessive distortion of the 'h-type' zonal mesh, rather than the time-step stability limit associated with the explicit solution procedure within the moving grid region. In any case, the convergence problem was not pursued, since it was considered satisfactory to operate at half the bending amplitude given the linear nature of the unsteady flow previously demonstrated in section 5.2.2.
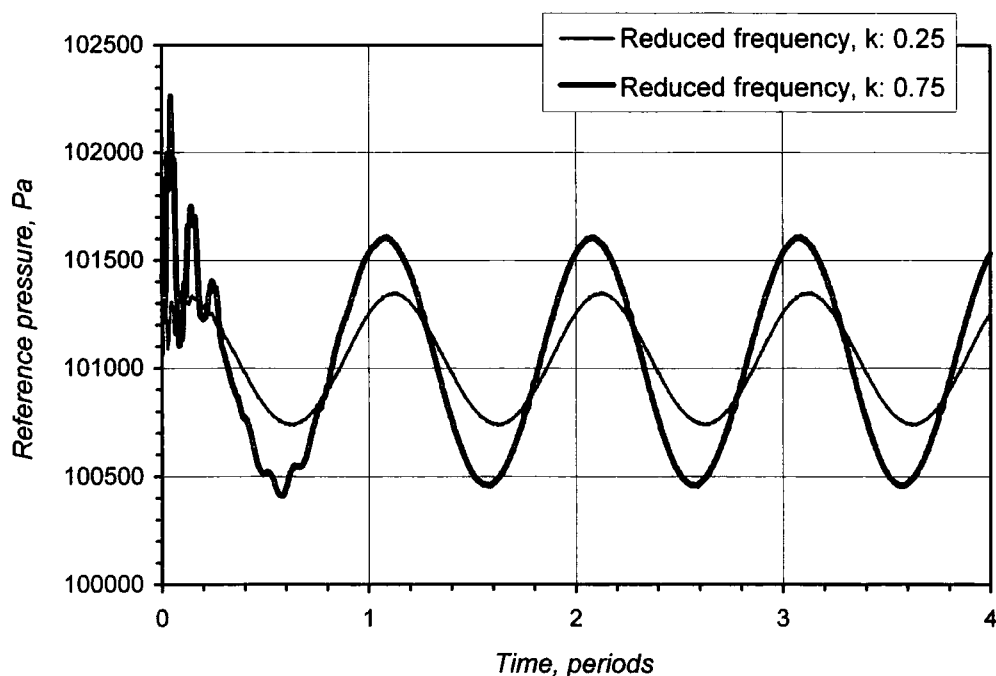
Figure 6.4: Typical convergence history, *k*: 0.25 and *k*: 0.75

(Reference pressure taken at mid-span, mid-chord on the suction surface)

103

The low reduced frequency of the unsteady test cases meant that the number of time steps per period of vibration was specified to satisfy the CFL stability criteria for the explicit numerical scheme, rather than that required for acceptable temporal resolution. Indeed, the number of time steps per period of vibration was at best 7000 for the highest reduced frequency case and at worst 35000 for the lowest reduced frequency. Fortunately, the computational expense incurred due the excessive number of time steps required per period of vibration is somewhat offset at low reduced frequencies by the rapid convergence in terms of the number of periods required to obtain a converged solution. In the present case it was found that a converged solution was generally obtained upon the third period of vibration when the computations were initiated with the steady flow solution, as indicated by figure 6.5. The computations were, however, continued for a minimum of two additional periods of vibration to verify convergence in each case.

6.3 Computational Results

Computational solutions of the experimental test cases provided in chapter 5 are presented in this section. These were obtained at the conditions already described for cases of both steady and unsteady flow.

6.3.1 Steady Flow Computations

The strong relationship between steady flow aerodynamic loading and unsteady pressure generation exhibited by the experimental measurements indicated the importance of obtaining a good quality steady flow prediction before embarking upon unsteady flow computations. Figure 6.5, which shows a comparison of predicted and measured blade surface pressure distribution, demonstrates that this was largely made possible in the inviscid computations through the contraction applied to the side and endwalls towards the outlet of the computational domain. While reasonable agreement with the experimental measurements is evident for prediction obtained with contraction, a marked deterioration in the predicted suction surface pressure distribution can be observed for the case without contraction in figure 6.5. This clearly shows the effective contribution of the contraction which sets a more realistic mass flow in the computations, thereby reducing the velocities required over the suction surface to satisfy continuity. The manner in which this contraction is applied also relieves the strong diffusion over the suction surface towards the trailing edge, which has a secondary effect of simulating the relief provided

by boundary layer growth over the blade surface and the sidewalls of the experimental working section.

Although the computational results presented in figure 6.5 are confined to the midspan location, they are representative of the steady flow blade pressure distribution predicted at all spanwise locations. This is because the omission of a tip clearance in the computational domain and the stipulation of uniform far field boundary conditions removed any source of three dimensional flow in the inviscid steady flow computations. Equally, the experimental measurements provided for the midspan location are representative of the actual blade surface pressure distribution between 10% and 90% span, although a slight deviation was evident in the measurements at 90% span due to the influence of tip leakage flow, as previously shown in figure 5.3.
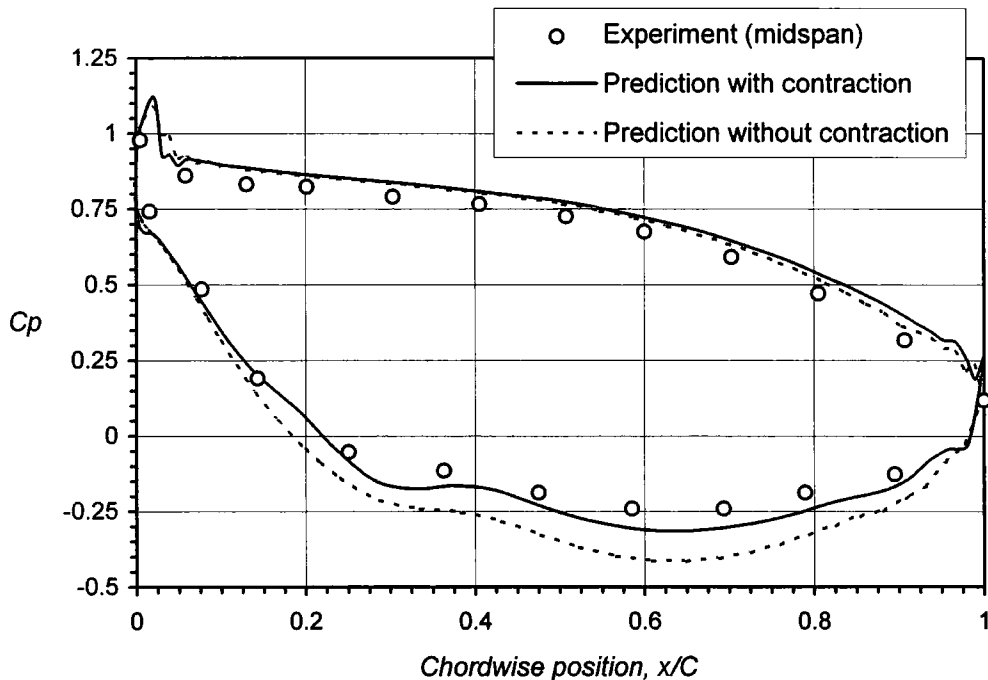
Figure 6.5: Predicted and measured blade surface pressure distribution at midspan (Improved prediction obtained through contracting side and endwalls)

6.3.2 Unsteady Flow Computations

Inviscid computational solutions of the four unsteady experimental test cases presented in chapter 5 are provided in figures 6.6 to 6.18. For each test case (reduced frequencies, k: 0.15, 0.25, 0.50 and 0.75) three plots are provided. The first shows a comparison of

predicted and measured amplitude of first harmonic pressure and the second, the predicted phase angle of this response. In the interests of clarity, the measurements and predictions presented in these plots are provided for just three spanwise locations: 10% span, midspan and 90% span. The contribution of the predicted and measured response at other spanwise locations is, however, accounted for in the third plot presented for each test case, which shows the spanwise variation in local aerodynamic damping. Finally, in figure 6.18, the results of the entire set of computational solutions are presented through a global comparison of the predicted and measured variation in the overall aerodynamic damping with reduced frequency.

The computational solutions presented in these figures, which to the authors knowledge are the first published 3D predictions of their kind to be supported by experimental measurements, are most encouraging. They are characterised by a very good qualitative and quantitative agreement with the experimental measurements, which is generally evident throughout the range of reduced frequency for predictions of amplitude of first harmonic pressure, phase angle and both local and overall aerodynamic damping - the latter two providing a global indication of the quality of these predictions. The computational solutions therefore indicate that the unsteady aerodynamic response is predominantly governed by inviscid unsteady flow mechanisms.

The predicted amplitude of first harmonic pressure for the three lowest reduced frequency cases (k: 0.15, 0.25 and 0.50), shown in figures 6.6, 6.9 and 6.12 respectively, exhibits excellent agreement with the experimental measurements at all spanwise locations over both the pressure surface and the suction surface. The amplitude of unsteady pressure is, however, generally under predicted for the highest reduced frequency case (k: 0.75) shown in figure 6.15, although the qualitative agreement with the test data remains very good. The predicted amplitude of first harmonic pressure very much supports the observed three dimensional behaviour of the unsteady aerodynamic response reported in chapter 5, with the solutions consistently demonstrating the same insensitivity of the unsteady pressure generation to the local bending amplitude. Like the experimental measurements, the predicted amplitude of first harmonic pressure is almost uniform along the blade span of the pressure surface, despite the significant variation in local bending amplitude. And the predicted variation along the blade span of the suction surface is also much less severe than the corresponding variation in local bending amplitude.

The predicted phase angle of the first harmonic pressure response, shown in figures 6.7, 6.10, 6.13 and 6.16, also demonstrates very good agreement with the experimental

106

measurements throughout the range of reduced frequency at all locations on the pressure surface. From the leading edge to approximately midchord on the suction surface there is also reasonable agreement between the predicted and measured phase angle of the first harmonic pressure response, which is consistent with a predominant inviscid behaviour of the unsteady aerodynamics. Aft of this location and towards the trailing edge on the suction surface there is by comparison, however, a marked deterioration in both the quantitative and qualitative level of agreement exhibited by the predicted phase angle with the test data. Whereas the inviscid predictions indicate a phase lead of the unsteady pressure response from the trailing edge position on the suction surface, with a pressure wave propagating upstream from this location, the experimental measurements show the converse to be true, with a drop in phase angle generally observed aft of the 70% chord location.

The disparity between the predicted and measured phase angle towards the trailing edge of the suction surface, where the flow is subject to a significant diffusion, is consistent with the arguments laid out in section 5.2. In this discussion, the drop in phase angle observed in the experimental measurements towards the trailing was explained in terms of the sensitivity of the thickened boundary layer to information convected downstream. In the inviscid computations such effects are obviously neglected and the local unsteady pressure distribution is more directly influenced by the condition of flow at the trailing edge. Information propagates upstream from this location, which manifests in the phase lead observed in the predicted unsteady pressure response from the trailing edge on the suction surface. This argument also holds true for the actual unsteady pressure response of the pressure surface, which is also featured by a phase lead from the trailing edge position.

It is also apparent that the marked variation in phase angle along the blade span of the suction surface aft of approximately 40% chord, most especially observed in the experimental measurements at the lower reduced frequencies (see figures 6.7 and 6.10 for example), is not captured by the inviscid predictions. This indicates that this three dimensional feature of the unsteady aerodynamic response is attributable to an unsteady viscous phenomenon, which is most likely to be induced by the differing change in passage area experienced along the blade span within the region of strong diffusion towards the trailing edge.

It is important to note that the discrepancies observed between the predicted and measured phase angle of the first harmonic pressure response on the suction surface are
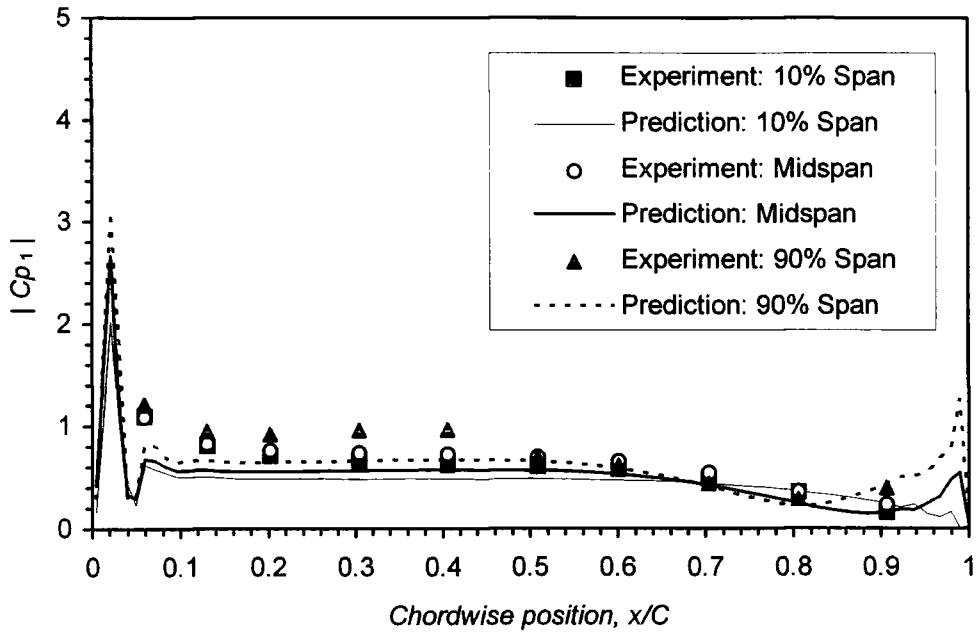
(i). Pressure surface response
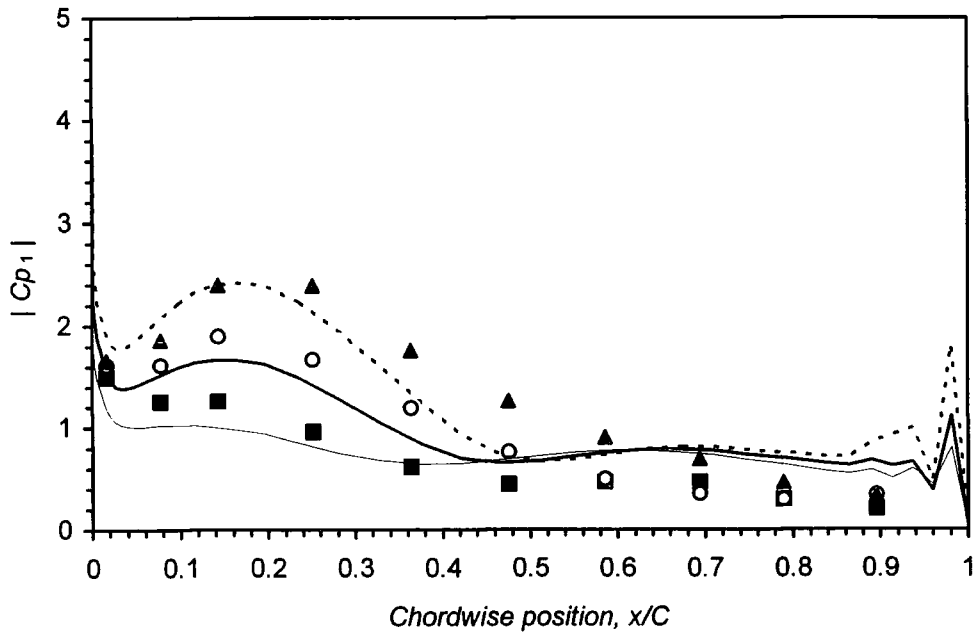
(ii). Suction surface response

Figure 6.6: Predicted and measured amplitude of first harmonic pressure, *k*: 0.15
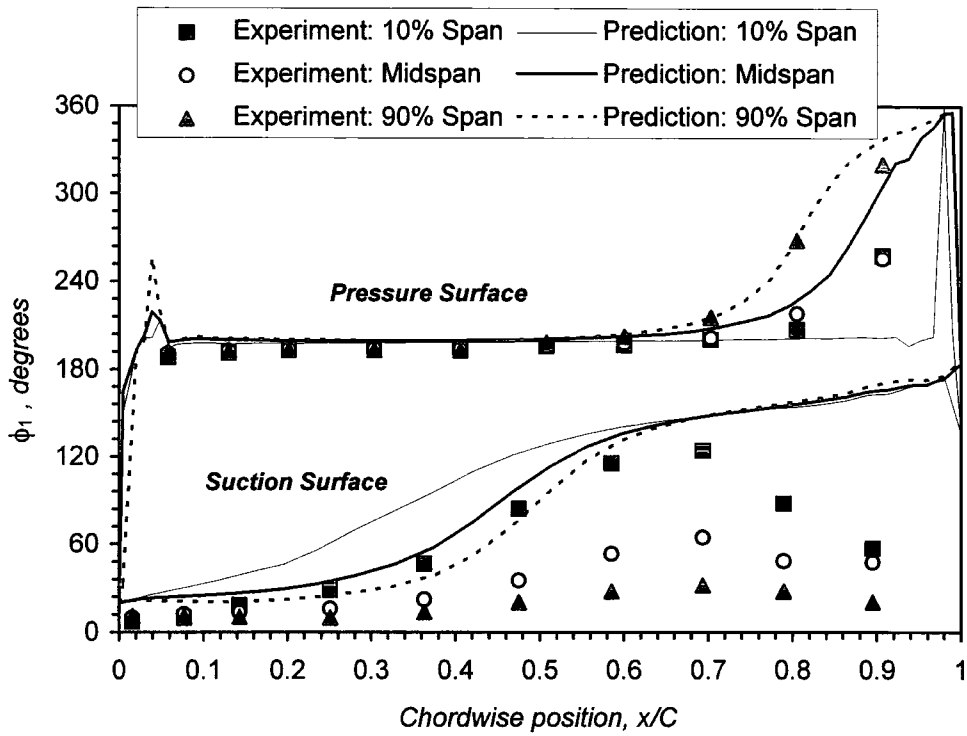
Figure 6.7: Predicted and measured phase angle of first harmonic pressure, k: 0.15
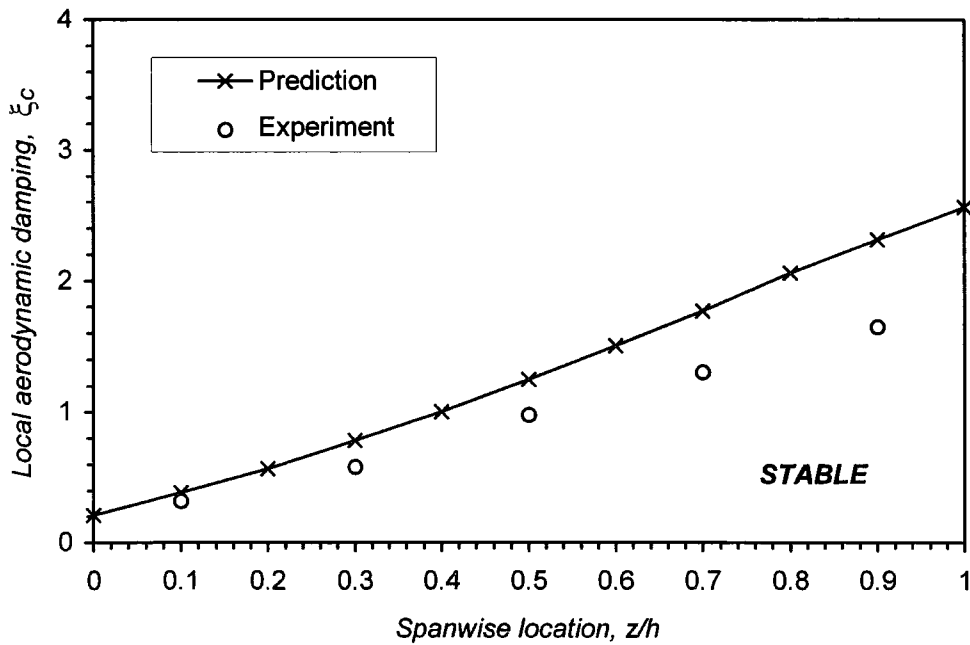
Figure 6.8: Predicted spanwise variation in local aerodynamic damping, k: 0.15

109
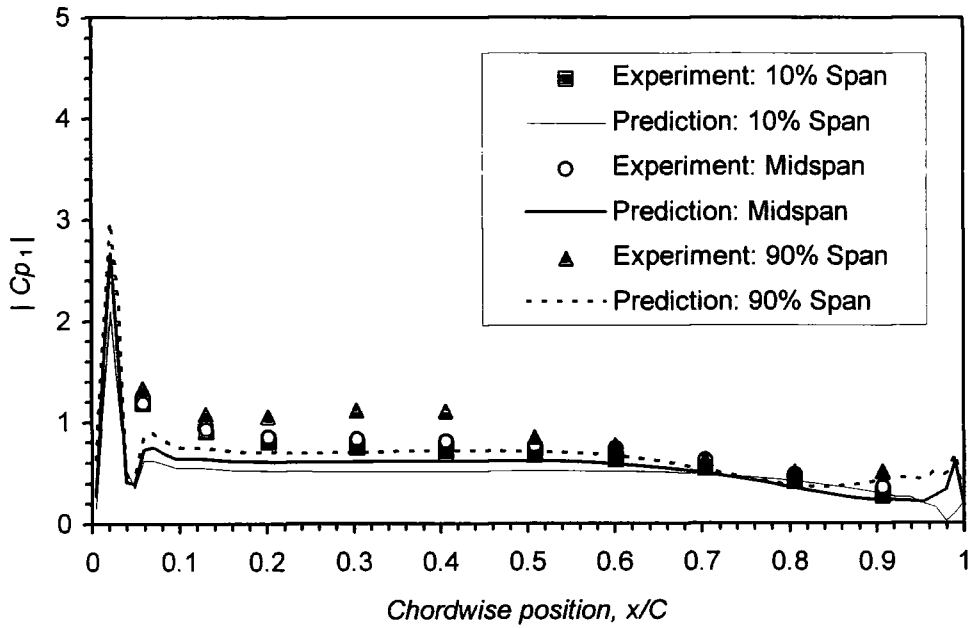
(i). Pressure surface response
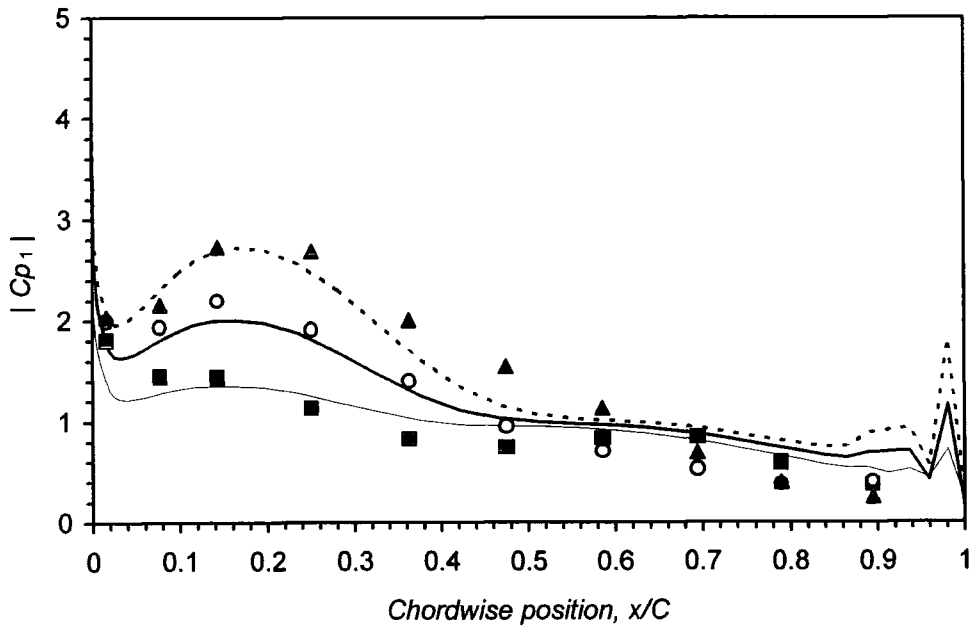
(ii). Suction surface response

Figure 6.9: Predicted and measured amplitude of first harmonic pressure, *k*: 0.25
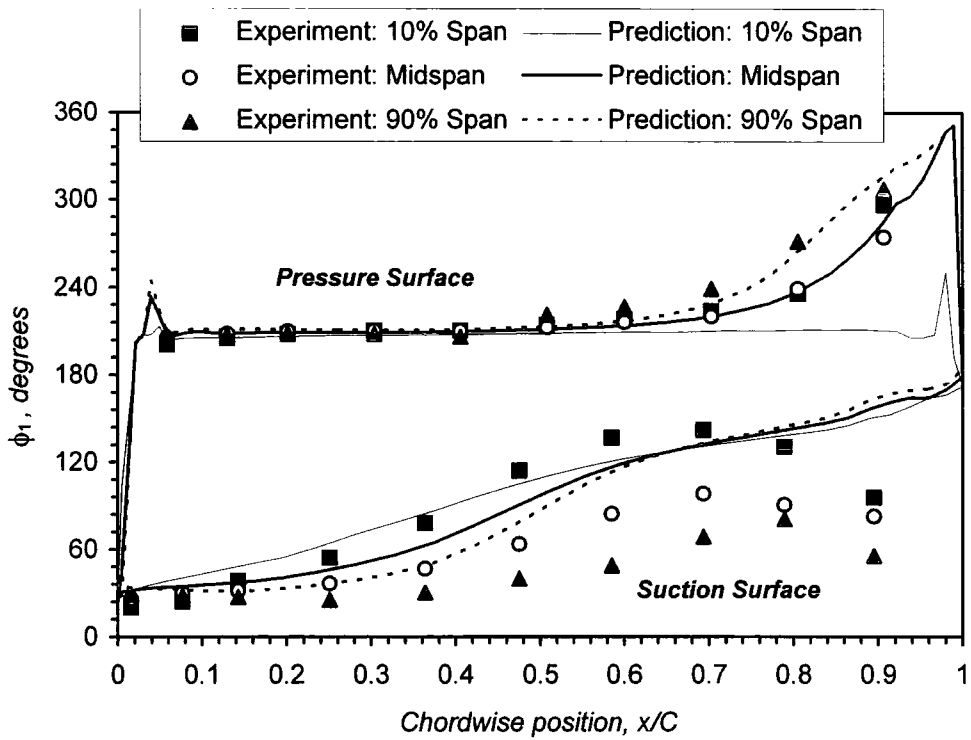
Figure 6.10: Predicted and measured phase angle of first harmonic pressure, *k*: 0.25
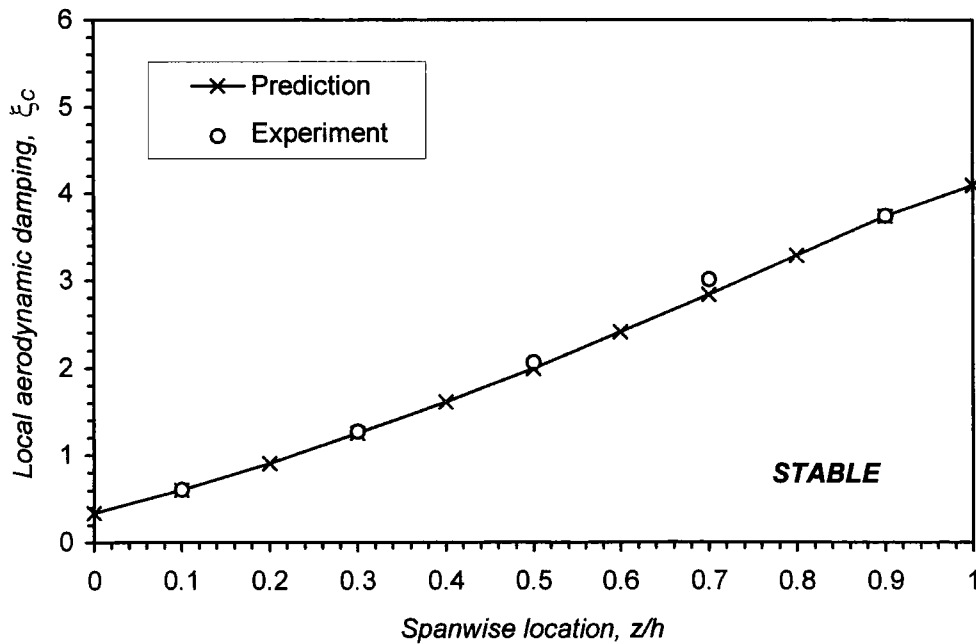
Figure 6.11: Predicted spanwise variation in local aerodynamic damping, *k*: 0.25
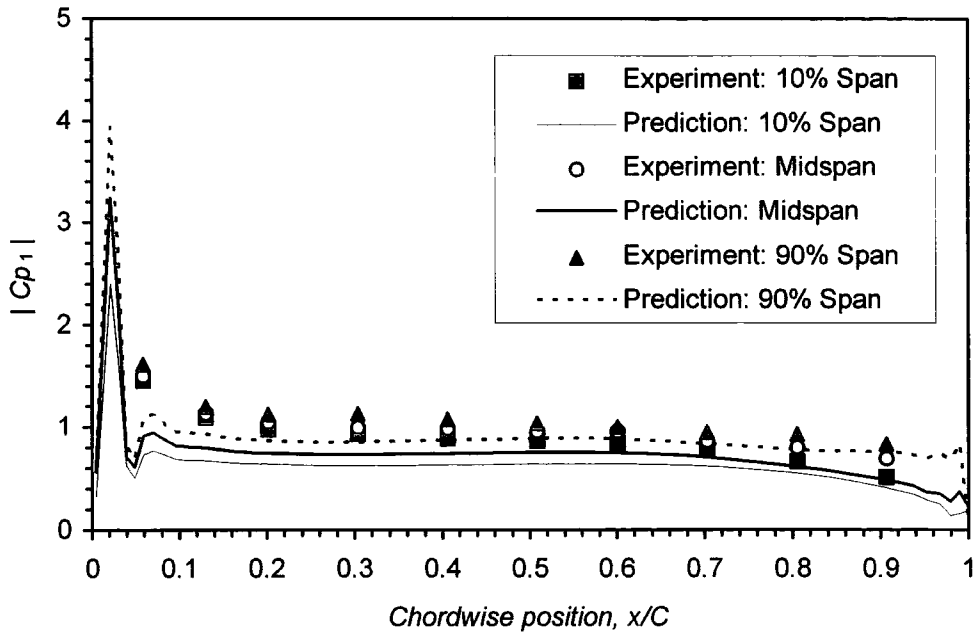
(i). Pressure surface response
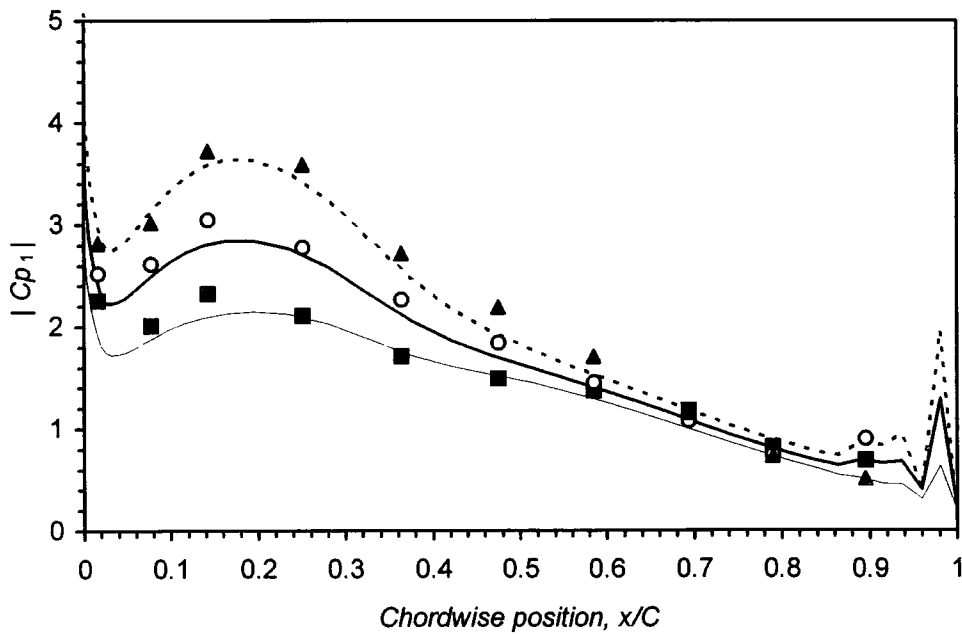
(ii). Suction surface response

Figure 6.12: Predicted and measured amplitude of first harmonic pressure, *k*: 0.50
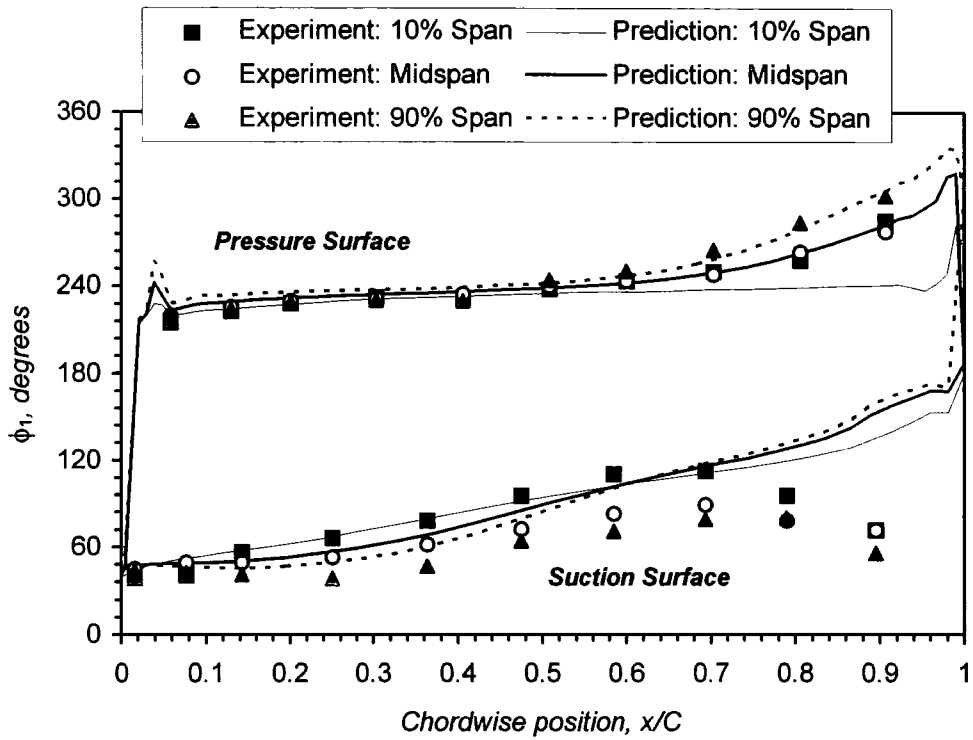
Figure 6.13: Predicted and measured phase angle of first harmonic pressure, *k*: 0.50
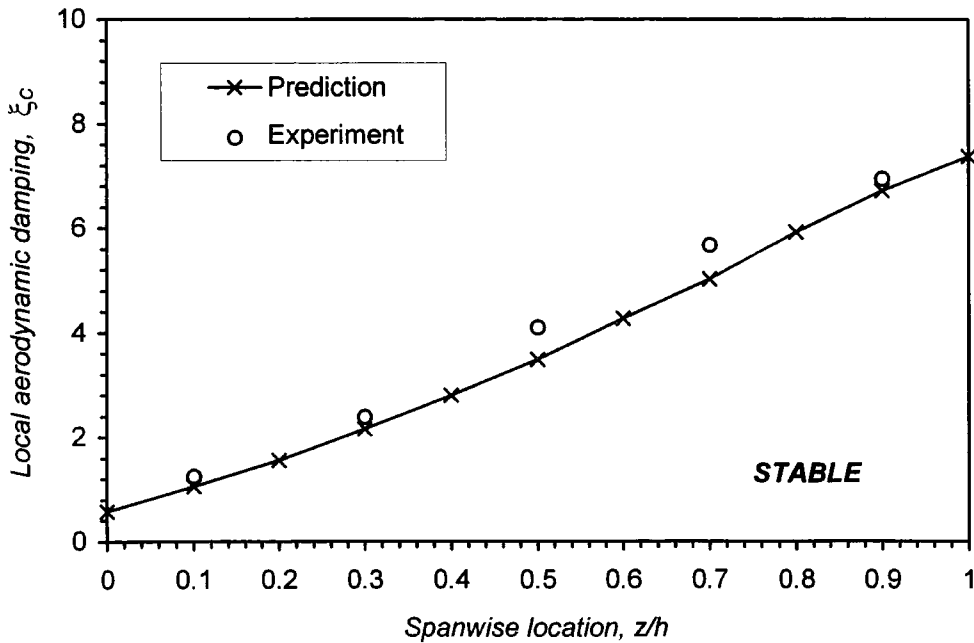
Figure 6.14: Predicted spanwise variation in local aerodynamic damping, *k*: 0.50

113
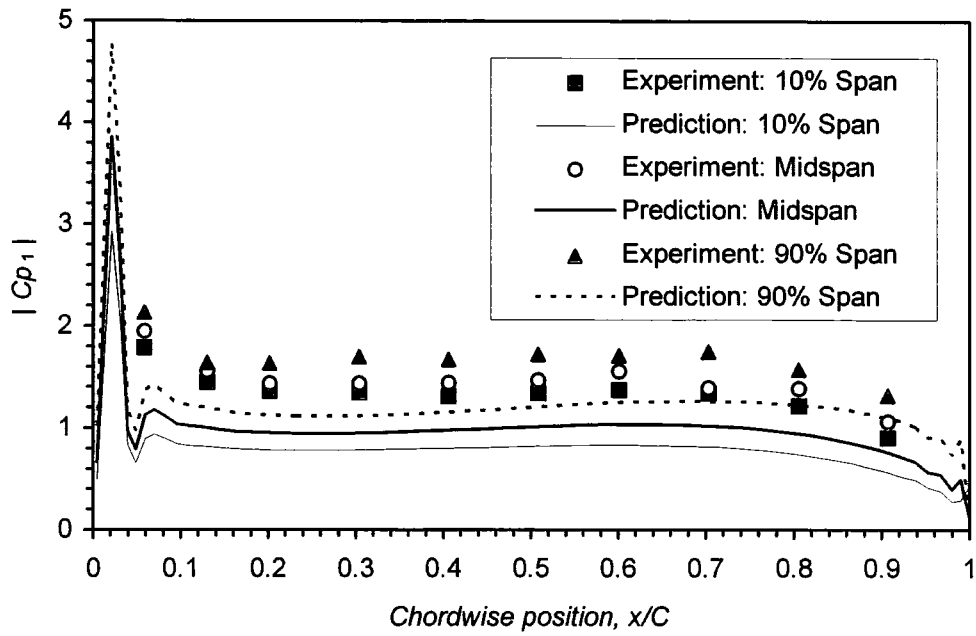
(i). Pressure surface response
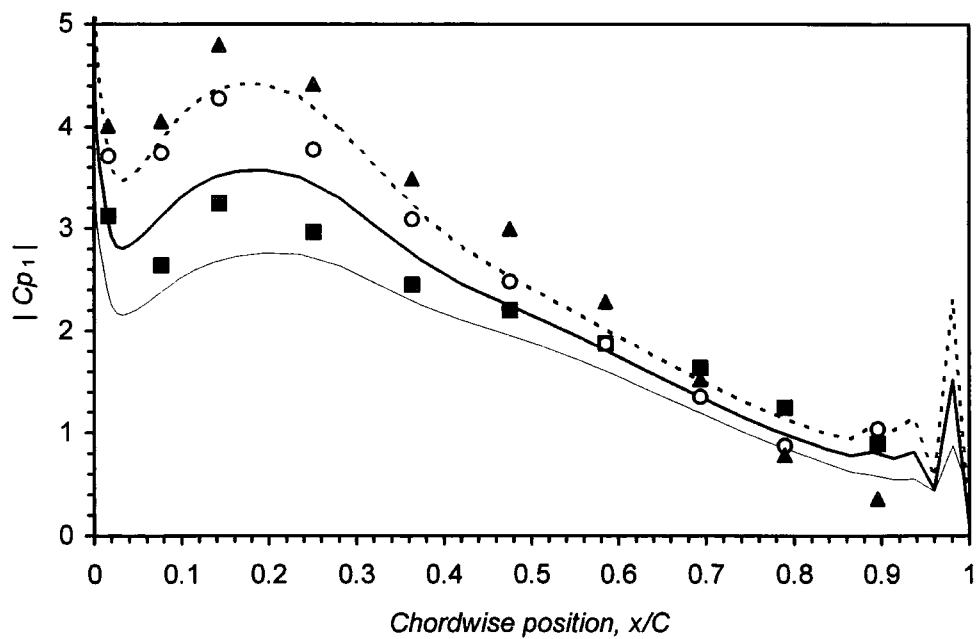
(ii). Suction surface response

Figure 6.15: Predicted and measured amplitude of first harmonic pressure, *k*: 0.75
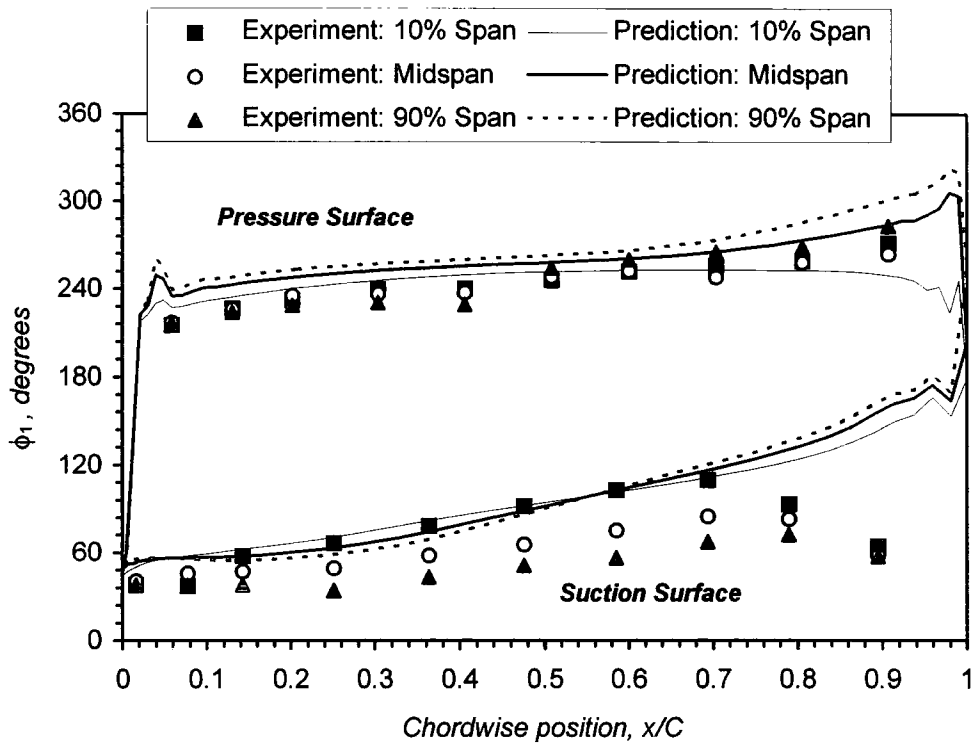
Figure 6.16: Predicted and measured phase angle of first harmonic pressure, *k*: 0.75
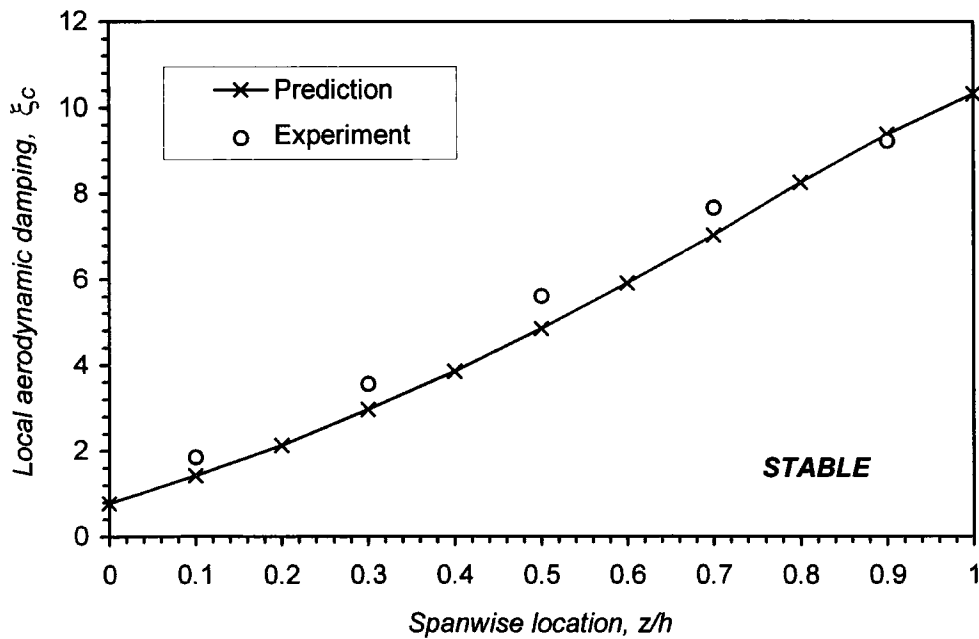
Figure 6.17: Predicted spanwise variation in local aerodynamic damping, *k*: 0.75
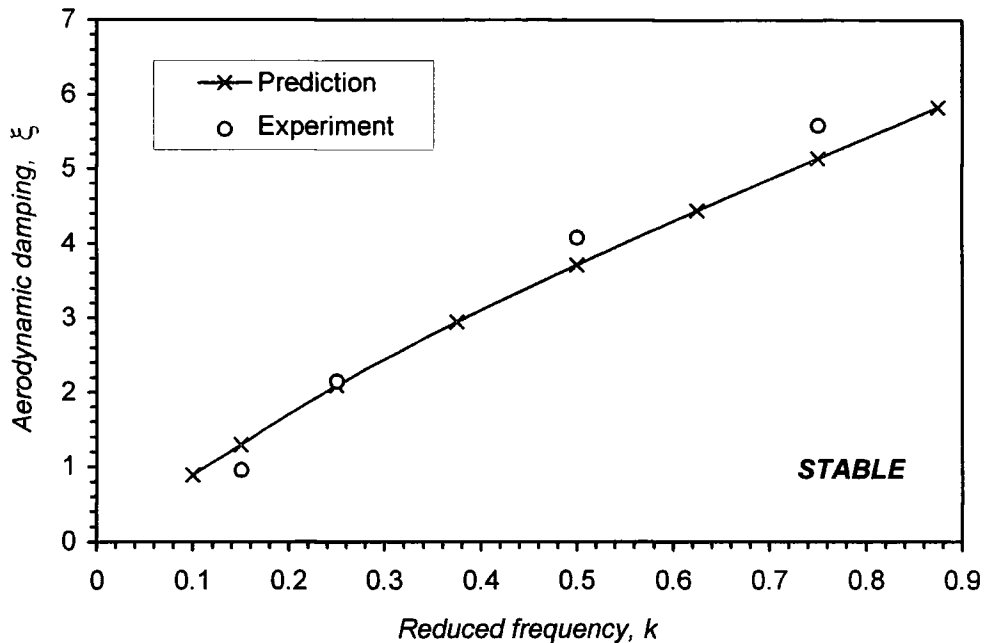
Figure 6.18: Predicted and measured variation aerodynamic damping (ξ) with reduced frequency

confined to a region of moderate to low unsteady pressure activity. The contribution of the unsteady aerodynamic response within this region (near the trailing edge) towards the aerodynamic damping is therefore relatively small. Indeed, this is reflected by the excellent agreement between the predicted and measured variation in local aerodynamic damping along the blade span, shown in figures 6.8, 6.11, 6.14 and 6.17 for each of the four test case reduced frequencies.

In terms of engineering practicality, the most important feature of the computational solutions is the accuracy and consistency with which they predict aerodynamic damping, since this will ultimately determine the capability of establishing stability margins. Figure 6.18 shows a most encouraging result in both these respects, with a very good quantitative comparison between the predicted and measured aerodynamic damping evident throughout the range of reduced frequency considered. Apart from demonstrating the capability of the computational method to predict the relevant unsteady aerodynamic phenomenon, the good level of agreement reinforces the observation that the predominant unsteady flow mechanisms are inviscid.

116

6.3.3 Quasi-3D Computations

The observed three dimensional behaviour of unsteady aerodynamic response, most especially in terms of the insensitivity of the unsteady pressure generation to the local bending amplitude, clearly challenges the validity of the conventional quasi-3D strip method for the prediction of oscillating blade flows of the present kind. To clarify the importance of this phenomenon and the capability of a quasi-3D approach to the prediction of the unsteady flow, a computational solution was subsequently obtained at a test case reduced frequency of 0.25 through a series of eleven 2D computations performed at equally spaced sections along the blade span. The performance of this quasi-3D prediction is evaluated in figures 6.19 and 6.20 through comparison with both the test data and the full-3D prediction.

Figure 6.19 shows the predicted and measured amplitude of first harmonic pressure on the suction surface at three spanwise sections: 10% span, midspan and 90% span. The prediction obtained with the quasi-3D method, shown in figure 6.19(i), clearly shows the inability of this method to capture the insensitivity of the amplitude of unsteady pressure to the local bending amplitude exhibited by the test data. Whereas the full 3D prediction, shown in figure 6.19(ii), demonstrates very good agreement with the test data at all spanwise sections, the quasi-3D version of this method grossly under predicts the amplitude of unsteady pressure at 10% span and grossly over predicts it at 90% span, although very good agreement is apparent at midspan.

The influence of the erroneous predictions, obtained from the quasi-3D method towards the hub and tip sections, upon local aerodynamic damping[†] is shown in figure 6.20. From the hub section to approximately 70% span the quantitative agreement with the test data exhibited by the quasi-3D prediction of local aerodynamic damping is fair, although it is clearly poorer than that obtained with the full 3D prediction. Towards the tip section, however, the level of agreement deteriorates quite markedly, with a pronounced over-prediction of local aerodynamic damping by the quasi-3D method. This is associated with the over predicted amplitude of unsteady pressure towards the tip section, which becomes exaggerated in the evaluation of local aerodynamic damping through the increased local bending amplitude imposed in this region. Although the under prediction of local

---

[†]   The local aerodynamic damping is evaluated using the local bending amplitude which increases linearly along the blade span. For a full definition of local aerodynamic damping refer to section 4.2.2 (Eq. 4.13).
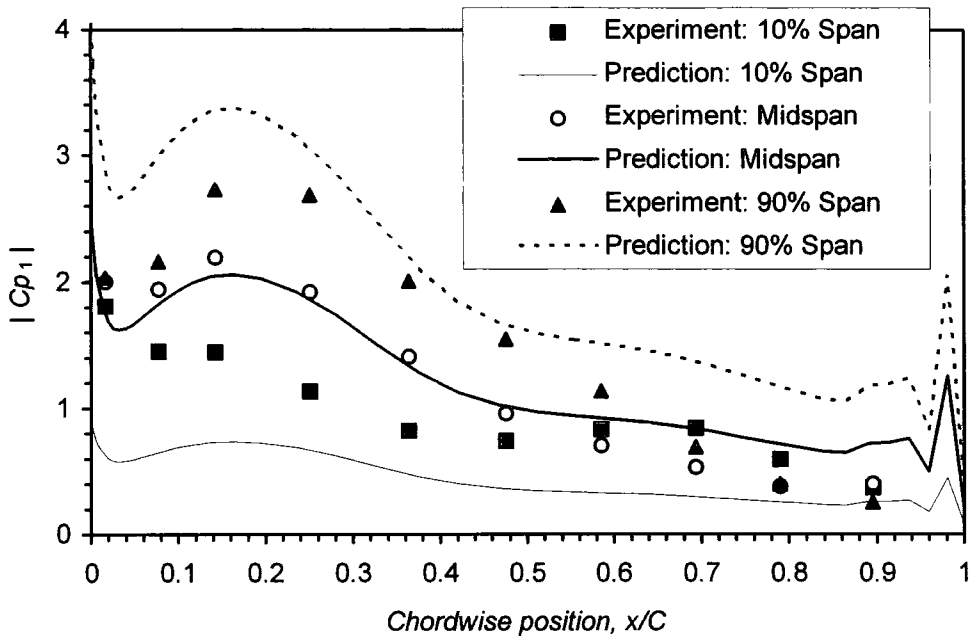
(i). Quasi-3D prediction
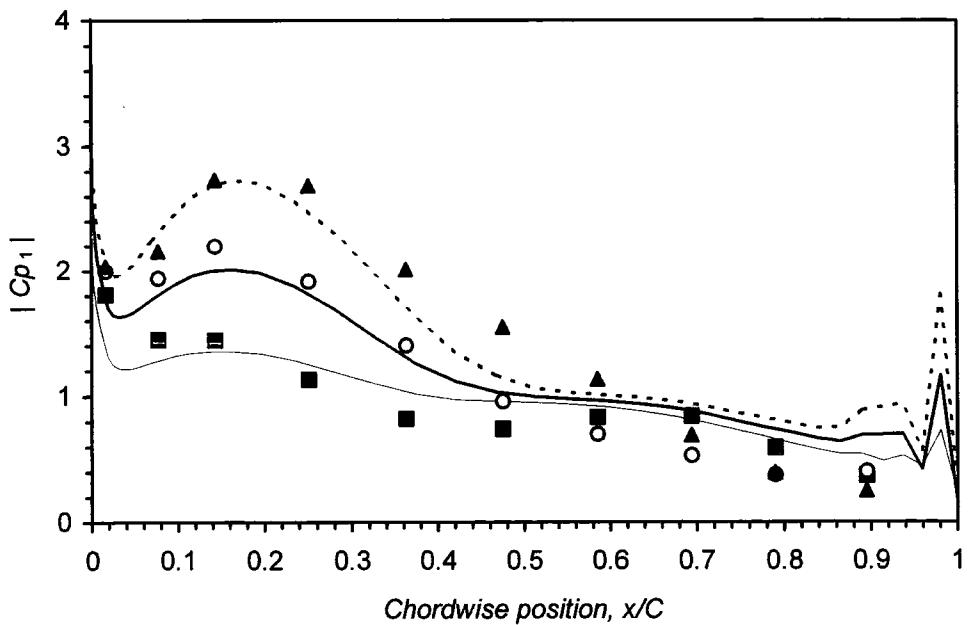
(ii). Full-3D prediction

Figure 6.19: Comparison of predicted amplitude of first harmonic pressure obtained with quasi-3D and full 3D Euler method (suction surface, k: 0.25)

118
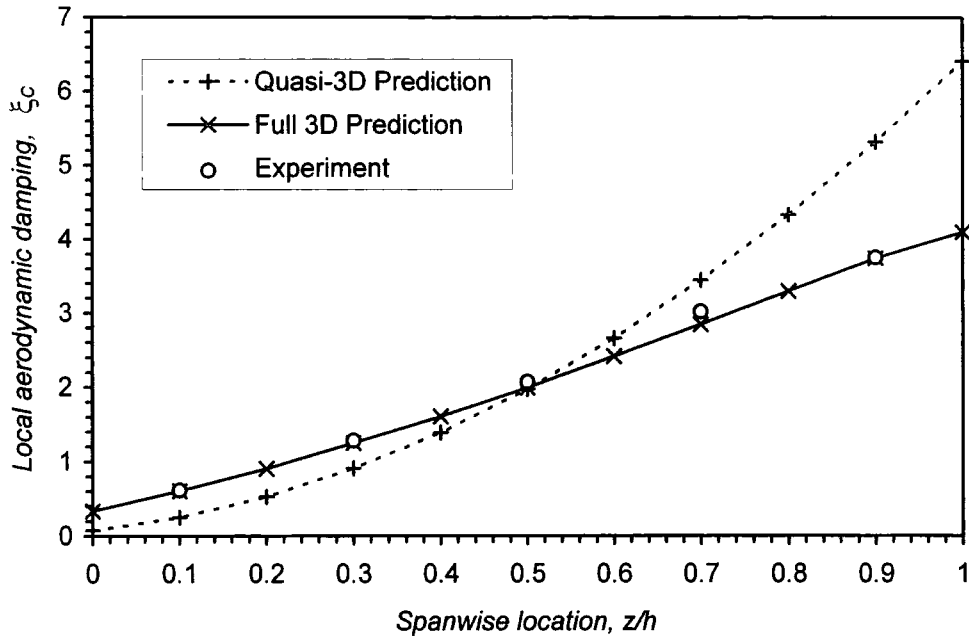
Figure 6.20: Comparison of predicted local aerodynamic ** **damping obtained with quasi-3D and full 3D method, *k*: 0.25**

**Note the definition of local aerodynamic damping, $\xi_C = \int_C \dfrac{-\pi B_L |Cp_1| Sin\phi_1}{CB_C} dA$

	Aerodynamic damping	Deviation from test data
Experimental Test Data:	2.143	
Full 3D prediction:	2.084	-2.8%
Quasi-3D prediction:	2.403	12.1%

Table 6.1: Comparison of predicted aerodynamic damping obtained with quasi-3D and full 3D Euler method

aerodynamic damping observed towards the hub section somewhat cancels the over-prediction at the tip, the disproportionate contribution from the tip region due to the increased local bending amplitude results in an over-prediction in the overall aerodynamic damping by 12% (compared to an under prediction by 3% from the full 3D method), as shown in table 6.1.

6.4 Summary

An extended, three dimensional time-marching Euler method for the prediction of flow around oscillating turbomachinery blades has been described, along with the modifications required for direct simulation of the experimental test cases presented in chapter 5.

The solutions obtained from the computational method, which are the first to be supported by 3D test data, were most encouraging. A good qualitative and quantitative agreement with the experimental test data was generally achieved and the method was observed to adequately capture the three dimensional behaviour of the unsteady flow. Apart from demonstrating the capability of the present method, the results also indicated that the unsteady flow was largely governed by inviscid mechanisms.

Quasi-3D solutions were also presented. These highlighted the strong three dimensional nature of the unsteady aerodynamic response and demonstrated apparent deficiencies of the conventional strip method approach to the prediction of unsteady flows of the present kind. The quasi-3D version of the computational method was unable to capture the insensitivity of the amplitude of unsteady pressure to the local bending amplitude, and the marked over-prediction of unsteady pressure observed towards the blade tip led to an over-prediction in aerodynamic damping.

Chapter Seven

The Influence of Tip Leakage on the Oscillating Turbine Blade Flow

An additional experimental investigation, designed to assess the influence of tip leakage upon the local unsteady aerodynamic response of the oscillating turbine blade, is documented here. The chapter opens with a brief overview of the motivation behind this investigation, followed by a description of the experimental set-up. A series of steady flow experimental measurements obtained at three different tip clearances are then provided, in order to identify features of the three dimensional tip leakage flow structure which may influence the local unsteady aerodynamic response of the oscillating turbine blade. In the final part of this chapter a comprehensive set of unsteady pressure measurements, acquired at each setting of tip clearance, are presented and discussed.

The steady flow measurements indicate a characteristic behaviour of the tip leakage flow throughout the range of tip clearance and demonstrate that despite the somewhat unusual configuration, the test facility provides a suitable vehicle for the investigation undertaken. The detailed nature of the unsteady pressure measurements presented also allows the influence of the tip leakage flow upon the local unsteady flow to be examined. And the results generally show the change in tip clearance to have limited effect upon the unsteady aerodynamic response of the oscillating turbine blade although subtle, but consistent, trends are evident in the unsteady pressure measurements obtained at 90% span.

7.1 Motivation

The high amplitudes of vibration endured towards the tip section of oscillating high aspect ratio, unshrouded turbomachinery blades - which are the type most susceptible to aeroelastic instability - means that a significant contribution towards aerodynamic damping can be expected from the unsteady aerodynamic response induced within this

region. The flow structure towards the tip section of these blades is, however, extremely complex, with three dimensional phenomenon associated with the tip leakage flow and to a lesser extent the blade passage secondary flow particularly prominent, as previously indicated in figure 1.3. Now although the deleterious steady flow nature of these secondary flow structures has been investigated at depth, their influence upon the aeroelastic stability of vibrating turbomachinery blades remains unexplored apart from the contribution of Norryd & Bölcs, which assessed the influence of tip clearance on the mid-span unsteady aerodynamic response of an oscillating linear turbine cascade. Their work highlighted a significant variation in the measured amplitude of unsteady pressure through a range tip gap settings, although the aerodynamic damping was largely unaffected

In regard to the potential influence of tip endwall secondary flow structures, it would appear significant that good quantitative agreement was obtained with the experimental test data through inviscid computations that neglected to model the tip clearance present in the experimental configuration. This would seemingly suggest that the three dimensional endwall flow structures - particularly the tip leakage flow which was identified in section 5.1 - largely unaffect the unsteady aerodynamic response of the oscillating turbine blade or at the most exert a very localised influence. For these particular cases it was apparent, however, that the steady flow blade loading within the instrumented section of the blade (10% to 90% span) was also largely unaffected by the tip leakage flow. Subsequently, it remains unclear how a more pronounced tip leakage flow, which is likely to exert a more marked influence upon the steady flow blade loading, would affect the unsteady aerodynamics. The present investigation is intended to address this matter through providing a more thorough, albeit preliminary, indication of the influence of tip leakage upon the unsteady aerodynamic response of the oscillating turbomachinery blade. This is achieved through comparison of detailed steady flow and unsteady pressure measurements obtained at various settings of tip clearance.

7.2 Experimental Set-Up

A series of steady and unsteady flow experiments were performed at three different settings of tip clearance (0.5%, 1.0% and 1.5% chord), under the free stream conditions previously described in table 3.2. At each setting of tip clearance, the steady flow blade surface pressure distribution was obtained from the five spanwise sections of tappings, distributed between 10% and 90% span, to allow any significant influence of the tip leakage flow upon the local blade loading to be readily identified. A five-hole probe traverse was also performed at the exit traverse plane, to provide an indication of the

strength and structure of the tip leakage flow for each case. In addition to the steady flow experiments, unsteady blade surface pressure measurements were acquired at four values of reduced frequency (k: 0.15, 0.25, 0.50 and 0.75 - as specified in table 3.2) for each setting of the tip clearance.

The previous experimental measurements were acquired under conditions of uniform inlet flow, which were realised through bleeding the wind tunnel wall boundary layers. However, in the interests of realism and to promote the generation of secondary flow structures in the present investigation, a thickened boundary layer was introduced at the tip endwall which is shown by the pitch-averaged inlet velocity profiled in figure 7.1.
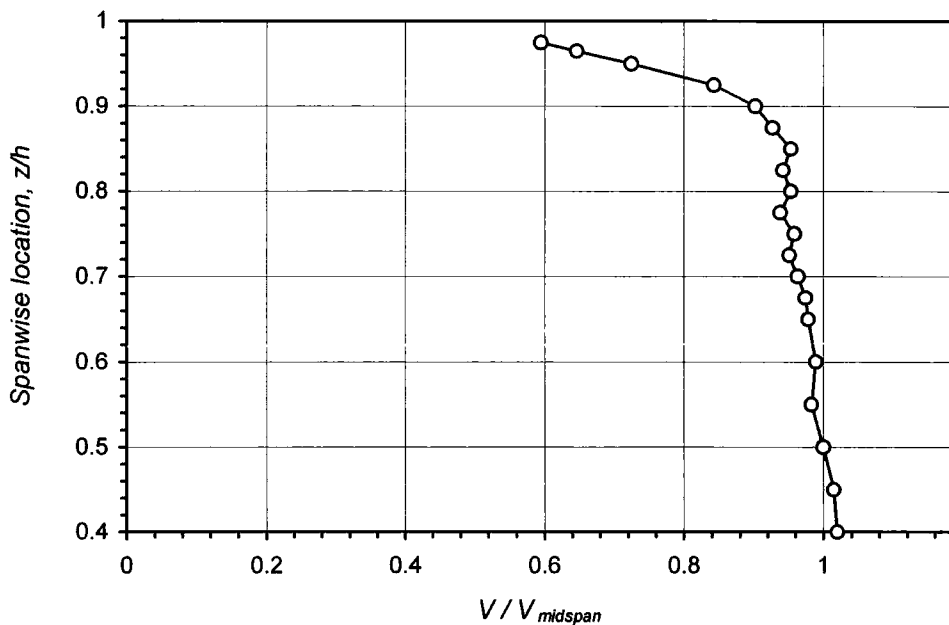
Figure 7.1: Pitch-averaged inlet velocity profile

(Five-hole probe measurements obtained at the inlet traverse plane)

7.3 Steady Flow Measurements

A detailed appraisal of the steady flow nature of tip leakage flows is beyond the scope of the present work, to this end the reader is directed to the overview of this substantive field of research made by Sjolander (1997). Rather, the purpose of this section is to provide the aerodynamic background for the unsteady experiments and identify features of the three dimensional steady flow structure which may influence the unsteady aerodynamic response of the oscillating turbine blade. The steady flow measurements obtained for each setting of tip clearance are presented in figures 7.2 to 7.5.
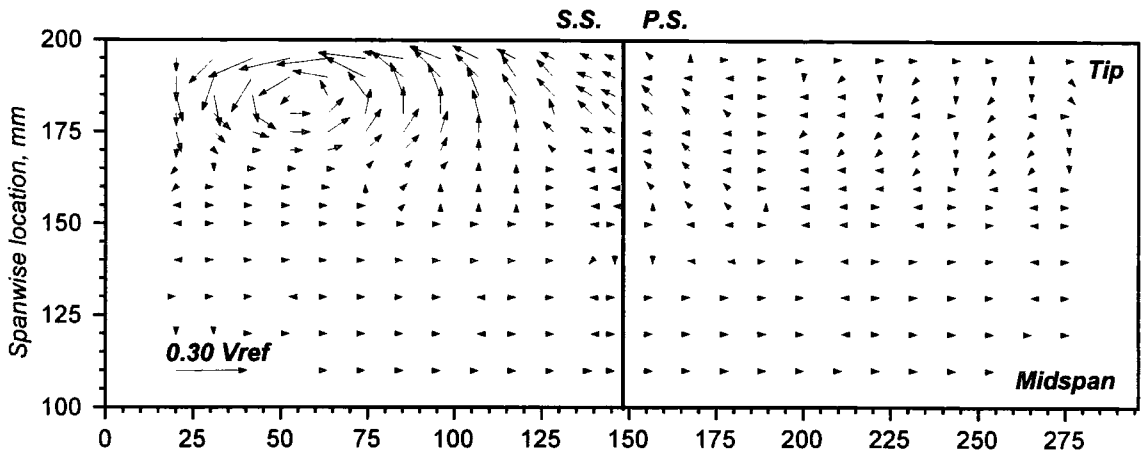
(i). Tip clearance: 0.5% chord
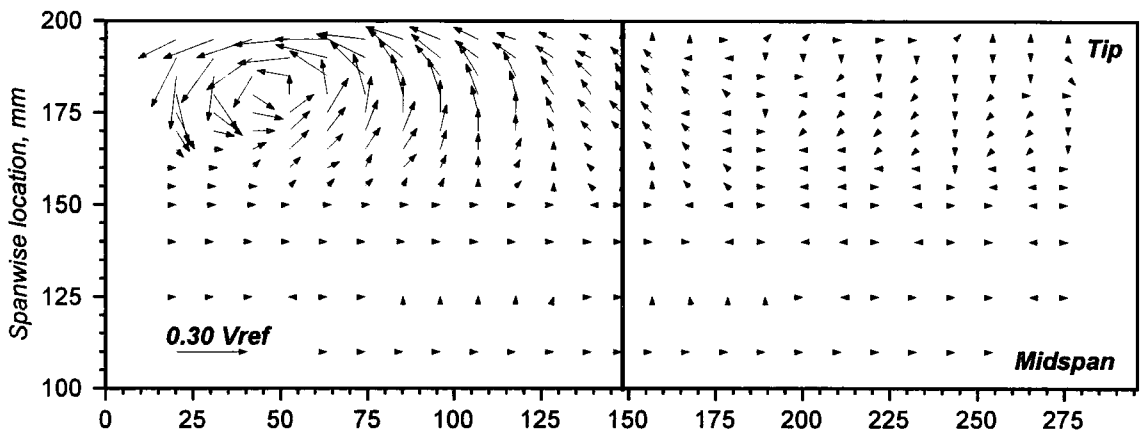
(ii). Tip clearance: 1.0% chord
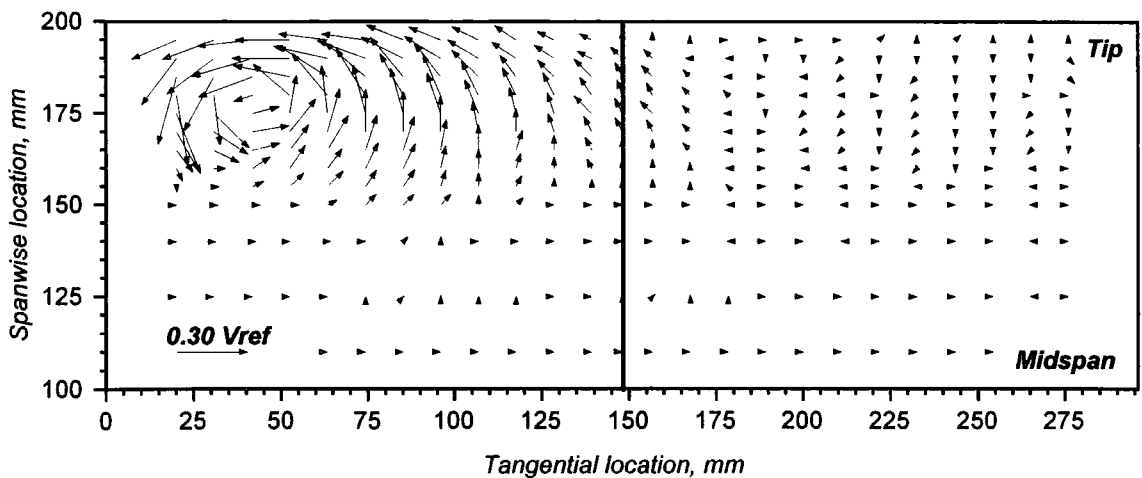
(iii). Tip clearance: 1.5% chord

Figure 7.2: Variation in secondary velocity with tip clearance
(Five-hole probe measurements at the outlet traverse plane)

124
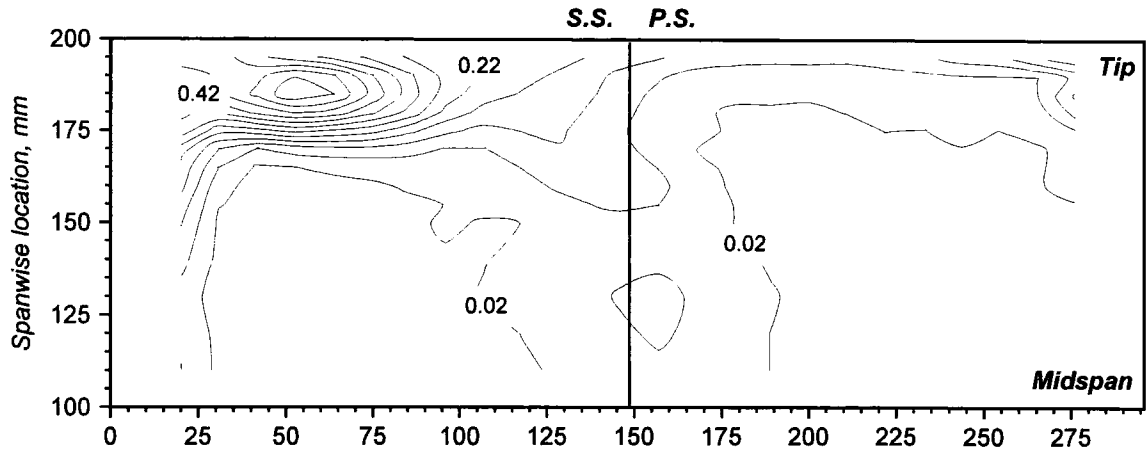
(ii). Tip clearance: 0.5% chord
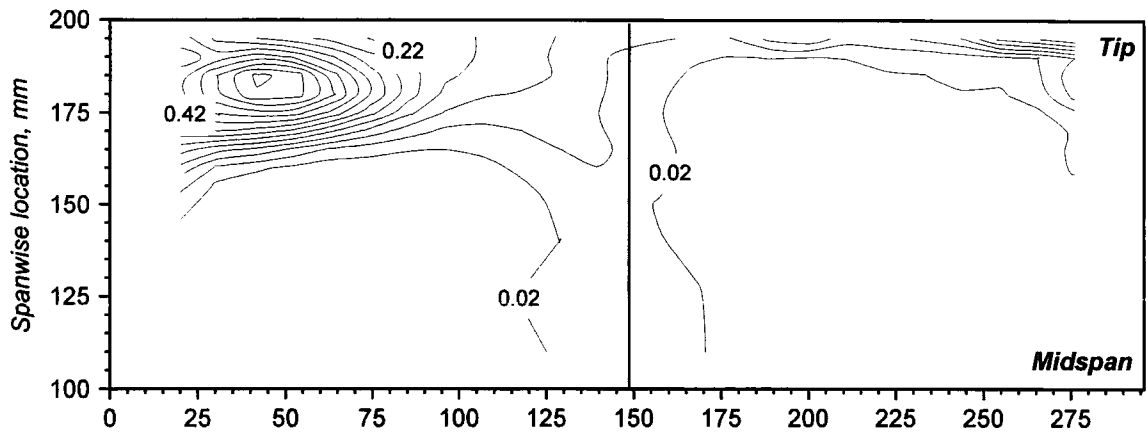
(ii). Tip clearance: 1.0% chord
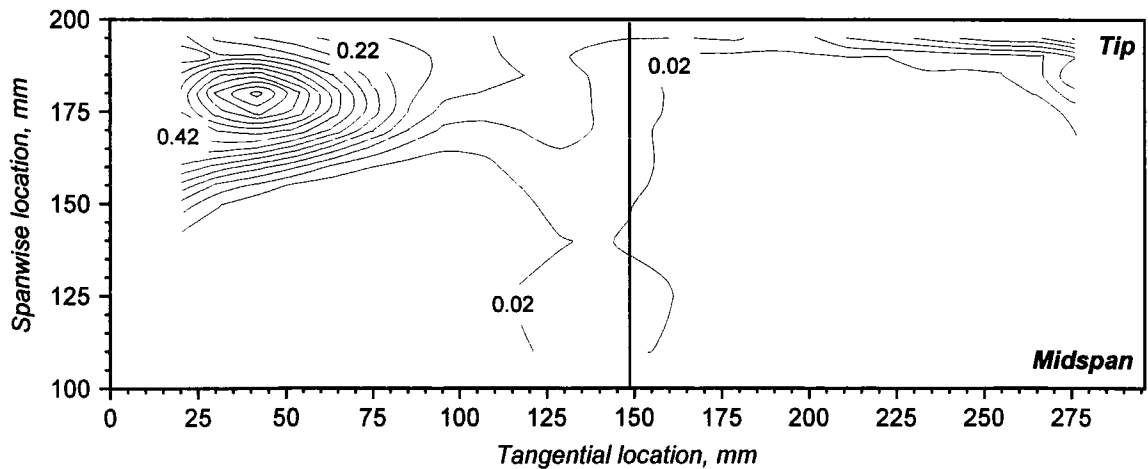
(iii). Tip clearance: 1.5% chord

Figure 7.3: Variation in coefficient of total pressure loss (Y) with tip clearance

at outlet traverse plane - contours drawn at increments of $dY = 0.05$
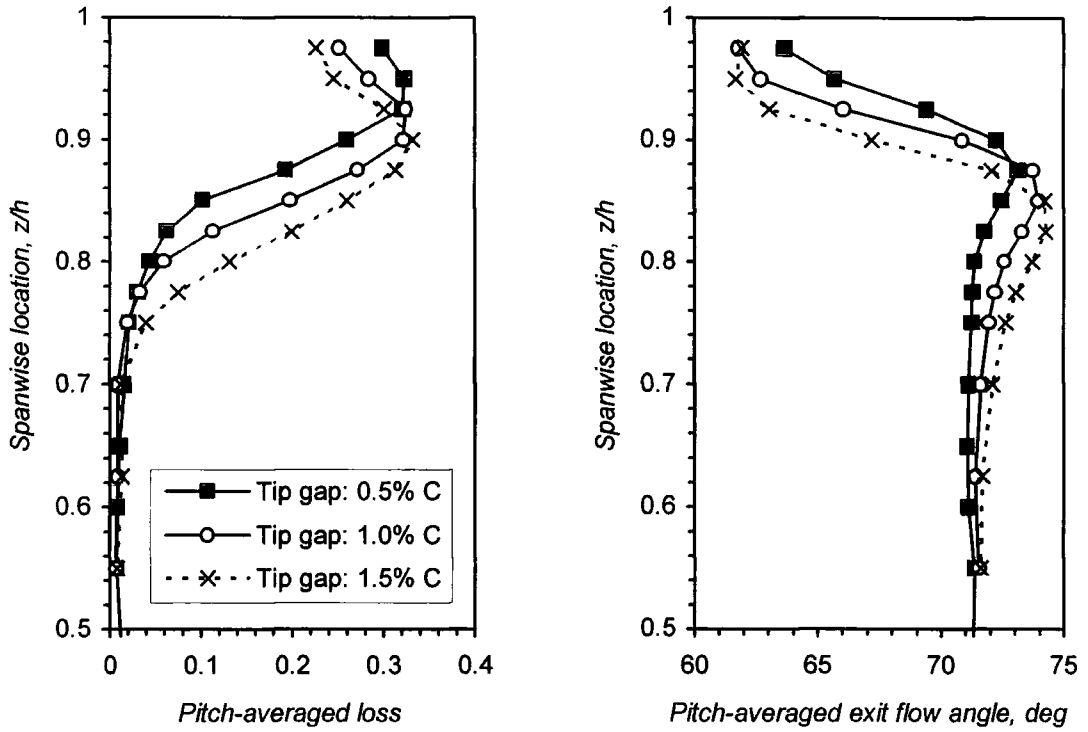
Figure 7.4: Spanwise variation in pitch-averaged total pressure loss ($\overline{Y}$) and exit flow angle ($\overline{\alpha}$) at downstream traverse plane
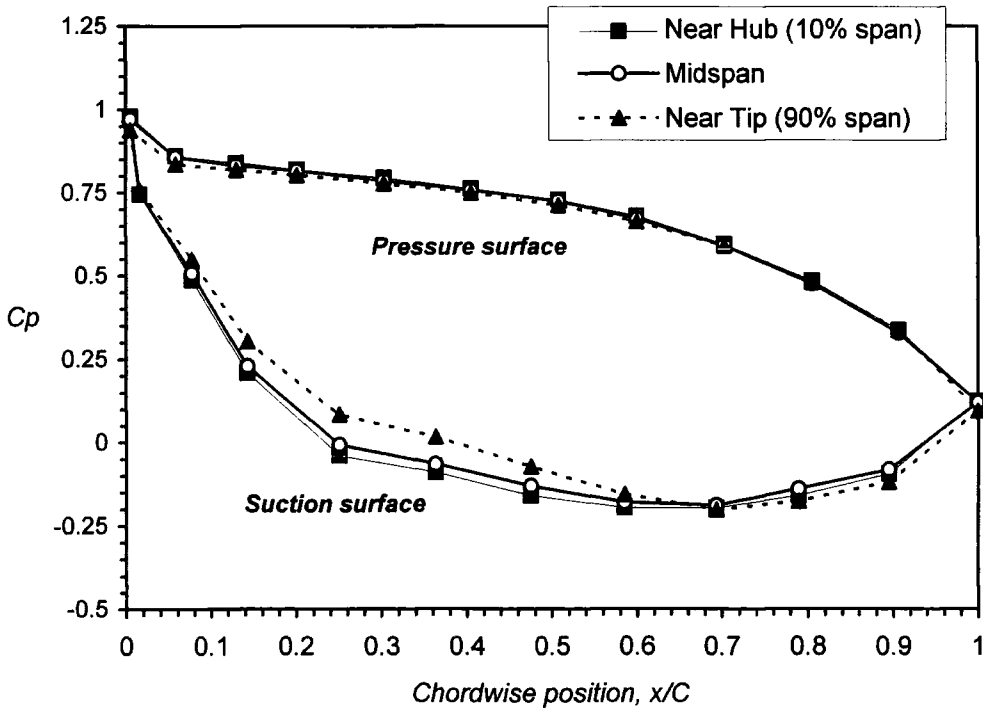
7.5(i): Blade surface pressure distribution (tip clearance: 0.5% chord)
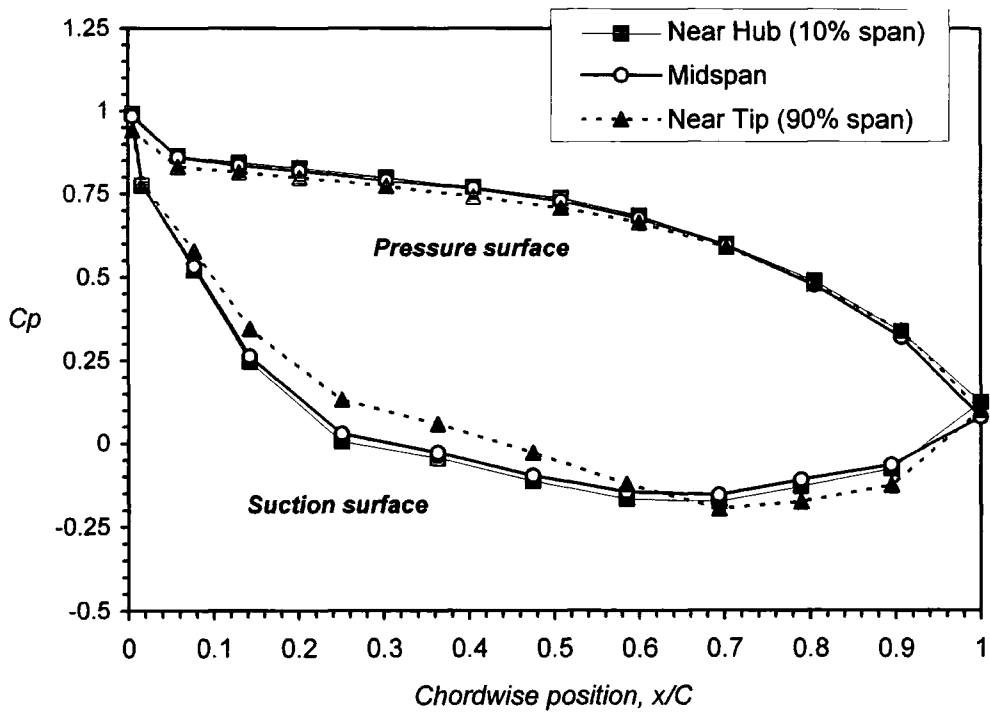
(ii). Tip clearance: 1.0% chord
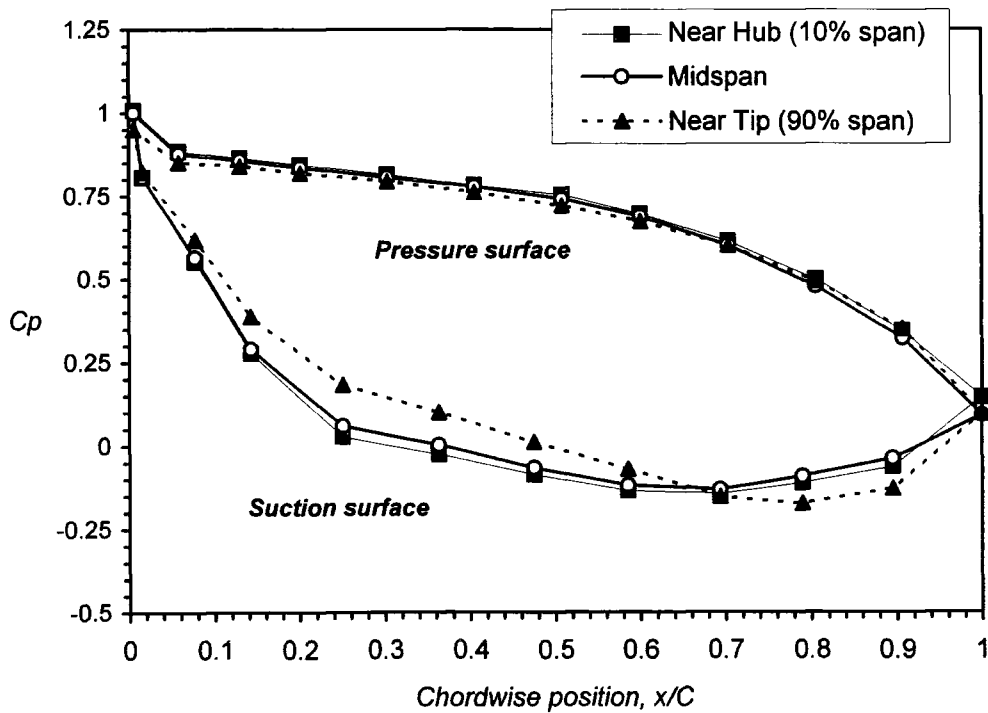
(iii). Tip clearance: 1.5% chord

7.5: Variation in blade surface pressure distribution with tip clearance

The results of the five-hole probe steady flow measurements performed at the exit traverse plane, located 75% chord downstream of the trailing edge, are presented for each tip clearance as secondary velocity vectors in figure 7.2, contours of total pressure loss in figure 7.3 and in pitch averaged form (total pressure loss and exit flow angle) in figure 7.4. The plots of secondary velocity vectors and contours of total pressure highlight the dominance of the tip leakage flow, whilst there is a notable absence of evidence to suggest the presence of an appreciable blade passage secondary flow for the present cases of moderate flow turning and significant tip clearance. Throughout the range of tip clearance, a significant tip leakage vortex can be observed at the downstream measurement plane in the near tip endwall region and towards the left side wall, as indicated by the anticlockwise rotation of secondary velocity vectors in figure 7.2 and the associated loss core in figure 7.3. It is apparent then, that the tip leakage flow has undergone a significant tangential migration due to the underturning which is associated with this phenomenon.

The secondary velocity vectors and contours of total pressure loss also indicate a characteristic behaviour of the tip leakage flow, with a marked and consistent increase in the size and strength of the tip leakage vortex as the tip gap is increased, which is fundamentally caused by the increase in mass flow through the tip clearance. This basic behaviour of the tip leakage flow subsequently results in a secondary phenomenon, whereby the centre of the vortex is observed to migrate further towards the left hand sidewall and away from the tip endwall with increases in the tip gap, as seen in figure 7.3.

The spanwise variations in the pitch-averaged total pressure loss and exit flow angle shown in figure 7.4 give a quantitative indication of the characteristic behaviour of the tip leakage flow through the range of tip clearance, which supports the qualitative trends observed in figures 7.2 and 7.3. The spanwise variation in pitch-averaged total pressure loss (figure 7.4) clearly shows the increasing size of the loss core through the range of tip clearance, with the spanwise height subtended by the loss core increasing quite linearly with tip clearance. As the tip leakage vortex deepens with increasing tip gap, the peak in loss can also be observed to move away from the tip endwall, although the magnitude of this peak remains fairly uniform. The spanwise variation in exit flow angle (figure 7.4) captures a marked region of underturning towards the tip endwall region which is a characteristic feature of this secondary flow phenomenon. Through the range of tip clearance the peak magnitude of underturning increases, with a maximum underturning of -7.5° recorded for a tip gap of 0.5% chord and -10° for a tip gap of 1.5% chord. Alike the

variation recorded for total pressure loss, the region of underturning subtends a greater spanwise distance from the tip endwall with increasing tip clearance, with a quite linear pattern in evidence. Further away from the endwall the underturning is balanced somewhat by a comparatively weak region of overturning, which also increases in size and strength with tip clearance.

The plots presented in figure 7.5 show the changes in steady flow blade loading induced by the variation in tip clearance, through the comparison of pressure distributions at three spanwise sections: 10% span (near the hub), midspan, and 90% span (near the tip). Upon close inspection of the three plots, which are provided for each level of tip clearance, it is apparent that there is a general shift in the suction surface pressure distribution at all spanwise locations between the three cases, with an overall unloading of the blade with increasing tip clearance indicated by the measurements. Whilst in contrast, the pressure surface response is unaffected by the change in tip clearance, at least between 10% and 90% span. Sjolander & Amrud (1987) observed a similar scenario in an investigation of the influence of tip leakage on turbine blade loading, and offered a plausible explanation of the phenomenon in terms of a reduction in incidence induced by the increasing strength of the tip leakage vortices emerging at the tip of the suction surface.

Between 10% and 70% span the blade pressure distribution is reasonably two dimensional, although a subtle increase in loading is in evidence towards the hub endwall. At the 90% span location, however, the pressure distribution over the suction surface deviates quite markedly from that observed at the midspan, with the deviation becoming more pronounced with increasing tip clearance. From approximately 10% to 60% chord there is an unloading of the suction surface compared to the midspan response, which becomes more prominent with consistent increases in tip clearance. An increase in suction, compared to midspan, also becomes increasingly evident for the two largest tip clearances aft of 70% chord and towards the trailing edge of the suction surface. Measurements presented by Sjolander & Amrud (1987) and Sjolander (1997) also showed a qualitatively similar pattern in the loading of the suction surface towards the tip section. Visualisation of spanwise flow structures in their work showed the decrease in loading to be caused by the deflection of flow away from the tip of the suction surface on entering the blade passage, whilst the increase in suction further down the blade chord developed as the tip leakage vortex rolls up along the suction surface. This induces higher velocities over the blade surface, which manifests as the increase in suction observed aft of 70% chord at 90% span. Both these secondary flow mechanisms become more pronounced as

the tip leakage flow becomes more powerful, i.e. as the tip clearance is increased, which is reflected by the trends in blade loading towards the tip of the suction surface.

In contrast to the trends observed for the suction surface, the pressure surface loading is largely unaffected by the tip leakage between 10% and 90% span, although significant changes are typically observed nearer the tip section, e.g. Sjolander & Amrud (1987).

The steady flow measurements presented within this section show a marked change in the size and strength of the tip leakage flow through the range of tip clearance examined, but moreover, the results consistently indicate a characteristic behaviour of the tip leakage flow. This demonstrates that despite the somewhat unusual test configuration, a suitable environment is provided to assess the influence of tip leakage flow on the unsteady aerodynamic response of the oscillating turbine blade.

7.4 Unsteady Pressure Measurements

The processed results of unsteady pressure measurements, which were obtained over a range of reduced frequency for each setting of tip clearance, are presented here.

The extensive data generated by the series of unsteady experiments meant that it was easiest to compare results obtained for each setting of tip clearance through consideration of global parameters, i.e. local and overall aerodynamic damping. Figure 7.6 shows the variation in overall aerodynamic damping through a range of reduced frequency of 0.15 to 0.75 for each setting of tip clearance. The plot clearly indicates the overall aerodynamic damping to be largely unaffected by the change in tip clearance throughout the range of reduced frequency examined, with the limited variation between the three curves of a comparable order of magnitude to the experimental error. Equally, figure 7.7 shows there to be limited variation in the local aerodynamic damping throughout the range of tip clearance.

The uniform levels of aerodynamic damping observed through the range of tip clearance - which it must be remembered are evaluated from unsteady pressure measurements confined to locations between 10% and 90% span - clearly suggest that the tip leakage flow exerts a negligible influence on the overall unsteady aerodynamic response of the oscillating blade. Comparison of global parameters alike aerodynamic damping can, however, prove misleading when unsupported by a more detailed analysis of unsteady pressure data, as demonstrated by the fair level of predicted overall aerodynamic damping

by the quasi-3D computations in section 6.3.2. Indeed, in the present case it was found that the change in tip clearance induced a subtle but consistent variation in the first harmonic pressure response at the 90% span location, whilst other spanwise sections were unaffected.
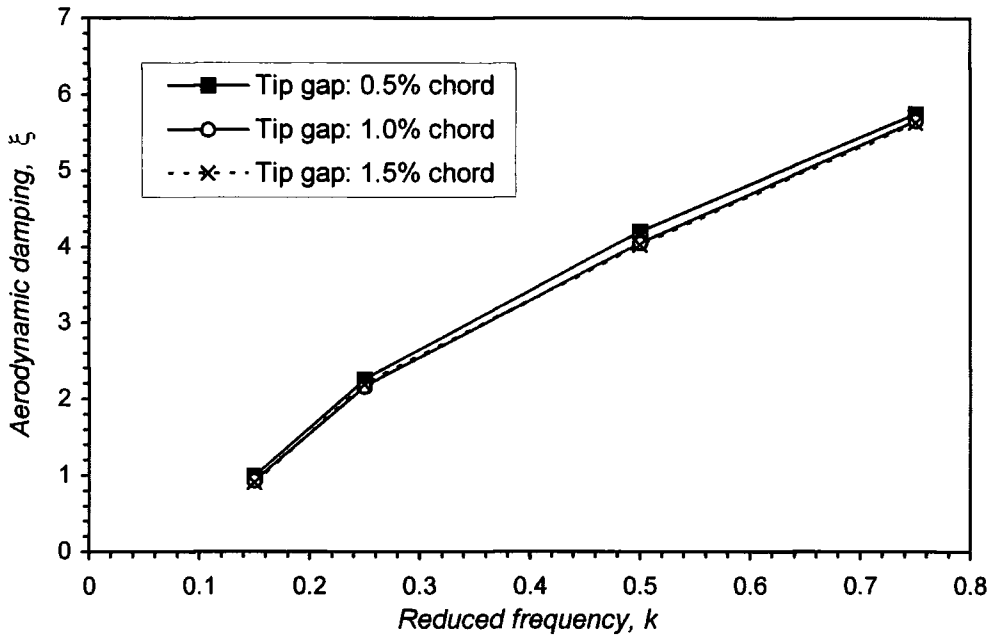
Figure 7.6: Variation in aerodynamic damping with tip clearance (k: 0.15 to 0.75)

Figure 7.8 shows the amplitude, and figure 7.9 the phase angle, of the first harmonic pressure response recorded at 90% span for the extreme tip gaps (0.5% and 1.5% chord). The results are arbitrarily selected for reduced frequencies of 0.25 and 0.75, although the trends observed for these cases are typical of the full range of reduced frequency. Differences in the amplitude of the first harmonic pressure response of the suction surface are evident at 90% span for the different settings of tip clearance, as seen in figure 7.8. It is apparent in this figure that as the tip clearance increases, the amplitude of the unsteady pressure consistently reduces for all measurement positions between the leading edge and 30% chord on the suction surface. In contrast, aft of 60% chord the amplitude of unsteady pressure can be observed to increase with tip gap. The amplitude of unsteady pressure recorded for the pressure surface is, however, seemingly unaffected by the change in tip clearance. Differences are also present in the phase angle of the first harmonic pressure response for the suction surface. The phase angle reduces more rapidly towards the trailing edge as the tip clearance increases, although the maximum deviation represents less than 15°.

131
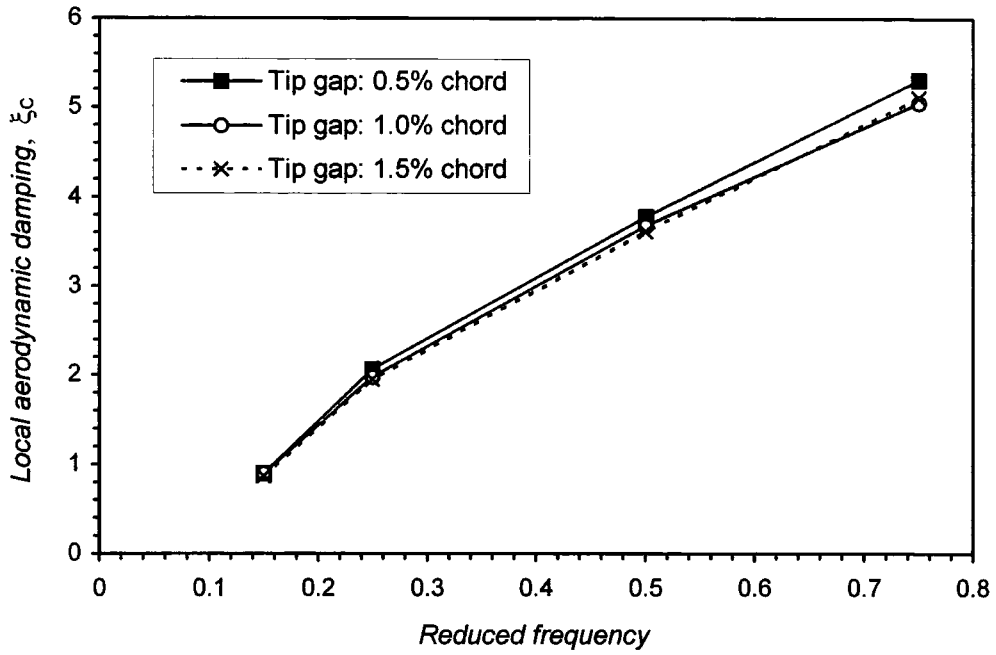
(i). Local aerodynamic damping at midspan (k:0.15 to 0.75)
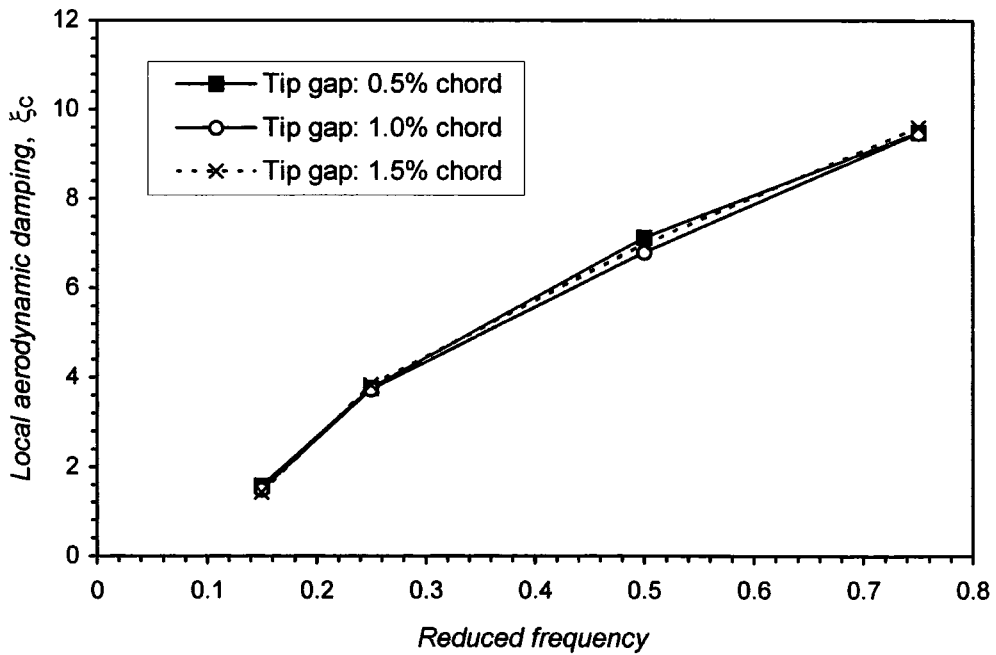
(ii). Local aerodynamic damping at 90% span (k:0.15 to 0.75)

Figure 7.7: Variation in local aerodynamic damping with tip clearance
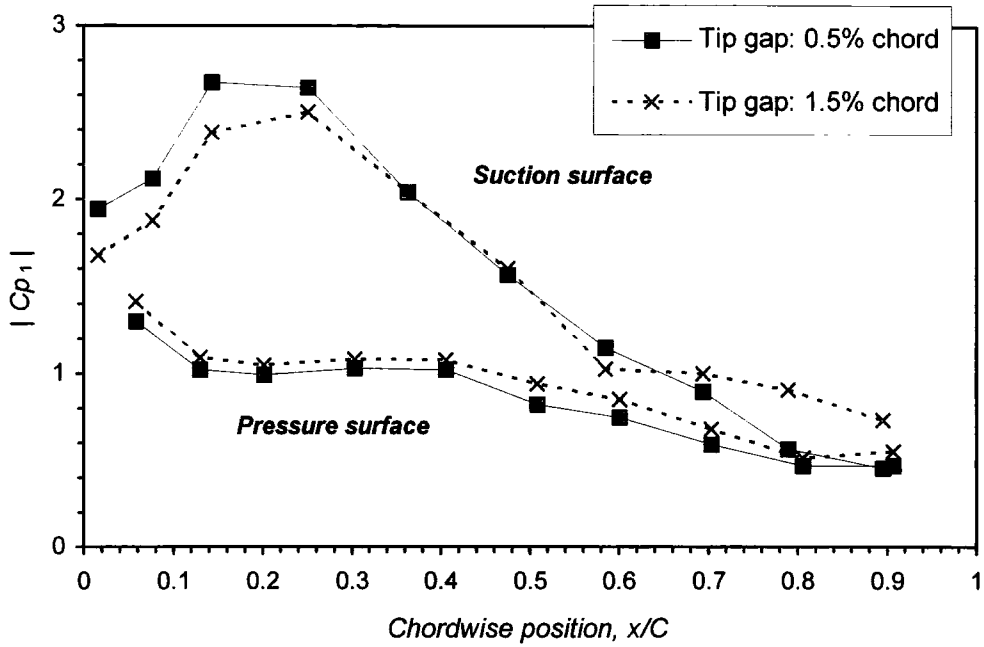
(i). Reduced frequency: 0.25
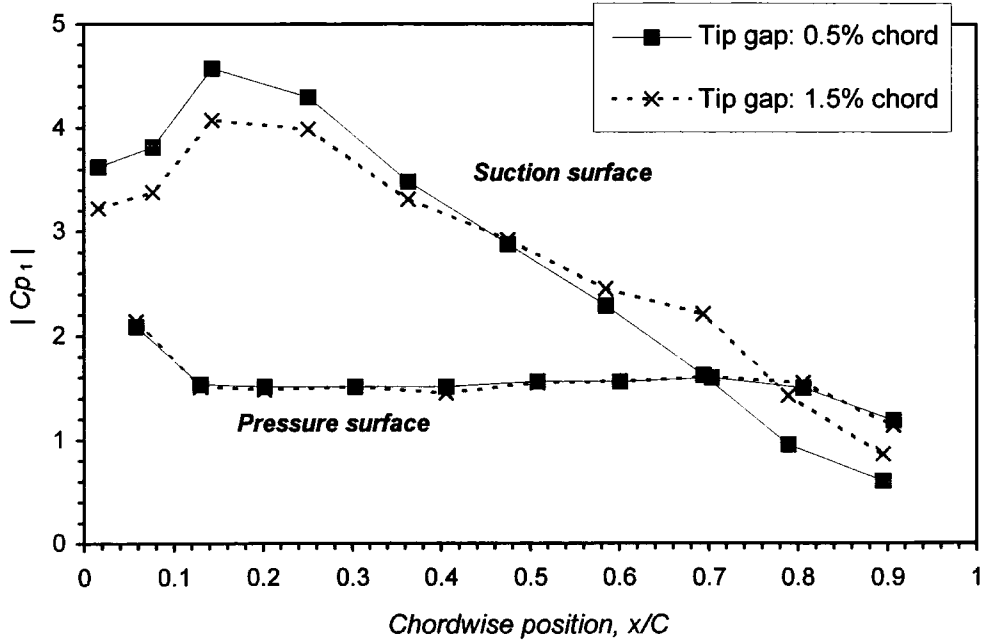
(ii). Reduced frequency: 0.75

Figure 7.8: Variation in amplitude of first harmonic pressure at 90% span with tip clearance, *k*: 0.25 and 0.75

133
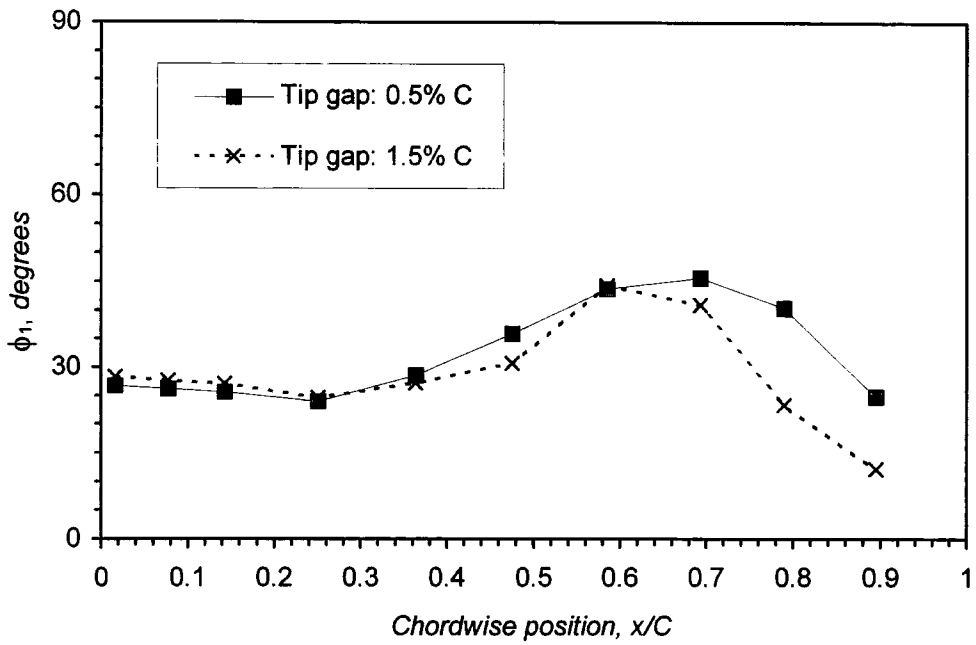
(i). Reduced frequency: 0.25
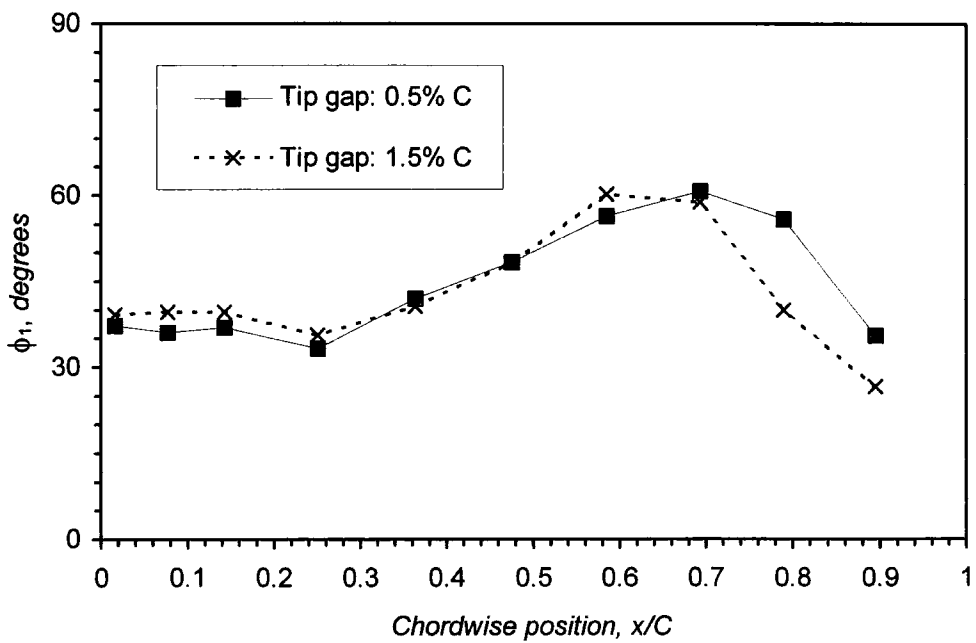
(ii). Reduced frequency: 0.75

Figure 7.9: Variation in phase angle of first harmonic pressure on the suction surface at 90% span with tip clearance, *k*: 0.25 and 0.75

134

It is notable, and believed significant, that the trends in amplitude of unsteady pressure with tip clearance are in correspondence with the deviation observed in steady flow blade loading from the midspan response. The slight increases in unloading observed for the suction surface with increasing tip gap, coincide with the reduction in $|Cp_1|$, whilst the increases in suction observed towards the trailing edge of the suction surface for increasing tip gap coincide with the increases in amplitude of unsteady pressure.

It is recognised that the trends in amplitude of the unsteady pressure response, observed for the changes in tip gap, do not represent substantial changes in the unsteady aerodynamic response. However, the consistent nature of results throughout the range of reduced frequency support the presumption that these trends are true aerodynamic effects of the variation in tip clearance. The fact that these effects have been observed at the 90% span location, where only moderate variation in the blade loading is induced by the tip leakage, also gives rise to conjecture that the influence of tip leakage on the unsteady aerodynamic response will be considerably more significant nearer the tip section where the tip leakage flow will exert a more pronounced influence on the blade loading. It must also be recalled here, that the contribution towards aerodynamic damping is disproportionately weighted towards the tip section due to the high amplitudes of vibration. Subsequently, it remains unclear whether the tip leakage flow could have a significant effect on the *actual* aerodynamic damping through generating very high spanwise gradients in both the steady and unsteady loading within the very near tip region, i.e. above the 90% span location.

The test configuration clearly neglects to model certain features of realistic tip geometries. The blade is clearly thicker than that normally encountered towards the tip section of high aspect ratio blades, and the test facility does not allow the influence of rotation of the outer casing relative to the tip section to be addressed. It is therefore difficult to extrapolate the findings of this particular study to predict the precise influence of tip leakage in the unsteady aerodynamic response of realistic turbomachinery configurations. Nonetheless, the results indicate that the considerable tip leakage flow observed within test facility largely unaffects the overall aerodynamic response of the oscillating turbine blade, with deviations in the unsteady aerodynamic response confined to a localised section of the blade where tip leakage flow exerts an discernible influence on the steady flow loading characteristic.

Chapter Eight

Concluding Remarks

8.1 Conclusions

A detailed experimental and computational study into the behaviour of flow around a turbine blade oscillating in a three dimensional bending mode has been presented. The work documented in the preceding chapters, which was motivated by the urgent need to improve current understanding and provide 3D test data for the validation of advanced computational methods for the prediction of blade flutter, is divided into four complimentary parts. These deal with:

- The development, from conception, of a low speed experimental test facility
- The presentation and analysis of experimental results, which constitute the first 3D test cases for aeroelastic application in turbomachines
- The development and performance of an extended 3D time-marching Euler method for the prediction of oscillating blade flows
- The influence of tip leakage flow on the unsteady aerodynamics of oscillating turbomachinery blades

8.1.1 The Development of a Low Speed Flutter Test Facility

A low speed flutter test facility was commissioned for the purposes of the present work, with the objective to provide detailed and reliable 3D test data for aeroelastic applications. The facility employs an unusual configuration at the working section, in which a single turbine blade is mounted within a profiled duct and driven in a three dimensional bending mode. At some cost in terms of modelling a realistic turbomachinery configuration, the test facility offers an important benefit of clearly defined boundary conditions which has

136

proved troublesome in previous oscillating linear cascade experiments due to the difficulty encountered in establishing a periodic unsteady flow. Detailed measurement of the unsteady pressure response of the oscillating turbine blade is also enabled, through the use of externally mounted pressure transducers which is permitted by the low operating speed and scale of the test facility.

The validity of technique employed for the measurement of blade surface unsteady pressure is examined in detail within chapter 4. And comparison of calibration measurements - which correct for the phase shift and attenuation of unsteady pressure signals along the tubing which separates the blade surface tappings with the outboard pressure transducers - with predictions presented by Tijdeman (1975) demonstrated a good level of agreement, thereby supporting the approach adopted. An evaluation of repeatability and experimental error, also presented in chapter 4, indicated an excellent level of repeatability and good level of accuracy to be achieved in the measurement of unsteady pressure.

8.1.2 Experimental Results

The steady flow and extensive set of unsteady pressure measurements presented in chapter 5 provide the first 3D test data of its kind, to be made available in open literature. The steady flow blade surface pressure distribution and results of five-hole probe measurements performed at inlet and exit traverse planes demonstrate a predominant <u>two dimensional steady flow</u> structure throughout the working section. Whilst in contrast the blade surface unsteady pressure measurements, which are provided for five spanwise sections between 10% and 90% span, reveal a consistent <u>three dimensional behaviour of the unsteady aerodynamics</u> throughout a range of reduced frequency (k: 0.15 to 0.75). This is most especially evident in the measured amplitude of blade surface unsteady pressure which is largely insensitive to the local bending amplitude. An experimental assessment of linearity also indicated a linear behaviour of the unsteady aerodynamic response of the oscillating turbine blade.

8.1.3 Computational Results

An extended version of a three dimensional time-marching Euler method for the prediction of unsteady flows around oscillating turbomachinery blades was developed in order to model the experimental test configuration. The computational predictions

obtained from this method, which are the first to be supported by 3D test data, exhibited a consistently high level of qualitative and quantitative agreement with the experimental test data throughout the range of reduced frequency examined. This clearly demonstrated the ability of the computational method to predict the relevant unsteady aerodynamic phenomenon and further indicated the unsteady aerodynamic response to be largely governed by inviscid flow mechanisms. Some discrepancies were, however, apparent in the prediction of phase angle towards the trailing edge of the suction surface which were attributed to viscous effects induced by the strong diffusion experienced in this region. Fortunately, these discrepancies were confined to a region of low unsteady pressure activity and subsequently did not significantly influence the overall level of prediction, as demonstrated by the favourable comparison with the measured aerodynamic damping.

Additional solutions, obtained from a quasi-3D version of the computational method, highlighted the strong three dimensional behaviour of the unsteady aerodynamics and demonstrated the apparent inadequacies of the conventional quasi-3D strip methodology. The quasi-3D method was clearly unable to capture the insensitivity of the unsteady pressure generation to the local bending amplitude, whilst this phenomenon was adequately predicted by the full 3D Euler method. The marked over prediction of unsteady pressure amplitude by the quasi-3D method towards the tip of the blade, where the amplitude of vibration is high, also led to a considerable over-prediction in aerodynamic damping.

8.1.4 The Influence of Tip Leakage on the Oscillating Turbine Blade Flow

An additional, and entirely original, experimental investigation was performed in order to make a preliminary assessment of the unknown influence of tip leakage flow on the unsteady aerodynamic response of oscillating turbomachinery blades. This was achieved through a comprehensive set of steady flow and unsteady pressure measurements at three different settings of tip clearance. The steady flow measurements presented in chapter 7 indicated a characteristic behaviour of the tip leakage flow throughout the range of tip clearance considered, demonstrating that despite the unusual configuration, the test facility provides a suitable vehicle for the investigation undertaken. The unsteady pressure data, obtained from tappings between 10% and 90% span, showed the unsteady aerodynamics to be largely unaffected by the variation in clearance, with negligible impact on the measured aerodynamic damping observed. Close examination of the

unsteady pressure measurements did, however, reveal subtle, but consistent, trends the first harmonic pressure response at the 90% span location, which were notably observed to coincide with localised regions where the tip leakage flow had a discernible impact on the steady flow blade loading characteristic.

8.2 Recommendations for Further Work

Despite the original contribution of the present work in providing the first three dimensional test data for aeroelastic applications, the fundamental problem faced by developers of advanced computational methods for the prediction of blade flutter largely remains unchanged: That of robust validation of over a wide range of aerodynamic operating conditions. This is not only important in terms of the assessing capabilities of existing methods, but moreover, it is required in order to establish areas of deficiency and direct future developments. It is clear then, that a significant effort should be expended in order to compile an extensive three dimensional test database, which should be made available in open literature and address flutter problems at aerodynamic conditions of practicable interest, for instance transonic and separated flow regimes. Pursuit of this objective should also yield improved understanding of three dimensional nature of blade flutter, which is of vital importance to the design engineer.

Future experimental work directed at the three dimensional unsteady flow phenomenon should also be conducted in more realistic turbomachinery configurations, most likely in an oscillating linear cascade to enable detailed measurement of 3D unsteady flow structures. This would offer the ability to address a wider range of flow conditions than possible with the present configuration and allow an assessment of the influence of parameters such as incidence angle and interblade phase angle on the three dimensional nature of the unsteady flow. Care must be taken, however, to ensure the realisation of clearly defined boundary conditions and when adopting the linear influence coefficient technique that the unsteady phenomenon exhibits a linear behaviour. Additional work is also required to improve understanding of flutter under realistic modes of blade vibration which at present can only be achieved through testing in instrumented turbomachines.

It is also proposed that the basic configuration of the present test facility, which bounds the unsteady flow around the oscillating turbine blade with the sidewalls of a profiled duct, may prove particularly beneficial in the acquisition of reliable transonic test cases for oscillating blade flows. This is because, the particularly serious problems currently

encountered in establishing a periodic steady and unsteady flow in cascades operating at transonic speeds are removed by oscillating a single blade in a profiled duct, whilst the basic ingredients required for understanding the important behaviour of oscillating transonic blade flows are retained - i.e. that of unsteady shock behaviour.

In terms of the computational work presented, it was notable that the inviscid method was unable to adequately capture the unsteady response towards the trailing edge of the suction surface where the flow was subject to significant diffusion. In light of this, computation of the experimental test configurations with a viscous computational method would seem prudent, both to give a preliminary indication of performance of such a method and provide further insight into the behaviour of the unsteady viscous flow and relevant modelling issues.

Although the experimental investigation into the influence of tip leakage on the unsteady aerodynamic response of the oscillating turbine blade showed there to be limited effect on the unsteady pressure measurements between 10% and 90% span, it remains unclear as to the influence of tip leakage on the unsteady blade loading much nearer the tip section. Further investigation is therefore recommended to assess the influence of tip leakage on the unsteady flow within the very near tip region, since the contribution towards aerodynamic damping from this localised section of the blade could quite conceivably have a significant impact on the overall aeroelastic stability.

Appendix A

References and Bibliography

Ayer, T.C. & Verdon, J.M. (1998), "Validation of a Nonlinear Unsteady Aerodynamic Simulator for Vibrating Blade Rows," *Transactions of the ASME, Journal of Turbomachinery*, Volume 120, pp. 113-121.

Barton, H.A. & Halliwell, D.G. (1987), "Detailed On-Blade Measurements on a Transonic Fan in Unstalled Supersonic Flutter," *Proceedings of the 4th International Symposium on Unsteady Aerodynamics and Aeroelasticity of Turbomachines (ISUAAT)*, Aachen, Germany.

Bell, D.L. & He, L. (1997a), "Three Dimensional Unsteady Pressure Measurements for an Oscillating Turbine Blade," *ASME Paper* 97-GT-105.

Bell, D.L. & He, L. (1997b), "Three Dimensional Unsteady Flow Around a Turbine Blade Oscillating in Bending Mode - An Experimental and Computational Study," *Proceedings of the 8th ISUAAT*, Stockholm, Sweden.

Bell, D.L. & He, L. (1998), "Three Dimensional Unsteady Flow for an Oscillating Turbine Blade and the Influence of Tip Leakage," Submitted for *ASME Turbomachinery Exposition* 1998.

Bölcs, A. & Fransson, T.H. (1986), "Aeroelasticity in Turbomachines: Comparison of Theoretical and Experimental Cascade Results," *Communication du Laboratoire de Thermique Appliquée et de Turbomachines, No. 13, Lusuanne, EPFL*.

Buffum, D.H. & Fleeter, S. (1993), "Wind Tunnel Wall Effects in a Linear Oscillating Cascade," *Transactions of the ASME, Journal of Turbomachinery*, Volume 115, No. 1, pp. 147-156.

Buffum, D.H., Capece, V.R., King, A.J. & El-Aini, Y.M. (1998), "Oscillating Cascade Aerodynamics at Large Mean Incidence," *Transactions of the ASME, Journal of Turbomachinery*, Volume 120, No. 1, pp. 122-130.

Carta, F.O. & St. Hilaire, A.O. (1978), "Experimentally Determined Stability Parameters of a Subsonic Cascade Oscillating Near Stall," *Transactions of the ASME, Journal of Engineering for Power*, Volume 100, No. 1, pp. 111-120.

Carta, F.O. & St. Hilaire, A.O. (1980), "Effects of Interblade Phase Angle on Cascade Pitching Stability," *Transactions of the ASME, Journal of Engineering for Power*, Volume 102, pp. 391-396.

Carta, F.O. (1983), "Unsteady Aerodynamics and Gapwise Periodicity of Oscillating Cascaded Airfoils," *Transactions of the ASME, Journal of Engineering for Power*, Volume 105, pp. 565-574.

Collar (1947), "The Expanding Domain of Aeroelasticity," *Journal of the Royal Aeronautical Society* 51-1.

Denton, J.D. (1983), "An Improved Time-Marching Method for Turbo-machinery Flow Calculations," *Transactions of the ASME, Journal of Engineering for Power*, Volume 105, No. 3, pp. 514-524.

Denton, J.D. (1993), "The 1993 IGTI Scholar Lecture: Loss Mechanisms in Turbomachines," *Transactions of the ASME, Journal of Turbomachinery*, Volume 115, No. 4, pp. 621-656.

Dominy, R.G. & Hodson, H.P. (1993), "An Investigation of Factors Influencing the Calibration of Five-Hole Probes for Three-Dimensional Flow Measurements," *Transactions of the ASME, Journal of Turbomachinery*, Volume 115, pp. 513-519.

Erdos, J.I. & Alzner, E. (1977), "Computation of Unsteady Transonic Flows Through Rotating and Stationary Cascades, I - Method of Analysis," *NASA Scientific and Technical Information Office*, NAS3-16807.

Fleeter, S., Novick, A.S., Riffel, R.E. & Caruthers, J.E. (1977), "An Experimental Determination of the Unsteady Aerodynamics in a Controlled Oscillating Cascade," *Transactions of the ASME, Journal of Engineering for Power*, Volume 99, pp. 88-96.

Fleeter, S., Jay, R.L. & Bennet, W.A. (1978), "Rotor Wake Generated Unsteady Aerodynamic Response of a Compressor Stator," *ASME Journal of Engineering for Power*, Volume 100, pp. 664-675.

Fleeter, S. & Jay, R.L. (1987), "Unsteady Aerodynamic Measurements in Flutter Research," *AGARD Manual on Aeroelasticity in Axial-Flow Turbomachines*, Volume 1 - Unsteady Turbomachinery Aerodynamics, AGARD-AG-298.

Fransson, T.H. & Pandolfi, M. (1986), "Numerical Investigation of Unsteady Subsonic Compressible Flows Through an Oscillating Linear Cascade," *ASME Paper* 86-GT-304.

Gerolymos, G.A. (1993a), "Advances in the Numerical Integration of the Three-Dimensional Euler Equations in Vibrating Cascades," *Transactions of the ASME, Journal of Turbomachinery*, Volume 115, pp. 781-790.

Gerolymos, G.A. (1993b), "Coupled Three-Dimensional Aeroelastic Stability Analysis of Bladed Disks," *Transactions of the ASME, Journal of Turbomachinery*, Volume 115, pp. 791-799.

Giles, M.B. (1987), "Calculation of Unsteady Wake/Rotor Interactions," *Proceedings of the AIAA 25th Aerospace Sciences Meeting*, Nevada, USA. Paper No. AIAA-87-0006.

Gorlin, S.M. & Slezinger, I.I. (1964), "Wind Tunnels and their Instrumentation," Translated from Russian by the Israel Program for Scientific Translations.

Hall, K.C. & Crawley, (1989), "Calculation of Unsteady Flows in Turbomachinery Using the Linearised Euler Equations," *AIAA Journal*, Volume 27, No. 6, pp. 777-787.

Hall, K.C. & Lorence, C.B. (1993), "Calculation of Three-Dimensional Unsteady Flows in Turbomachinery using the Linearized Harmonic Euler Equations," *Transactions of the ASME, Journal of Turbomachinery*, Volume 115, pp. 800-809.

Hall, K.C., Clark, W.S. & Lorence, C.B. (1994), "A Linearized Euler Analysis of Unsteady Transonic Flows in Turbomachinery," *Transactions of the ASME, Journal of Turbomachinery*, Volume 116, pp. 477-488.

Hanamura, Y., Tanaka, H. & Yamaguchi, K. (1980), "A Simplified Method to Measure Unsteady Forces Acting on Vibratory Blades in Cascade," *Bulletin of the JSME*, Volume 23, No. 180, pp. 880-887.

Hanamura, Y. & Yamaguchi, K. (1995), "Experimental Observation of Mach Number Effects upon a Vibrating Highly-Turned Turbine Cascade," *Proceedings of the 7th ISUAAT*, Fukuoka, Japan, pp. 401-417.

He, L. (1990a), "An Euler Solution for Unsteady Flows Around Oscillating Blades," *Transactions of the ASME, Journal of Turbomachinery*, Volume 112, pp. 714-722.

He, L. (1990b), "Unsteady Flow Around Oscillating Turbomachinery Blades," PhD thesis, University of Cambridge, UK.

He, L. & Denton, J.D. (1991), "An Experiment on Unsteady Flow over an Oscillating Airfoil," *ASME Paper* 91-GT-181.

He, L. (1992), "Method of Simulating Unsteady Turbomachinery Flows with Multiple Perturbations," *AIAA Journal*, Volume 30, No. 11, pp. 2730-2736.

He, L. (1993), "A New Two-Grid Acceleration Method for Unsteady Navier-Stokes Calculations," *AIAA Journal of Power and Propulsion*, Volume 9, No. 2, pp 272-280.

He, L. & Denton, J.D. (1993a), "Inviscid-Viscous Coupled Solution for Unsteady Flows Through Vibrating Blades: Part 1 - Description of Method," *Transactions of the ASME, Journal of Turbomachinery*, Volume 115, pp. 95-100.

He, L. & Denton, J.D. (1993b), "Inviscid-Viscous Coupled Solution for Unsteady Flows Through Vibrating Blades: Part 2 - Computational Results," *Transactions of the ASME, Journal of Turbomachinery*, Volume 115, pp. 101-109.

He, L. & Denton, J.D. (1994), "Three Dimensional Time-Marching Inviscid and Viscous Solutions for Unsteady Flows Around Vibrating Blades," *Transactions of the ASME, Journal of Turbomachinery*, Volume 116, pp. 469-476.

He, L. & Ning, W. (1997), "Nonlinear Harmonic Analysis of Unsteady Transonic Inviscid and Viscous Flows," *Proceedings of the 8th ISUAAT*, Stockholm, Sweden.

He, L. (1998a), "Unsteady Flow in Oscillating Turbine Cascade, Part 1. Linear Cascade Experiment," *Transactions of the ASME, Journal of Turbomachinery*, Volume 120, No. 2, pp. 262-268.

He, L. (1998b), "Unsteady Flow in Oscillating Turbine Cascade, Part 2. Computational Study," *Transactions of the ASME, Journal of Turbomachinery*, Volume 120, No. 2, pp. 269-275.

Hennings, H. & Send, W. (1996), "Experimental Investigation and Theoretical Prediction of Flutter Behaviour of a Plane Cascade in Low-Speed Flow," *ASME Paper* 96-GT-417.

Holmes, G.D., Mitchell, B.E. & Lorence, C.B. (1997), "Three Dimensional Navier-Stokes Calculations for Flutter and Forced Response," *Proceedings of the 8th ISUAAT*, Stockholm, Sweden.

Huff, D.L. (1987), "Numerical Simulations of Unsteady, Viscous, Transonic Flow over Isolated and Cascaded Airfoils using a Deformed Grid," *AIAA Paper* 87-1316.

Jameson, A., Schmidt, W. & Turkel, E. (1981), "Numerical Solutions of the Euler Equations by Finite Volume Method using the Runge-Kutta Timestepping Scheme," *AIAA Paper* 81-1259.

Jutras, R.R., Stallone, M.J. & Bankhead, H.R. (1980), "Experimental Investigation of Flutter in Mid-Stage Compressor Designs," *AIAA* Paper 80-0786.

Kobayashi, H. (1989), "Effects of Shock Waves on Aerodynamic Instability of Annular Cascade Oscillation in a Transonic Flow," *Transactions of the ASME, Journal of Turbomachinery*, Volume 111, pp. 222-230.

Kobayashi, H., Oinuma, H. & Araki, T. (1995), "Shock Wave Behaviour of Annular Blade Row Oscillating in Torsional Mode with Interblade Phase Angle," *Proceedings of the 7th ISUAAT*, Fukuoka, Japan, pp. 383-400.

Körbächer, H.K. & Bölcs, A. (1995), "Experimental Investigation of the Unsteady Behaviour of a Compressor Cascade in an Annular Ring Channel," *Proceedings of the 7th ISUAAT*, Fukuoka, Japan, pp. 383-400.

Körbächer, H.K. & Bölcs, A. (1996), "Steady-State and Time Dependent Experimental Results of a NACA-3506 Cascade in an Annular Channel," *ASME Paper* 96-GT-334.

Kuk, V. (1995), Private communication.

Lane, F. (1956), "System Mode Shapes in the Flutter of Compressor Blade Rows," *Journal of Aeronautical Science*, Volume 23, pp. 54-66.

Lindquist, D.R. & Giles, M.B. (1994), "Validity of Linearized Unsteady Euler Equations with Shock Capturing," *AIAA Journal*, Volume 32, No. 1, pp. 46-53.

Lynn, P.A. & Fuerst, W. (1996), "Introductory Digital Signal Processing with Computer Applications," *Revised Edition, John Wiley & Sons.*

Manwaring, S.R. & Wisler, D.C. (1993), "Unsteady Aerodynamics and Gust Response in Compressors and Turbines," *Transactions of the ASME, Journal of Turbomachinery*, Volume 115, No. 4, pp. 724-740.

Manwaring, S.R., Rabe, D.C, Lorence, C.B. & Wadia, A.R. (1997), "Inlet Distortion Generated Forced Response of a Low Aspect Ratio Transonic Fan," *Transactions of the ASME, Journal of Turbomachinery*, Volume 119, pp. 665-676.

Manwaring, S.R. & Kirkeng, K.L. (1997), "Forced Response of a Low Pressure Turbine due to Circumferential Temperature Distortions," *Proceedings of the 8th ISUAAT*, Stockholm, Sweden.

Marshall, J.G. (1997), "Prediction of Turbomachinery Aeroelasticity Effects using a 3D Non-Linear Integrated Method", PhD thesis, Imperial College of Science, Technology & Medicine, University of London, UK.

Marshall, J.G. & Giles, M.B. (1997), "Some Applications of a Time-Linearized Euler Method to Flutter and Forced Response in Turbomachinery," *Proceedings of the 8th ISUAAT*, Stockholm, Sweden.

Mikolajczak, A.A., Arnoldi, R.A., Snyder, L.E. & Stargardter, H. (1975), "Advances in Fan and Compressor Blade Flutter Analysis and Predictions," *AIAA Journal of Aircraft*, Volume 12, No. 4, pp. 325-331.

Mikolajczak, A.A. (1976), "Technology Status for Blade Flutter in Axial Turbomachinery" *Transactions of the ASME, Journal of Fluids Engineering*, September 1976, pp. 337-339.

Norryd, M. & Bölcs, A. (1997), "Experimental Investigation of Unsteady Pressure Behaviour in a Linear Turbine Cascade," *Proceedings of the 8th ISUAAT*, Stockholm, Sweden.

Ning, W. & He, L. (1997), "Computation of Unsteady Flows Around Oscillating Blades Using Linear and Nonlinear Harmonic Euler Methods," *ASME Paper 97-GT-229*, to appear in the *Transactions of the ASME, Journal of Turbomachinery*.

Rothrock, M.D., Jay, R.L. & Riffel, R.E. (1982), "Time-Variant Aerodynamics of High-Turning Blade Elements," *Transactions of the ASME, Journal of Engineering for Power*, Volume 104, No. 2, pp. 412-419.

Schlichting, H. (1979), "Boundary Layer Theory," McGraw-Hill 7th edition.

Scalzo, A.J., Allen, J.M. & Antos, R.J. (1986), "Analysis and Solution of a Nonsynchronous Vibration Problem of the Last Row Turbine Blade of a Large Industrial Combustion Turbine," *Transactions of the ASME, Journal of Engineering for Gas Turbines and Power*, Volume 108, pp. 591-598.

Shannon, J.F. (1945), "Vibration Problems in Gas Turbine, Centrifugal and Axial Flow Compressors," *A.R.C., R & M 2226*.

Shibata, T. & Kaji, S. (1995), "Experimental Study of the Unstarted Flutter in a Compressor Cascade," *Proc. of the 7th ISUAAT*, Fukuoka, Japan, pp. 365-381.

Sisto, F. (1987a), "Introduction and Overview," *AGARD Manual on Aeroelasticity in Axial-Flow Turbomachines*, Volume 1 - Unsteady Turbomachinery Aerodynamics, AGARD-AG-298.

Sisto, F. (1987b), "Stall Flutter," *AGARD Manual on Aeroelasticity in Axial-Flow Turbomachines*, Volume 1 - Unsteady Turbomachinery Aerodynamics, AGARD-AG-298.

Sjolander, S.A. & Amrud, K.K. (1987), "Effects of Tip Clearance on Blade Loading in a Planar Cascade of Turbine Blades," *Transactions of the ASME, Journal of Turbomachinery*, Volume 109, pp. 237-224.

Sjolander, S.A. (1997), "Physics of Tip Clearance Flows I & II," *VKI Lecture Series on 'Secondary and Tip Clearance Flows in Axial Turbomachines,'* 1997-01.

Snyder, L.E. & Commerford, G.L. (1974), "Supersonic Unstalled Flutter in a Fan Rotor: Analytical and Experimental Results," *Transactions of the ASME, Journal of Engineering for Power*, Volume 96, No. 4, pp 379-386.

Srinivassen, A.V. (1997), "The 1997 IGTI Scholar Lecture: Flutter and Resonant Vibration Characteristics of Engine Blades," *ASME Paper* 97-GT-533.

Stargadter, H. (1977), "Optical Determination of Rotating Fan Blade Deflections," *Transactions of the ASME, Journal of Engineering for Power*, Volume 99, pp. 204-209.

Tijdeman, H. (1975), "On the Propagation of Sound Waves in Cylindrical Pipes," *Journal of Sound and Vibration*, Volume 39, No. 1, pp. 1-16.

Treaster, A.L. & Yocum, A.M. (1979), "The Calibration and Application of Five-hole Probes," *ISA Transactions*, Volume 18, No. 3, pp. 23-34.

Verdon, J.M. & Casper, J.R. (1982), "Development of a Linear Unsteady Aerodynamic Analyses for Finite-Deflection Subsonic Cascades," *AIAA Journal*, Volume 20, No. 9, pp. 1259-1267.

Verdon, J.M. (1993), "Review of Unsteady Aerodynamic Methods for Turbomachinery Aeroelastic and Aeroacoustic Applications," *AIAA Journal*, Volume 31, No. 2, pp. 235-249.

Walker, P. (1992), "Sizing of Boundary Layer Trips," GEC ALSTHOM TA373

Whitehead, D.S. (1982), "The Calculation of Steady and Unsteady Transonic Flows in Cascades," CUEDA/A - Turbo/TR 118, Cambridge University, England.

Appendix B

Blade Profile Specification

Axial	Tangential	Axial	Tangential	Axial	Tangential
0.012060	0.000077	0.005939	0.009774	0.006463	0.014459
0.012059	0.000054	0.005536	0.010241	0.006896	0.013939
0.012047	0.000035	0.005131	0.010705	0.007293	0.013390
0.012029	0.000022	0.004724	0.011167	0.007661	0.012821
0.012006	0.000020	0.004314	0.011628	0.008004	0.012237
0.011985	0.000027	0.003905	0.012088	0.008327	0.011642
0.011970	0.000044	0.003495	0.012549	0.008631	0.011037
0.011816	0.000433	0.003086	0.013010	0.008920	0.010424
0.011583	0.001003	0.002679	0.013473	0.009194	0.009805
0.011337	0.001568	0.002275	0.013938	0.009454	0.009180
0.011079	0.002128	0.001874	0.014406	0.009700	0.008549
0.010810	0.002682	0.001478	0.014878	0.009935	0.007914
0.010528	0.003230	0.001087	0.015354	0.010159	0.007274
0.010235	0.003772	0.000748	0.015784	0.010372	0.006632
0.009929	0.004307	0.000574	0.016151	0.010576	0.005986
0.009613	0.004836	0.000705	0.016511	0.010770	0.005337
0.009285	0.005357	0.001089	0.016639	0.010957	0.004686
0.008946	0.005872	0.001676	0.016642	0.011137	0.004033
0.008598	0.006380	0.002351	0.016587	0.011311	0.003378
0.008240	0.006882	0.003019	0.016478	0.011480	0.002722
0.007873	0.007377	0.003674	0.016306	0.011641	0.002064
0.007499	0.007867	0.004307	0.016065	0.011792	0.001404
0.007118	0.008351	0.004908	0.015754	0.011933	0.000742
0.006730	0.008830	0.005470	0.015377		
0.006337	0.009304	0.005989	0.014942	Co-ordinates in metres	